34468

National Library of Canada | Bibliothèque nationale du Canada

CANADIAN THESES ON MICROFICHE | *THÈSES CANADIENNES SUR MICROFICHE*

NAME OF AUTHOR/*NOM DE L'AUTEUR* THOMAS GERARD RYAN

TITLE OF THESIS/*TITRE DE LA THÈSE* Radiation Induced Chain Reaction in Water At High Temperatures and Electron Ranges and Applications to Hydrocarbons

UNIVERSITY/*UNIVERSITÉ*

DEGREE FOR WHICH THESIS WAS PRESENTED/*GRADE POUR LEQUEL CETTE THÈSE FUT PRÉSENTÉE* Ph.D.

YEAR THIS DEGREE CONFERRED/*ANNÉE D'OBTENTION DE CE GRADE* 1977

NAME OF SUPERVISOR/*NOM DU DIRECTEUR DE THÈSE* DR. G. R. FREEMAN

Permission is hereby granted to the NATIONAL LIBRARY OF CANADA to microfilm this thesis and to lend or sell copies of the film.

The author reserves other publication rights, and neither the thesis nor extensive extracts from it may be printed or otherwise reproduced without the author's written permission.

L'autorisation est, par la présente, accordée à la BIBLIOTHÈQUE NATIONALE DU CANADA de microfilmer cette thèse et de prêter ou de vendre des exemplaires du film.

L'auteur se réserve les autres droits de publication; ni la thèse ni de longs extraits de celle-ci ne doivent être imprimés ou autrement reproduits sans l'autorisation écrite de l'auteur.

DATED/*DATÉ* July 25/1977 SIGNED/*SIGNÉ* Thomas Ryan

PERMANENT ADDRESS/*RÉSIDENCE FIXÉ* McMaster University
Chemistry Department
Hamilton, Ontario

NOTICE

The quality of this microfiche is heavily dependent upon the quality of the original thesis submitted for microfilming. Every effort has been made to ensure the highest quality of reproduction possible.

If pages are missing, contact the university which granted the degree.

Some pages may have indistinct print especially if the original pages were typed with a poor typewriter ribbon or if the university sent us a poor photocopy.

Previously copyrighted materials (journal articles, published tests, etc.) are not filmed.

Reproduction in full or in part of this film is governed by the Canadian Copyright Act, R.S.C. 1970, c. C-30. Please read the authorization forms which accompany this thesis.

THIS DISSERTATION
HAS BEEN MICROFILMED
EXACTLY AS RECEIVED

AVIS

La qualité de cette microfiche dépend grandement de la qualité de la thèse soumise au microfilmage. Nous avons tout fait pour assurer une qualité supérieure de reproduction.

S'il manque des pages, veuillez communiquer avec l'université qui a conféré le grade.

La qualité d'impression de certaines pages peut laisser à désirer, surtout si les pages originales ont été dactylographiées à l'aide d'un ruban usé ou si l'université nous a fait parvenir une photocopie de mauvaise qualité.

Les documents qui font déjà l'objet d'un droit d'auteur (articles de revue, examens publiés, etc.) ne sont pas microfilmés.

La reproduction, même partielle, de ce microfilm est soumise à la Loi canadienne sur le droit d'auteur, SRC 1970, c. C-30. Veuillez prendre connaissance des formules d'autorisation qui accompagnent cette thèse.

LA THÈSE A ÉTÉ
MICROFILMÉE TELLE QUE
NOUS L'AVONS REÇUE

THE UNIVERSITY OF ALBERTA

RADIATION INDUCED CHAIN REACTIONS IN WATER AT HIGH TEMPERATURES AND ELECTRON RANGES AND MOBILITIES IN HYDROCARBONS

BY

© THOMAS GERARD RYAN

A THESIS

SUBMITTED TO THE FACULTY OF GRADUATE STUDIES AND RESEARCH

IN PARTIAL FULFILMENT OF THE REQUIREMENTS FOR THE DEGREE

OF

DOCTOR OF PHILOSOPHY

DEPARTMENT OF CHEMISTRY

EDMONTON, ALBERTA

FALL, 1977

THE UNIVERSITY OF ALBERTA

FACULTY OF GRADUATE STUDIES AND RESEARCH

The undersigned certify that they have read, and recommend to the Faculty of Graduate Studies and Research for acceptance, a thesis entitled

"RADIATION INDUCED CHAIN REACTIONS IN WATER AT HIGH TEMPERATURES AND ELECTRON RANGES AND MOBILITIES IN HYDROCARBONS"

submitted by THOMAS GERARD RYAN in partial fulfilment of the requirements for the degree of Doctor of Philosophy.

.....
Supervisor

.....

.....

.....

.....

.....
External Examiner

July 22/1977
Date

PART I

A B S T R A C T

The γ-radiolysis of water and deuterium oxide solutions of nitrous oxide have been examined at various temperatures. For each of the conditions studied a plot of nitrogen yield versus radiation dose was constructed and the 100 eV yield of nitrogen was calculated from the slope. At all temperatures studied the yield of nitrogen from deuterium oxide was higher than that from water. This was interpreted as a higher yield of free electrons in the former compound which resulted from a higher total ionization yield.

The addition of methanol or 2-propanol to aqueous nitrous oxide solutions resulted in a radiation induced chain reaction above 200°C. The yields of nitrogen and formaldehyde, from the methanol system, and nitrogen and acetone, from the 2-propanol system, were determined as a function of nitrous oxide concentration, alcohol concentration, dose rate and temperature. A chain mechanism was proposed which involved the reaction of nitrous oxide with a $\cdot CR_2OH$ radical producing a $\cdot OCR_2OH$ radical. A steady state treatment of the reaction mechanism yielded a set of equations which agreed with the experimental results.

PART I-I

A pulse radiolysis conductance technique has been used to measure free ion yields and electron mobilities in five paraffins. The five compounds studied, 2,3-dimethylbutane, 3-methylpentane, 3,3-dimethylpentane, 2,2-4-trimethylpentane and 2,2,4,4-tetramethylpentane were examined over almost their entire liquid range. The free ion yields were determined as a function of electric field strength and the Onsager theory was used to obtain thermalization ranges. The mean value of the thermalization ranges was found to be larger in the more branched compounds and to increase with temperature. Electron mobilities were determined as a function of electric field strength and for nearly all conditions were found to be field independent. The Arrhenius plots of electron mobility had a complex shape, showing that not only thermal activation effects were operative. Parallel behavior between thermalization ranges and mobilities indicates that thermal and epithermal electrons are affected in a similar way by changes in liquid density.

A C K N O W L E D G E M E N T S

I would like to thank my research director, Professor G. R. Freeman, for his guidance and patience during the course of this work.

Special thanks are due to Mrs. Mary Waters who typed the final draft of this thesis and to Dr. T. E. M. Sambrook who collaborated with me on some of the work.

I am very grateful for the technical assistance of Mr. R. J. Gardner and his staff. I also thank the members of the glass shop and machine shop for the excellent work they have done in making these experiments possible.

I owe a great deal to my friends in the radiation chemistry group who maintained an atmosphere of good fellowship and cooperation in the laboratory.

TABLE OF CONTENTS

LIST OF TABLES

LIST OF FIGURES

P A R T I

RADIATION INDUCED CHAIN REACTIONS IN WATER AT HIGH TEMPERATURES

I INTRODUCTION

A. General

Radiation chemistry is the study of the chemical effects resulting from the absorption of high energy ionizing radiation by material (1). The absorption of such radiation by a liquid produces ionic and free radical species which then react further to produce stable products.

Absorption processes for γ-rays of about 1 MeV energy are of two types. The photoelectric effect is the process where a γ-ray transfers all of its energy to an orbital electron, causing the electron to be ejected into the medium. This process is important for γ-ray absorption by materials of high atomic number.

The second process is called Compton scattering, where only part of the energy of the γ-ray is absorbed, resulting in an ejected high energy electron and a degraded γ photon. Compton scattering is the predominant mode of interaction between 1.17 MeV γ-rays and materials of low atomic number.

High energy electrons produced by either of the above processes cause further ionization until their kinetic energy is lower than the ionization potential of the molecules in the medium.

B. Spatial Distribution of Ion Pairs Produced by γ-Radiolysis

When a high energy electron passes through a liquid, ion pairs are produced along the track of the electron so that an nonhomogeneous distribution of ions is created. If the incident electron kinetic energy is of the order of 1 MeV about two thirds of the ion pairs will be at a large enough distance from other ion pairs that there is no coulombic interaction between them. For electrons with kinetic energy 5 KeV the ion pairs created along the track are bunched together so that coulombic interaction between them is important (2).

C. Irradiation of Liquid Water by γ-Rays

The radiolysis of liquid water by γ-rays involves a sequence of events. The first stage, energy transfer to the liquid, is complete in 10^{-15} s or less. The process occurring in this time period can be represented by reaction (1).

$$H_2O \xrightarrow{\sim\sim} e^- + H_2O^+ \qquad (1)$$

The above ionization is followed by the thermalization and hydration of the electron, reaction (2) (3),

$$e^- \longrightarrow e^-_{therm} \longrightarrow e^-_{aq} \qquad (2)$$

and a proton transfer to H_2O accompanied by hydration,

reaction (3)

$$H_2O^+ + H_2O \longrightarrow OH + H_3O^+ \longrightarrow H_3O^+_{aq} + OH \quad (3)$$

These processes are over in 10^{-11} s or less. The next step involves diffusion and reaction of e^-_{aq}, $H_3O^+_{aq}$ and OH. Reactions (4) and (5) describe the fate of $H_3O^+_{aq}$ and e^-_{aq} ions (4).

$$[H_3O^+_{aq} + e^-_{aq}] \longrightarrow [H_3O] \longrightarrow [H + H_2O] \quad (4)$$

$$\xrightarrow{\text{diffusion}} H_3O^+_{aq} + e^-_{aq} \quad (5)$$

The square brackets indicate that the entities are in spurs which means that they are close enough to each other that they might react together before they can diffuse apart. For irradiation by 1 MeV γ-rays about 30% of the ions will recombine (reaction 4) and the remainder will diffuse into the bulk of the liquid and become free ions (reaction 5).

The H and OH radicals in the spur can combine, reaction (6),

$$[H + OH] \longrightarrow [H_2O] \quad (6)$$

or diffuse out of the spur, reaction (7).

$$[H + OH] \xrightarrow{\text{diffusion}} H + OH \quad (7)$$

The spurs are destroyed by diffusion in a time period of

about 10^{-9} s.

D. Effect of N_2O on γ-Radiolysis of Water

Nitrous oxide reacts very rapidly with solvated electrons and relatively slowly with free radicals. If nitrous oxide is added to water the effect produced upon radiolysis depends on the N_2O concentration. At low N_2O concentrations (about 1 mM) essentially all the hydrated electrons that have escaped into the bulk of the medium (free electrons) will be scavenged by N_2O. The process is described by reactions (8), (9) and (10).

$$N_2O + e^-_{aq} \longrightarrow N_2O^- \qquad (8)$$

$$N_2O^- \longrightarrow N_2 + O^- \qquad (9)$$

$$O^- + H_2O \longrightarrow OH^- + OH \qquad (10)$$

If the N_2O concentration is greater than 0.17 M, not only electron free ions will be scavenged but also most of the hydrated electrons in spurs.

$$[e^-_{aq} + N_2O] \longrightarrow [N_2O^-] \qquad (11)$$

The N_2O^- ion gives N_2 and O^- as indicated in equation 9, so the scavenging of spur electrons produces an increase in the N_2 yield. The number of N_2 molecules produced by the absorption of 100 eV of energy is called $G(N_2)$.

E. Radiation Induced Chain Reactions

Radiation induced chain reactions are initiated by

the absorption of energy from radiation (5). A typical sequence of initiation, propagation and termination reactions for a radiation induced chain process is represented by reactions 12-19,

$$M \rightsquigarrow [R + R] \quad \text{initiation} \quad (12)$$

$$[R + M] \longrightarrow [RH + R'] \quad (13)$$

$$[R'] \longrightarrow [P_1 + R] \quad \text{propagation} \quad (14)$$

$$[R + R] \longrightarrow [P_2] \quad \text{termination} \quad (15)$$

$$[R + R] \xrightarrow{\text{diffusion}} 2R \quad (16)$$

$$R + M \longrightarrow RH + R' \quad (17)$$

$$R' \longrightarrow P_1 + R \quad \text{propagation} \quad (18)$$

$$R + R \longrightarrow P_2 \quad \text{termination} \quad (19)$$

where R and R' are free radicals. P_1 is a product the yield of which is proportional to the chain length, P_2 is a termination product, and M is a liquid which absorbs energy from the radiation. The square brackets in reactions 12-16 indicate that the reactants are in spurs.

Some aspects of the γ radiolysis of liquids at the dose rates normally used ($\sim 10^{17}$ eV/ml s, make it possible to evaluate the importance of the intraspur chain (reactions 12-16) as compared to the chain process in the bulk medium (reactions 16-19). The chain length is

proportional to the reciprocal of the radical concentration and the local concentration of radicals in the spurs is several orders of magnitude larger than the homogeneous concentration of radicals in the bulk liquid. This means that the yield of P_1 from the bulk medium chain is several orders of magnitude larger than the yield of P_1 from the intraspur process. One is therefore justified in neglecting the contribution from reactions 13-15 and in treating the radiation induced chain process using conventional homogeneous kinetics.

F. Previous Studies in the γ-Radiolysis of N_2O-H_2O Mixtures

Nitrous oxide has been used as an additive to water for a number of γ-radiolysis studies (4,6-16). Dainton and Peterson (8) determined yields of oxygen, hydrogen, and nitrogen for a range of N_2O concentrations from 2 mM to 23 mM. Yields were also studied as a function of pH using sulfuric acid and sodium hydroxide to make acidic and basic solutions containing 0.014 M N_2O. The value of $G(N_2)$ changed from 0.75 at pH <1 to 3.1 at 4< pH <11. At pH greater than 12 the $G(N_2)$ value was 4.1.

Allan and Beck (10) examined the γ-radiolysis of aqueous solution of 2-propanol and N_2O. A value of $G(N_2)$ of 2.80 ± 0.1 was obtained from the irradiation of samples containing 10 mM 2-propanol and 3-9 mM N_2O at pH 7. The N_2 yield was insensitive to 2-propanol

concentration which is consistent with the fact that alcohols are poor electron scavengers.

Head and Walker (16) measured the yields of nitrogen at N_2O concentrations between 10^{-5} M and 3×10^{-2} M for various pH values. The results were interpreted in terms of a competition between N_2O and H_3O^+ for electrons. Plots of $1/G(N_2)$ versus $1/[N_2O]$ were linear for a given pH in agreement with the assumption of a competition. At pH 7 and N_2O concentration ~15 mM, $G(N_2)$ was 3.1 the same as the value obtained by Dainton and Peterson (8).

Russel and Freeman (4) measured the yield of solvated electrons from the γ-radiolysis of aqueous solution containing 10% ethanol. Between 10^{-4} and 10^{-2} M N_2O concentration the value of $G(N_2)$ was 2.5 for neutral solution. At a N_2O concentration of 0.25 M the value of $G(N_2)$ was 4.0.

The above results lead to the conclusion that the yield of free solvated electrons in water is between 2.5 and 3.0. At low pH the yield of N_2 is determined by a competition between N_2O and H_3O^+ for electrons. A N_2O concentration of 10 mM at pH 12 or 0.25 M at pH 7 can lead to scavenging of virtually all electrons in spurs and give a $G(N_2)$ of 4.0.

Mixtures

Dainton and Peterson (8) have measured yields of N_2 from the γ-radiolysis of solutions of N_2O in D_2O. The value of $G(N_2)$ obtained for an N_2O concentration of 0.016 M and pH 6.3 was 3.54, about 12% higher than the corresponding value for N_2O in water.

H. Radiation Induced Chain Reactions in N_2O-Water Systems

A radiation induced chain reaction has been observed in aqueous solutions of N_2O and hydrogen (17-19). At pH ~12, 10 mM N_2O concentration and 0.6 mM hydrogen, the value of $G(N_2)$ was about 20. Above pH 13 the yield of nitrogen was $G(N_2)$ ~80.

High yields of products have been observed from the γ-irradiation of alkaline solutions of N_2O and 2-propanol (20-22). With 2-propanol and N_2O concentrations at 100 mM and ~7 mM respectively, and pH <11, the value of G(acetone) was between 5 and 15 (22). Changing the pH to greater than 12, and keeping other conditions the same, increased the value of G(acetone) to ~70. The results were interpreted in terms of reactions 20-29.

$$H_2O \xrightarrow{\sim\sim} e^-_{aq},\ H,\ OH,\ H_2,\ H_2O_2,\ H_3O^+_{aq} \qquad (20)$$

$$H + OH^- \longrightarrow e^-_{aq} \qquad (21)$$

$$OH + OH^- \longrightarrow H_2O + O^- \quad (22)$$

$$e^-_{aq} + N_2O \longrightarrow N_2 + O^- \quad (23)$$

$$O^- + (CH_3)_2CHOH \longrightarrow OH^- + (CH_3)_2\dot{C}OH \quad (24)$$

$$O^- + (CH_3)_2CHOH \longrightarrow OH^- + \dot{C}H_2(CH_3)CHOH \quad (25)$$

$$(CH_3)_2\dot{C}OH + OH^- \longrightarrow H_2O + (CH_3)_2CO^- \quad (26)$$

$$(CH_3)_2CO^- + N_2O \longrightarrow (CH_3)_2CO + N_2 + O^- \quad (27)$$

$$\dot{C}H_2(CH_3)CHOH + (CH_3)_2CHOH \longrightarrow (CH_3)_2CHOH + (CH_3)_2\dot{C}OH \quad (28)$$

$$2\dot{C}H_2(CH_3)CHOH \longrightarrow \text{non radical products} \quad (29)$$

Most of the experiments were done at pH 13.5 and for the kinetic analysis it was assumed that the OH^- concentration was high enough to convert all H, OH and $(CH_3)_2\dot{C}OH$ radicals to ions (reactions 21, 22, and 26). The concentration of N_2O was about 100 mM and it was considered that under these conditions reaction 27 would not be rate determining. If one considers reaction 29 to be the only significant termination step then a steady state treatment leads to equation (30)

$$G(\text{acetone}) = \frac{k_{24}}{k_{25}} G_R + \left(1 + \frac{k_{24}}{k_{25}}\right) k_{28} \left(\frac{G_R}{2k_{29}D}\right)^{\frac{1}{2}} [\text{2-propanol}] \quad (30)$$

where $G_R = Ge^-_{aq} + G_H + G_{OH}$ and D is the dose rate. A plot of G(acetone) versus 2-propanol concentration (0 - 0.2) was linear in agreement with equation (30). The intercept had a value of 32 ± 1. G(acetone) plotted against $/D^{\frac{1}{2}}$, at a 2-propanol concentration of 52 mM, gave a

straight line with an intercept of 34 ± 1.2. Setting $k_{24}/k_{25}G_R = 34$ and $G_R = 5.9$ gives $k_{24}/k_{25} = 5.8$.

Additional experimental information about the above system could be obtained by measuring the nitrogen yield, as the mechanism predicts that it will be about equal to the acetone yield.

I. Object of the Present Work

A good deal of work has been done on the γ-radiolysis of N_2O-water mixtures at room temperature but no information is available about the behavior of this system at higher temperatures. In the present study nitrogen yields are obtained for the γ-radiolysis of solution of N_2O in water and D_2O at 23°C, 81 ± 1°C, and 142 ± 2°C.

The chain processes for the N_2O-water-alcohol a d N_2O-water-hydrogen systems described above were studied earlier at room temperature only. In the present study two systems, N_2O-methanol-water, and N_2O-2-propanol-water, are examined at radiolysis temperatures between 200 and 310°C at natural pH. Both nitrogen and formaldehyde yields are measured in the N_2O-methanol-water system and in the N_2O-2-propanol-water system yields of nitrogen and acetone are determined. The results are interpreted in terms of a free radical chain mechanism.

II EXPERIMENTAL

A. MATERIALS

(a) Water

Triply distilled water was used for the final rinsing of the sample cells and for the samples. The first distillation was from a solution of sulfuric acid and potassium dichromate (6:1 mol ratio). The second was from alkaline permanganate and the third from a flask with no additive. The three distillations were done in a self contained unit that was protected from the lab atmosphere by U tubes containing distilled water.

(b) Deuterium Oxide

The deuterium oxide was obtained from Columbia Organic Chemicals Co. and had a purity of 99.77%. It was further purified by distilling from alkaline permanganate and distilled once more without additive. The alkali used in the permanganate distillation was KOH and the amount of H added to the D was less than 0.01 atom %. Prior to distillation the glassware was rinsed with D_2O. About the first 3% of product from the distillation was discarded and about 10% of the D_2O remained in the distilling flask after the distillation was completed. An analysis by N.M.R. showed that the product was .5 atom % H or 1.0 atom % HDO.

(c) Nitrous Oxide

Nitrous oxide supplied by Matheson Company was 98.5% pure as received. It was bubbled through the concentrated potassium hydroxide solutions to remove nitrogen dioxide.

(d) Liquid Additives

Methanol (Spectro Grade), n-hexane (Certified), and 2-propanol (Spectro Grade), were obtained from Fisher Scientific Co. They were used as supplied.

(e) Compounds Used for Analysis

Compound	Supplier
Acetone (Analytical Grade)	Mallinckrodt Canada Ltd.
Chromotropic Acid (Practical Grade) (4,5-dihydroxy-2,7-naphthalenedisulfonic acid)	Eastman Organic Chemicals
Formaldehyde (40% solution)	Fisher Scientific Co.
Salicylaldehyde (Reagent Grade)	Fisher Scientific Co.

The above reagents were used as supplied.

(f) Materials Used in Gas Chromatography

Compound	Supplier
Molecular Sieves 5A (1/16" pellets)	Union Carbide Corp.
Helium (99.995%)	Union Carbide Corp.

(g) Miscellaneous

Compound	Supplier
Calcium Chloride	B.D.H. (Canada) Ltd.
Drierite	Hammond Drierite Co.
Ethanol (95%, used for slush baths)	Standard Chemical Co.
Potassium Hydroxide	Baker Chemical Co.

B. APPARATUS

(a) The Vacuum System

The main manifold is shown schematically in Figure II-1. A vacuum of $\leq 10^{-3}$ Pa ($\leq 10^{-5}$ torr) was achieved using a Welch duo-seal vacuum pump in series with a mercury diffusion pump and traps at liquid nitrogen temperature (traps T_1 and T_2) in Figure II-1. The pressure was measured with a Philips Gauge (Consolidated Vacuum Corporation, Model 010A). The gauge-head was connected to the vacuum manifold by a Kovar seal.

The Pyrex glassware used to construct the vacuum system was cleaned by wetting with ethanol and adding concentrated nitric acid. The heat, produced from the reaction of the acid with the small amount of alcohol, heated the acid and improved its cleaning power. After the treatment the glassware was rinsed thoroughly with tap water and then with triply distilled water. During construction of the apparatus the glass blowing was done through a breath filter of Drierite.

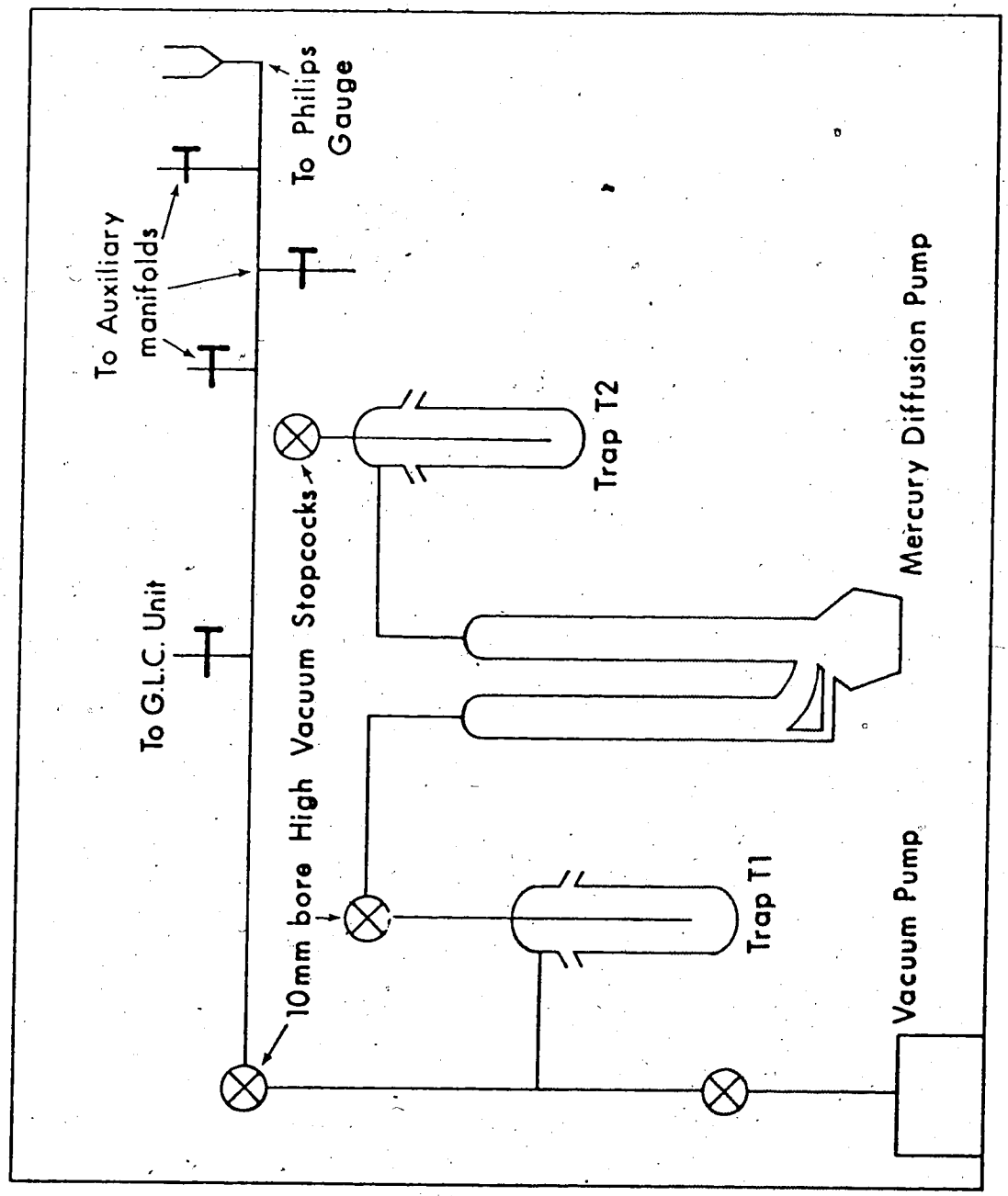

Figure II-1 Main Vacuum Manifold

(i) The Sample Preparation Manifold

The system shown in Figure II-2 was used for the preparation of water samples containing additives. The sample cells (Figure II-3 were constructed from 1.5 mm diameter Pyrex glass tubing. The preparation of samples involved the following procedure. The 10/30 inner ground joint was attached to the cell by glass blowing and the cell was then cleaned by the ethanol nitric acid method. The cells were then rinsed with tap water five times, once with 0.25 M $NaHCO_3$, and twenty times with triply distilled water, followed by drying in an oven (130°C) for almost four hours. They were then allowed to cool to room temperature and a small amount of silicone grease was applied to the 10/30 inner joint. The next step was to test for leaks by attaching the cells to the preparation manifold, Figure II-2, by means of a 10/30 outer ground glass joint. The cell was removed from the manifold and 5-6 ml of water, or D_2O, was added. At this point any additional liquid additives were introduced into the cells and the sample cells were again attached to the manifold. The samples were degassed by freeze-pump-thaw cycles until a pressure of about 5×10^{-6} torr showed on the vacuum gauge.

Nitrous oxide was the only gaseous additive and it was purified by using the system shown in Figure II-2. First the N_2O was bubbled through sintered glass discs in

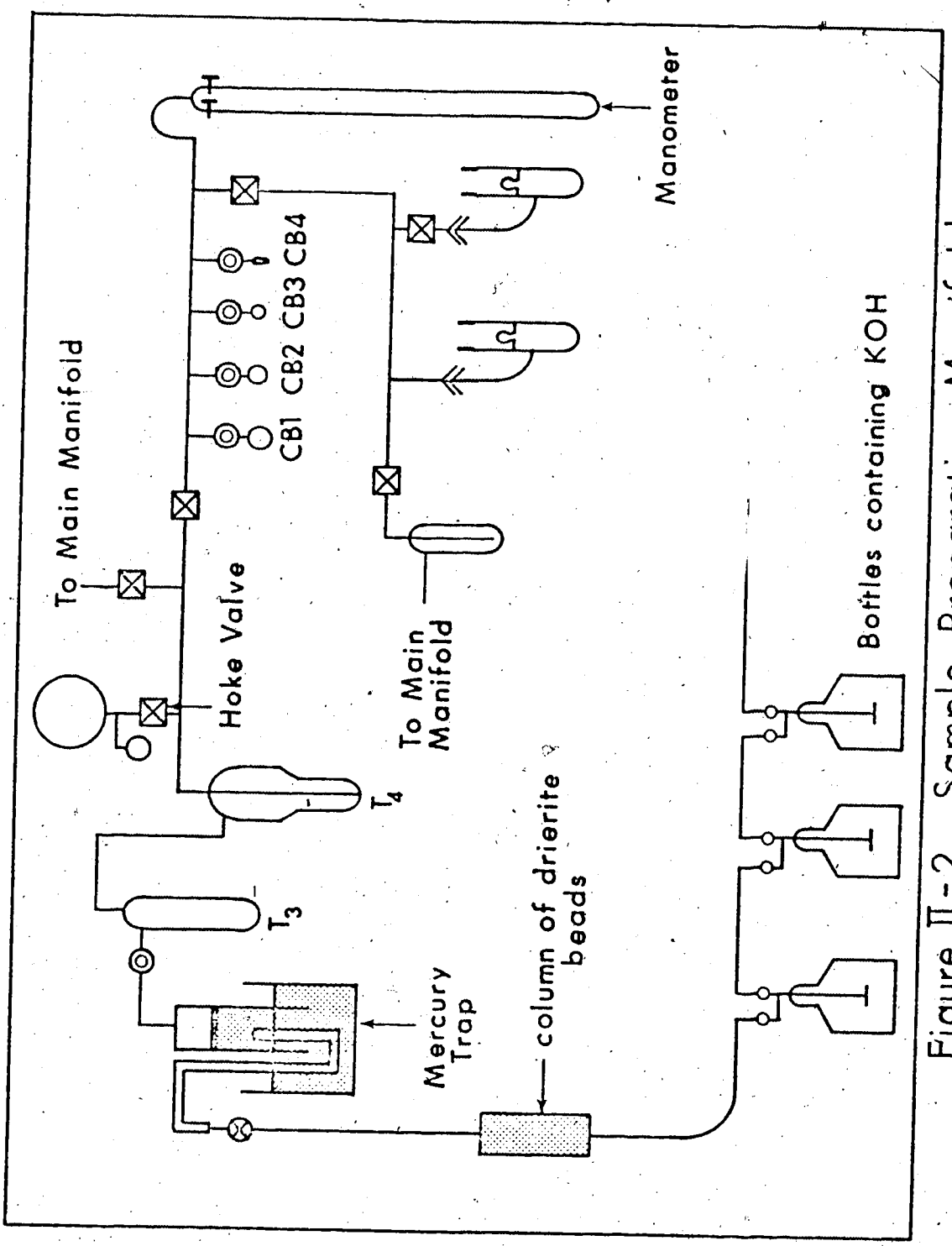

Figure II-2 Sample Preparation Manifold

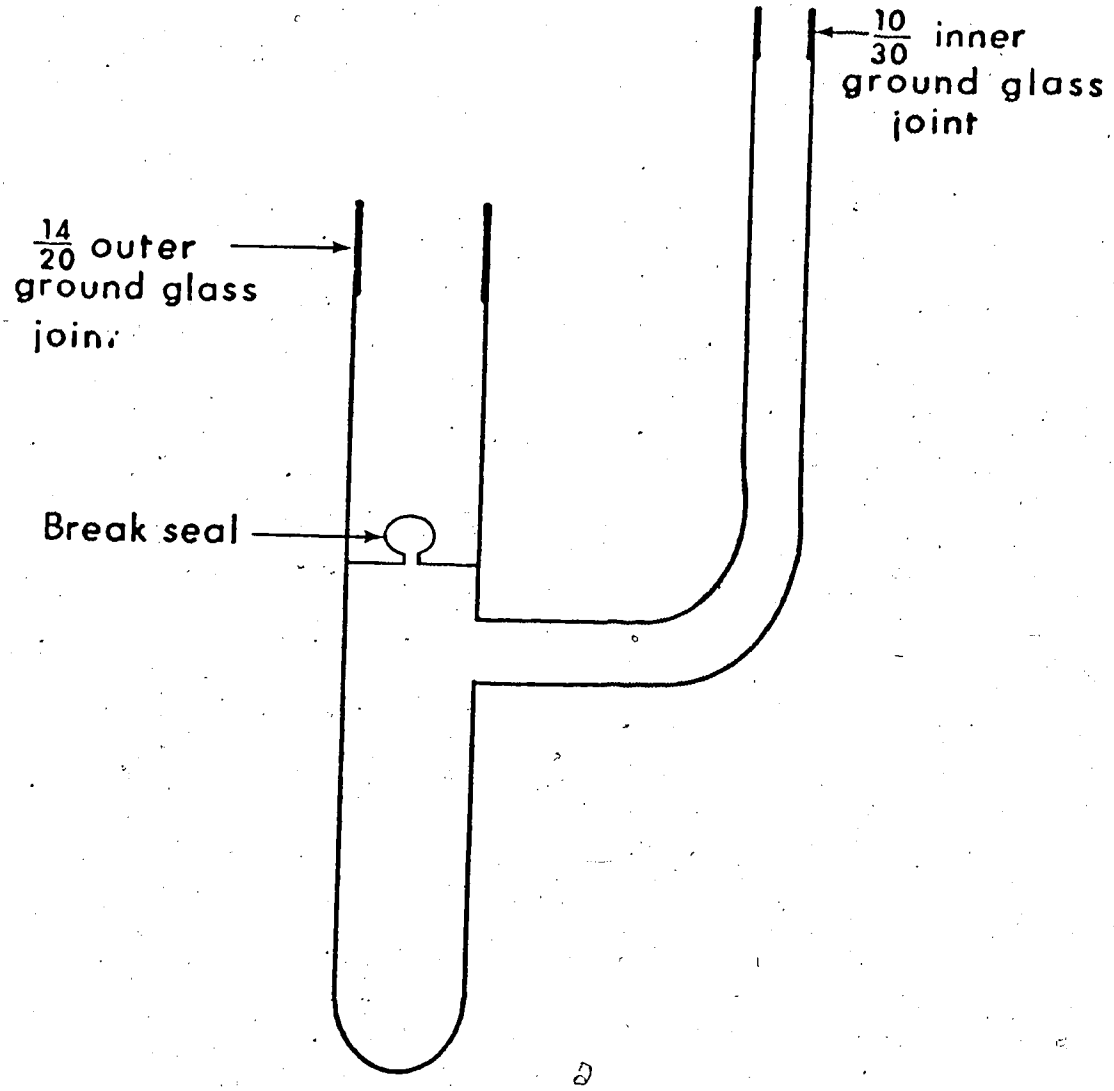

Figure II-3 sample cell

gas scrubber bottles containing concentrated potassium hydroxide solution. The gas was then passed through a 30 cm x 0.15 cm column of Drierite and was introduced into the sample preparation manifold through a mercury trap and sintered glass disc. The N_2O was condensed and degassed using traps T_3 and T_4 and stored in storage bulb SB1. When a quantity of N_2O was required for a sample it was measured using calibrated bulbs; CB1-CB4, to measure the volume and the manometer to measure the pressure. The N_2O was then added to the sample cell, containing a degassed sample as described above, by condensing it at 77K. While still at 77K the samples were sealed off with a flame.

(ii) The Sample Analysis Manifold

The sample analysis manifold is shown in Figure II-4. Bulbs SB2 and SB3 were used to store calibration gases. The Dewar vessel in the diagram was used to make a slow distillation of N_2O during analysis. The Dewar was evacuated by a glass tube connected to the main line. The Toepler pump was used to transfer product gases into the Macleod gauge for measurement and then into the chromatographic unit.

(b) The Gas Chromatographic Unit

The gas chromatographic unit consisted of a Molecular Sieves column, a thermal conductivity detector, a

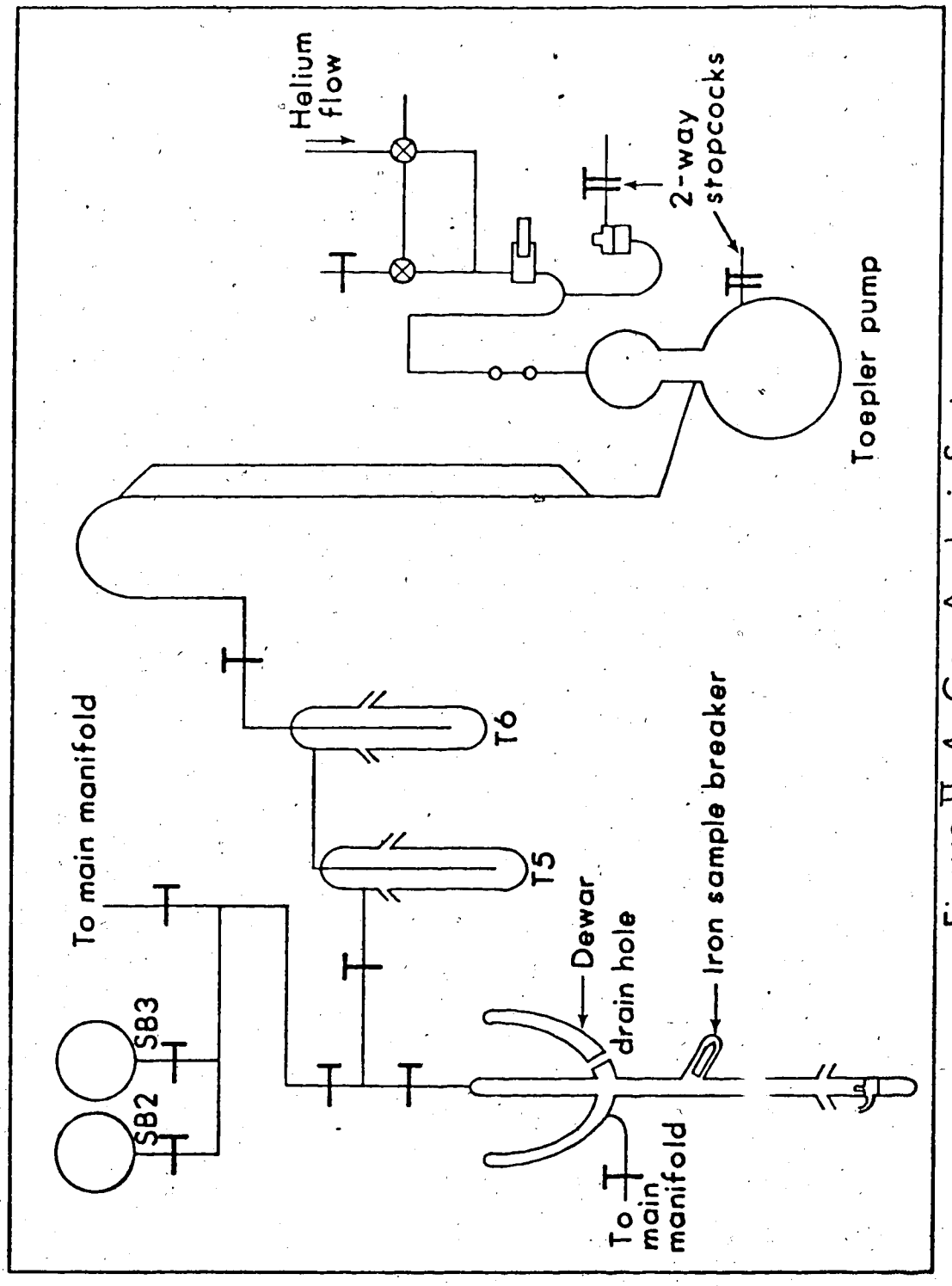

Figure II-4 Gas Analysis System

recorder, and a power supply. The power supply (Model 405CI) and the detector (Model TR2B) were supplied by Gow-Mac Instruments Co. The recorder (Model SR) was supplied by E. H. Sargent and Co. The column had a length of 2 m and was filled with 5A Molecular Sieves. The column was operated at room temperature and the detector at 43°C with a current of 250 mA. The helium carrier gas flow rate through the system was measured with a bubble flow-meter.

C. IRRADIATION

(a) The γ-Ray Source

A ^{60}Co Gammacell 220 (Atomic Energy of Canada) was used for most of the irradiations. When it was necessary to vary the dose rate a second ^{60}Co source in an irradiation cave was used. The room temperature irradiations were done by placing the sample tubes in a metal sample holder. For temperatures between room temperature and 150°C the sample holder was immersed in a Dewar vessel filled with glycerol. For temperatures above 150°C the apparatus shown in Figure II-5 was used. The distilled water in the pressure cell exerts its vapor pressure on the sample cell, equalizing the internal and external pressures.

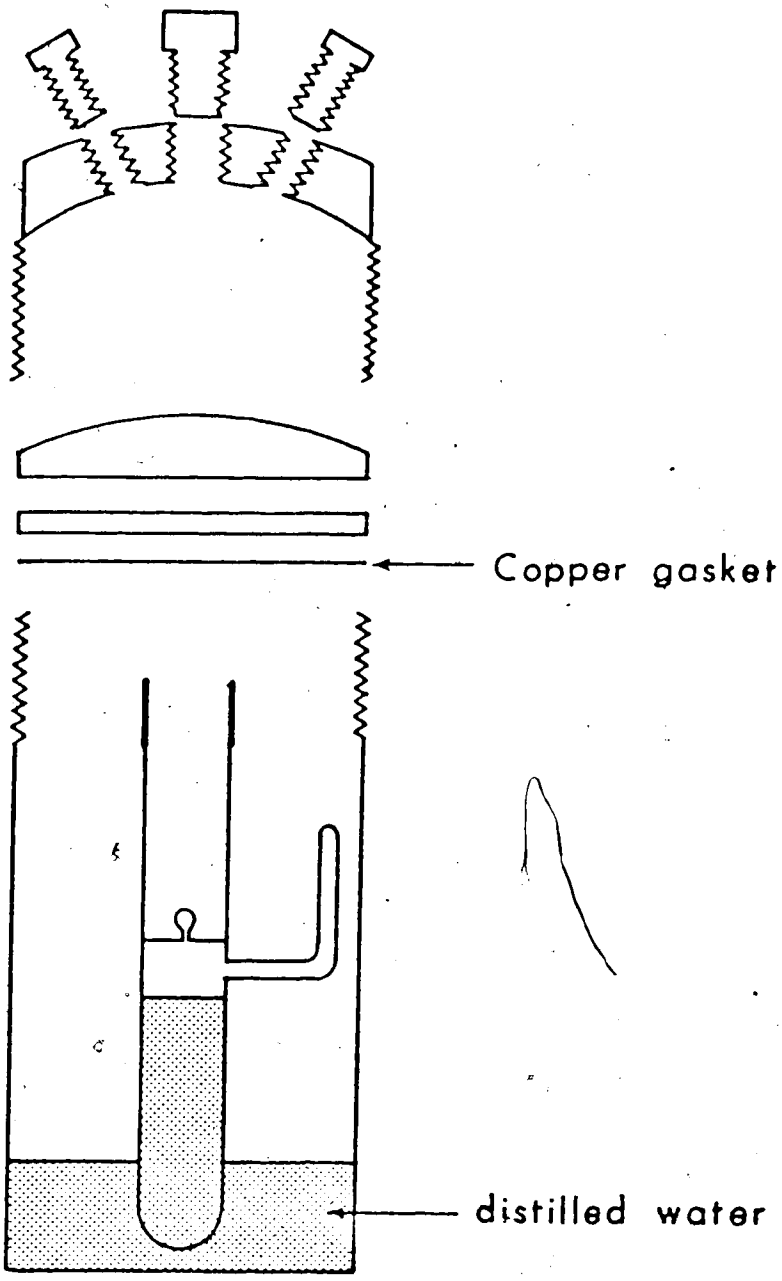

Figure II-5 Steel Pressure Cell

0.4 M H_2SO_4 and 10^{-3} M NaCl was used to determine all dose rates. A Beckmann DU Spectrophotometer set at a wavelength of 304 nm was used to measure the ferric ion concentration. The molar extinction coefficient used (2201, 25°C) was an average of values obtained in several laboratories. It had a standard deviation of 0.4% and a temperature coefficient of 16/°C. These values and $G(Fe^{+++}) = 15.6$ (23) were used to calculate the dose rate. The dose rates were determined at 23°C for samples placed inside of all sample holding devices used in the experiments and were corrected for the ^{60}Co radioactive decay.

D. SAMPLE ANALYSIS

(a) Gas Analysis

The system shown schematically in Figure II-4 was used to analyze the product gases. After irradiation the sample tube was attached to the analysis system by a 14/20 ground glass joint. After pumping down to a pressure of 10^{-6} torr the iron breaker was used to rupture the break seal. The products condensable at 77K were collected in the glass tube on the inside of the Dewar vessel which contained liquid nitrogen. The cork was then removed from the drain hole so that N_2O

slowly distilled into trap T_5 which was at 77°K. During this distillation the Toepler pump was put through twenty cycles or until no more gas could be collected. In a similar manner a distillation from trap T_5 to T_6 was carried out but the additional gas collected from this second distillation was never more than 5% of the total. Traps T_5 and T_6 were removed and cleaned after every two samples. The gases non-condensable at 77°K were collected and measured in the Macleod gauge. They were then passed through the Teflon valve, at the top of the gauge, and finally injected into the carrier gas stream. The helium flow rate was maintained at 60 ml/min by using a flow-meter. The gaseous products were separated by the column and their amounts displayed on the recorder-chart. The triangulation method was used to measure the peak areas.

Calibrations were done for nitrogen, oxygen, and carbon monoxide. Dry air was used to calibrate for nitrogen and oxygen. The volume, pressure, and temperature of an air sample were determined using the Macleod gauge. The sample was then injected into the chromatograph and the peak areas were measured. By doing many samples in this way a calibration curve relating moles of nitrogen and oxygen to peak area was obtained. The same procedure was used to calibrate for CO using 99.99% pure CO.

(b) Spectrophotometric Analysis

Formaldehyde was determined using chromotropic acid (24). One ml of the irradiated sample was pipetted into a test tube containing 0.5 ml of chromotropic acid reagent (2.5 g in 25 ml triply distilled water). Five ml of concentrated sulfuric acid was carefully added with stirring. The test tube was then stoppered and placed in a boiling water bath for 0.50 hr. The solution was cooled, poured into a 50 ml volumetric flask, and 40 ml of triply distilled water was added. After cooling to room temperature the solution was diluted to 50.0 ml. Aliquots were pipetted into 15 ml optical cells, and the formaldehyde complex concentration was measured spectrophotometrically at 570 nm with a Beckmann DU spectrophotometer. Non-irradiated samples were carried through the above stages and used as blanks. It was found advisable to use fresh chromotropic acid solutions for each batch of samples analyzed. The exact concentration of the formaldehyde solution used for calibration was determined through its methone derivative (25).

Acetone was determined using salicylaldehyde (26). One ml of the irradiated sample was pipetted into a 50 ml volumetric flask and 2 ml of 10.6 M sodium hydroxide was added. Triply distilled water was introduced to a volume of about 25 ml and 0.6 ml of neat salicylaldehyde was then added using a 1 ml syringe. The flask was shaken

and 20 ml of 10.6 M sodium hydroxide was introduced and the volume was made up to 50.0 ml with distilled water. The flask was allowed to stand for 2.0 hours and the absorbance was read against a reagent blank at 474 nm. Calibration was done using standard acetone solutions.

III RESULTS

A. Definition of Terms

G. Value

The G value of a product is defined as the number of molecules of product formed per 100 eV of energy absorbed by the system. A G value for ionic yield is the number of ion pairs per 100 eV of energy absorbed.

Ostwald Solubility Coefficient

The Ostwald solubility coefficient is the number of ml of a gas dissolved in 1 ml of a liquid when liquid and gas are at the same temperature and pressure.

Blank Sample

In this work a blank sample is a sample that is carried through all the preparation and analysis procedure but is not irradiated.

B. Product Yields from the Radiolysis of Water-N_2O Mixtures

Water samples containing N_2O were irradiated at a dose rate of 3×10^{17} eV/g min at 23°C, 81 $\pm$ 1°C, and 142 $\pm$ 2°C.

In the following Tables the molar N_2O concentration, the yield of N_2 in μmoles/ml, and the dose of radiation absorbed per ml of water solution are given. Each Table is accompanied by a Figure where the yield of N_2 in

μmoles/ml is plotted against the dose in eV/ml. A best fit line is drawn through the data for each experimental condition and the values of $G(N_2)$ is calculated from the slope. The intercept for each curve corresponds to the nitrogen yield from a blank sample. Wherever a blank sample was not done for a given set of conditions, the plot was made using a blank sample yield from the closest possible experimental conditions. The N_2O concentration shown at the bottom of each Figure contains appropriate variation limits. These variations arise because it was not possible to make several samples of exactly the same concentration of N_2O with the technique used.

Figure III-1 shows a plot of the Ostwald solubility coefficients for O_2, N_2, and N_2O as a function of temperature (27,28). For the 23°C, 81 ± 1°C and 142 ± 2°C samples the N_2O concentration was calculated by taking the Ostwald coefficient from the curve in Figure III-1B. The extrapolated curves from 180°C to 300°C for N_2O in Figure III-1B were drawn by comparing with the N_2 and O_2 curves in Figure III-1A. An estimated upper limit for the Ostwald coefficient for N_2O at 300°C is 1.4 and a lower limit is 0.3. A change in the Ostwald coefficient from 0.3 to 1.4 would produce a 2-fold change in the N_2O concentration and a change from 0.3 to ∞ would produce a 2.6-fold change in the N_2O concentration. A value of the Ostwald coefficient of 0.7 was used to calculate the N_2O

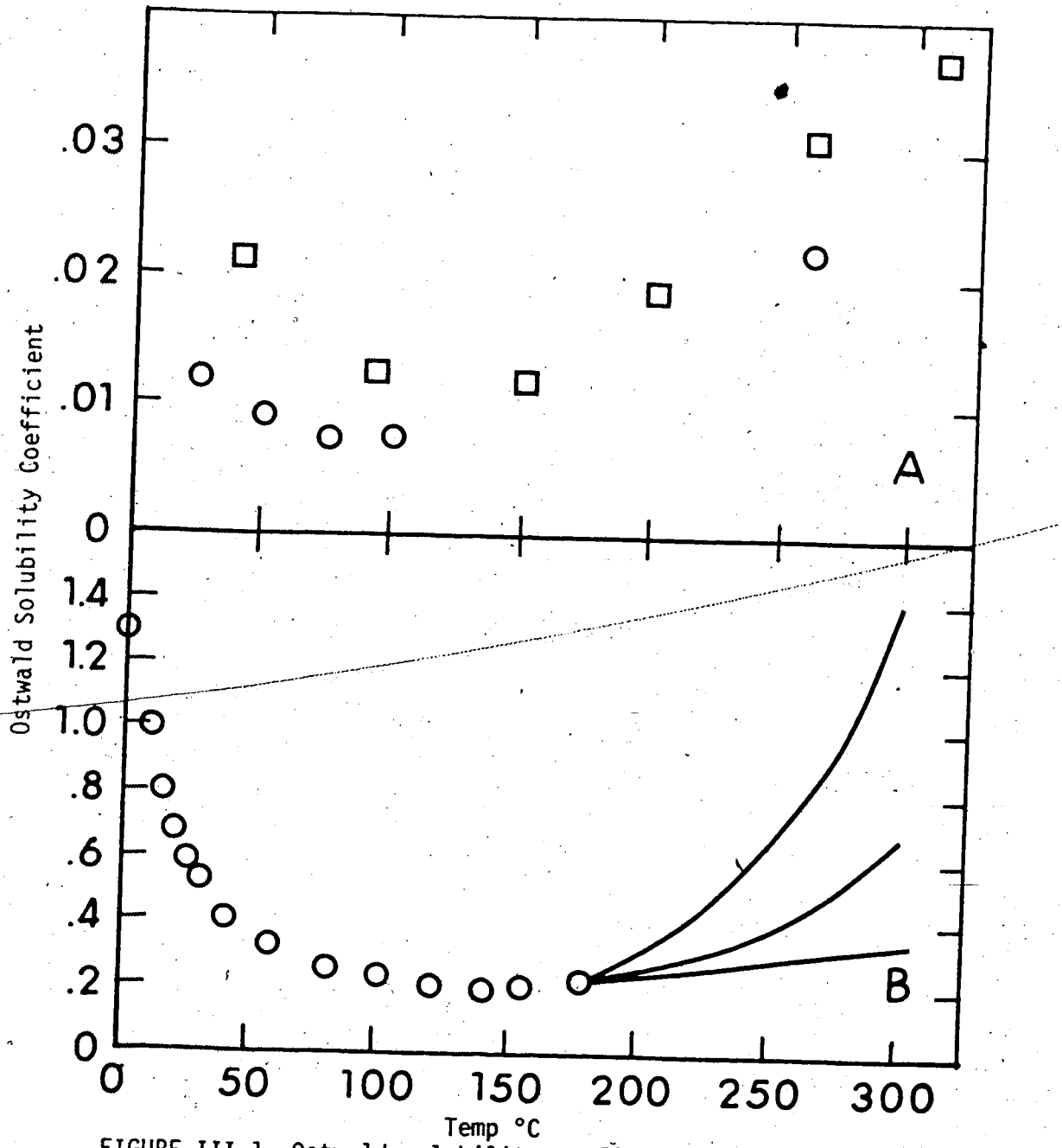

FIGURE III-1 Ostwald solubility coefficient of N_2, O_2 and N_2O in water as a function of temperature:

A ○, N_2; □, O_2

B ○, N_2O

concentration at 300°C.

Tables III-1 to III-3 and Figures III-2 to III-4 show the results from the irradiation of water-N_2O mixtures at 23°C. Over the dose range studied the yield of N_2 is linear with dose and the value of $G(N_2)$ is obtained from the slope. The N_2O concentration was changed from 0.23 mM to 133 mM and $G(N_2)$ values obtained are between 2.7 and 4.3.

TABLE III-1

Yields of N_2 from Water Samples Containing N_2O at 23°C

$[N_2O]$ mM	Yield N_2 µmoles/ml	Dose 10^{18} eV/ml
.25	0.023	0.0
.24	0.044	0.575
.23	0.062	0.862
.87	0.019	0.0
.97	0.017	0.0
.92	0.055	0.592
.87	0.063	0.888
.87	0.093	1.78
.87	0.110	1.98
1.0	0.124	2.37

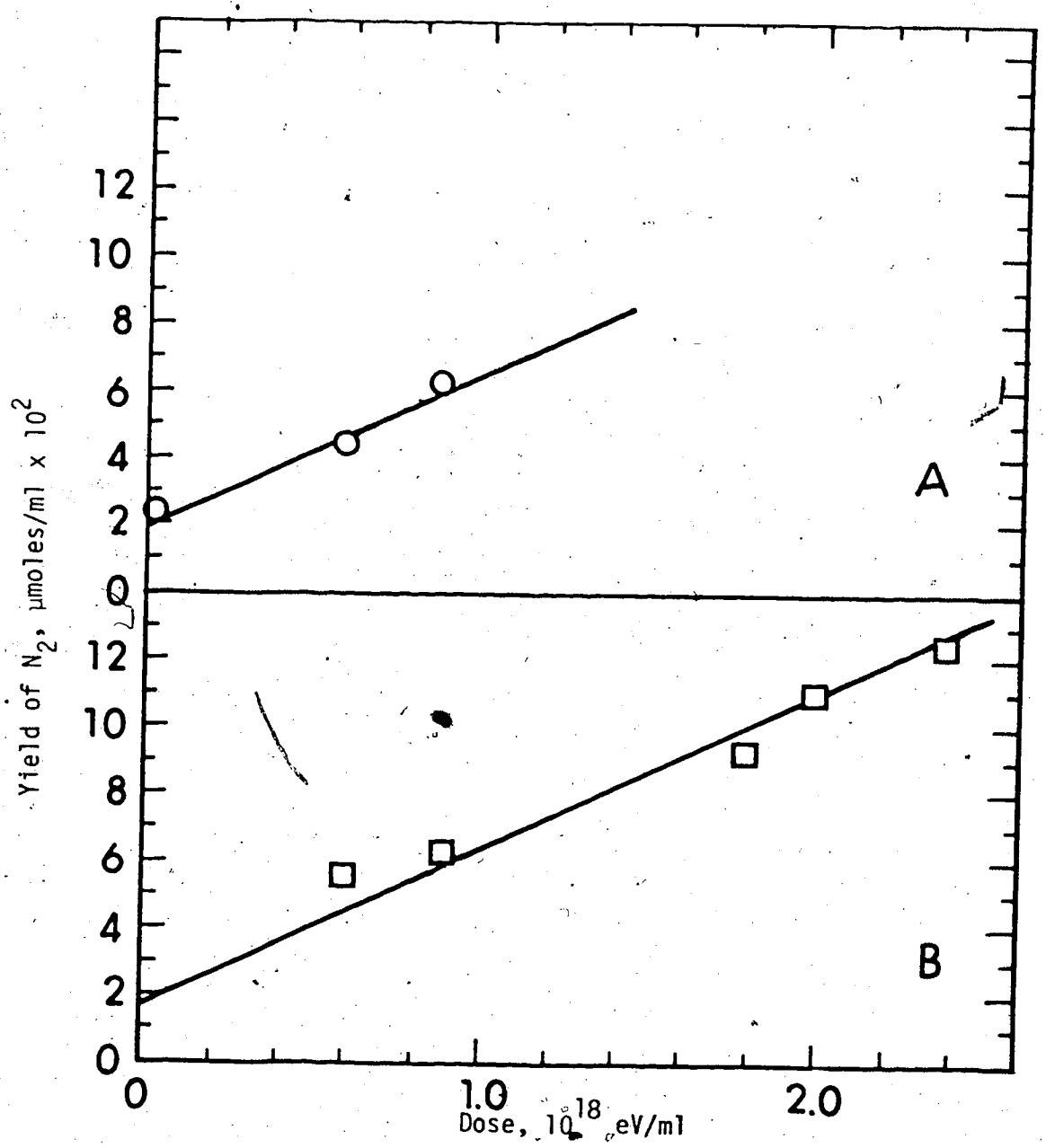

FIGURE III-2 Nitrogen yields as a function of dose at 23°C (H_2O)

A ○, 0.24 ± 0.1 mM N_2O, $G(N_2)$ = 2.7 ± 0.1

B □, 0.90 ± 0.1 mM N_2O, $G(N_2)$ = 2.8 ± 0.05

TABLE III-2

Yields of N_2 from Water Samples Containing N_2O at 23°C

$[N_2O]$ mM	Yield N_2 µmoles/ml	Dose 10^{18} eV/ml
2.7	0.012	0.0
3.2	0.058	0.917
3.3	0.099	1.835
6.2	0.059	0.862
6.2	0.076	1.150
15.4	0.013	0.0
15.9	0.071	0.87
15.4	0.110	1.74
33.3	0.012	0.0
34.9	0.060	0.87
34.4	0.10	1.16
32.8	0.12	1.74

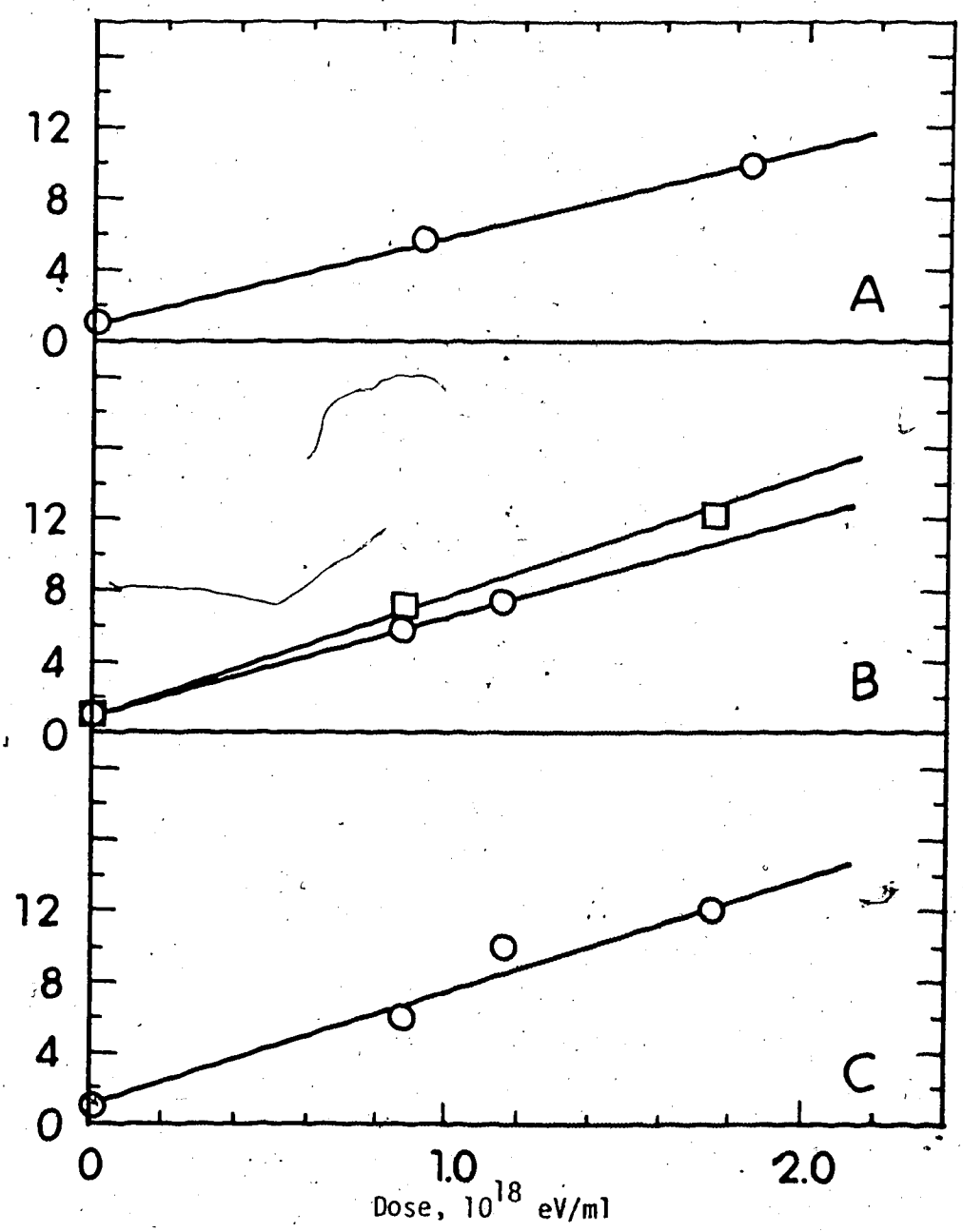

FIGURE III-3 Nitrogen yields as a function of dose at 23°C (H_2O)

A ○, 2.0 ± 0.3 mM N_2O, $G(N_2)$ = 2.9 ± 0.1
B ○, 6.2 ± 0.2 mM N_2O, $G(N_2)$ = 3.3 ± 0.1
□, 15.4 ± 1 mM N_2O, $G(N_2)$ = 4.0 ± 0.05
C ○, 34 ± 2 mM N_2O, $G(N_2)$ = 3.8 ± 0.3

TABLE III-3

Yields of N_2 from Water Samples Containing N_2O at 23°C

$[N_2O]$ mM	Yield N_2 µmoles/ml	Dose 10^{18} eV/ml
77.0	0.22	2.90
133.3	0.012	0.0
128.2	0.071	0.870
128.2	0.13	1.74
133.3	0.22	2.90
133.3	0.29	4.35

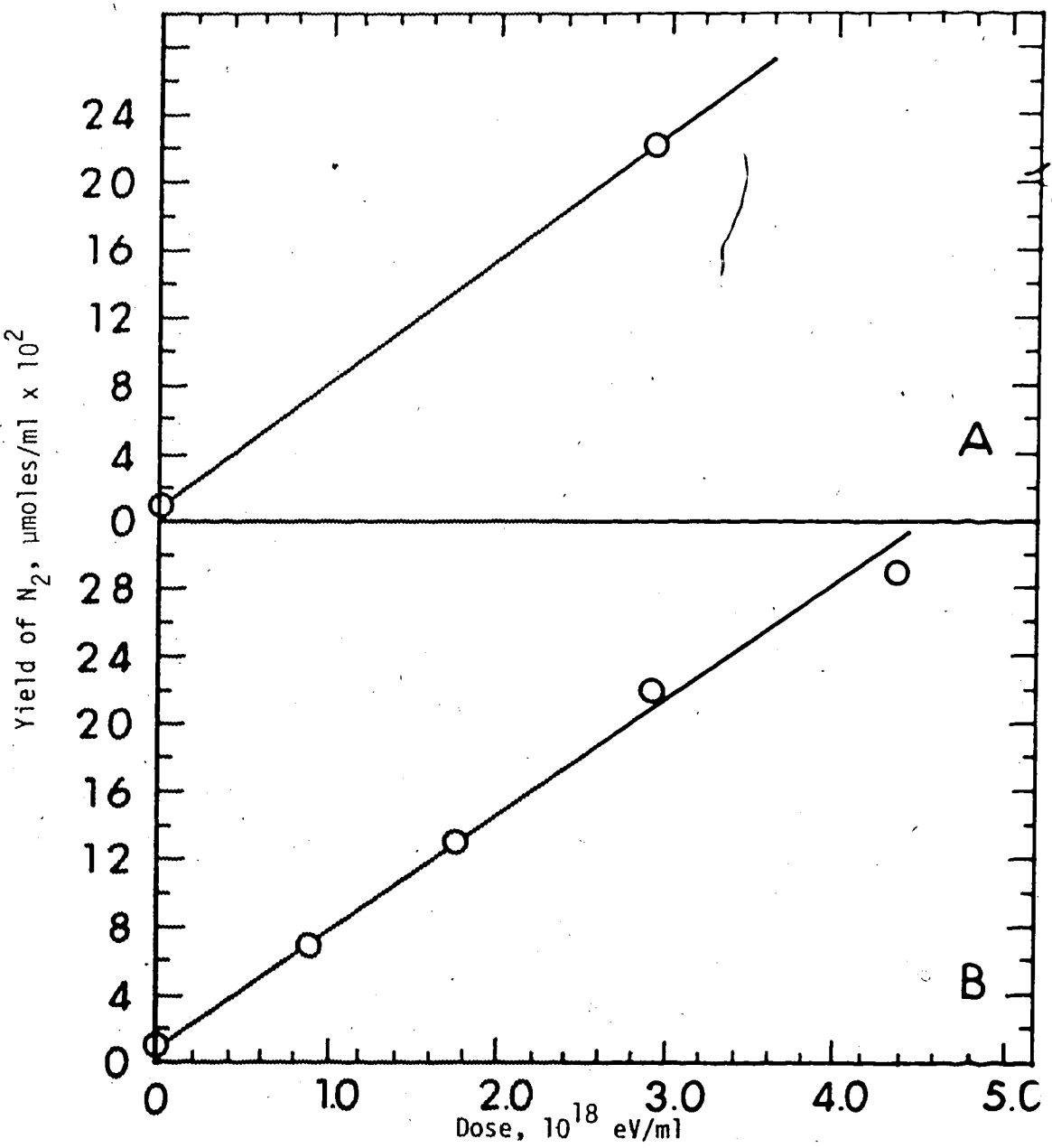

FIGURE III-4 Nitrogen yields as a function of dose at 23°C (H_2O).

A ○ , 77 ± 3 mM N_2O, $G(N_2)$ = 4.3 ± 0.2

B ○, 130 ± 5 mM N_2O, $G(N_2)$ = 4.1 ± 0.1

Tables III-4 and III-5 and Figures III-5 and III-6 show the results from irradiation of water samples at 81 ± 1°C. The N_2O concentration was varied from 0.25 mM to 73 mM and the values of $G(N_2)$ obtained are between 3.3 and 5.6. As indicated in Table III-5, 0.1 ml of methanol was added to one 40 mM (N_2O) sample and 10^{-3} ml of n-hexane to another. No perceptible effect of these additives was observed.

TABLE III-4

Yields of N_2 from Water Samples Containing N_2O at 81 ± 1°C

$[N_2O]$ mM	Yield N_2 μmoles/ml	Dose 10^{18} eV/ml
0.25	0.046	0.560
0.93	0.016	0.0
0.93	0.039	0.373
0.93	0.051	0.560
1.9	0.030	0.373
2.1	0.045	0.560
8.0	0.011	0.0
8.7	0.038	0.373
8.7	0.056	0.746

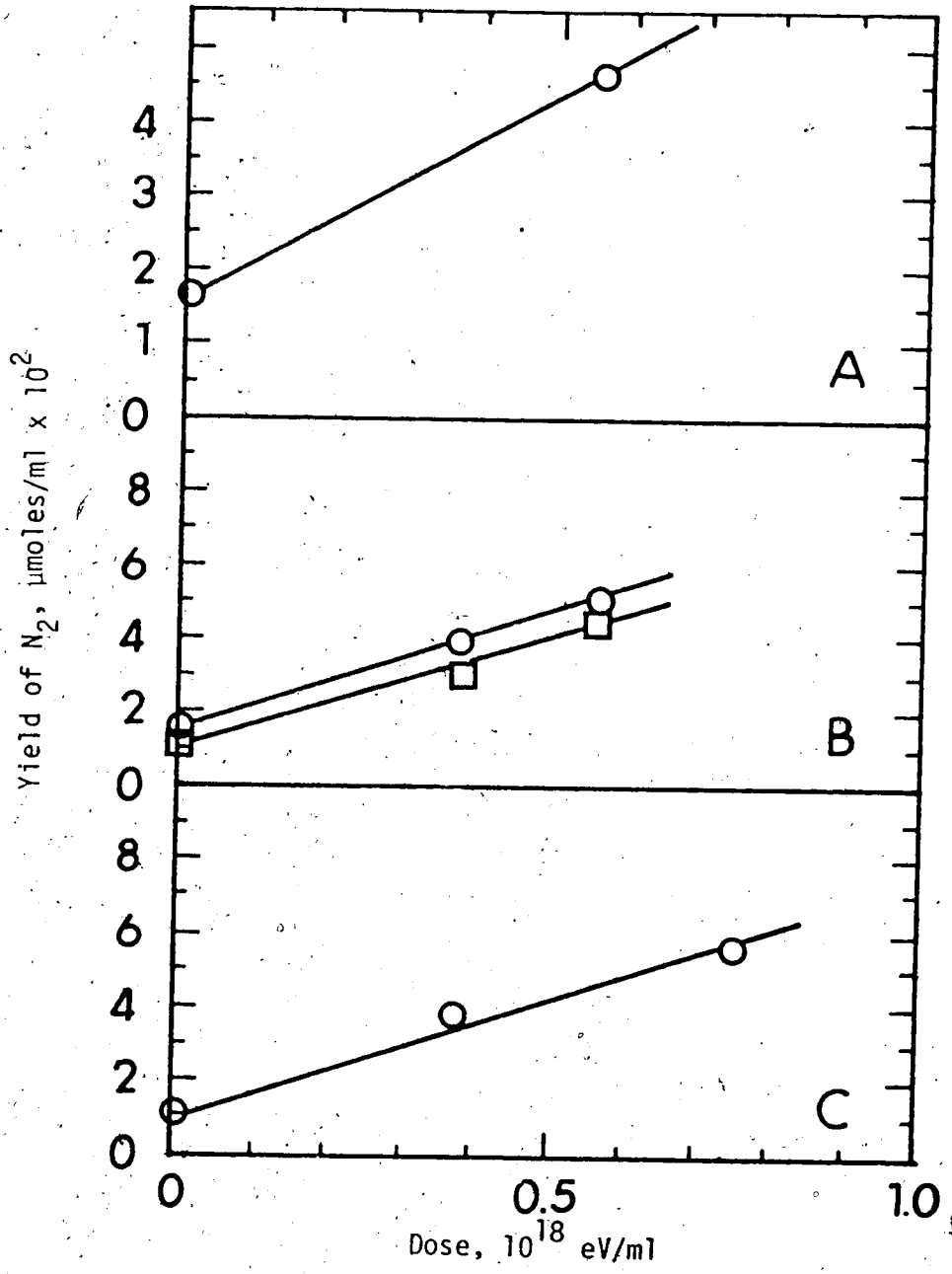

FIGURE III-5 Nitrogen yields as a function of dose at 81 ± 1°C (H_2O).

A ○, 0.25 ± 0.01 mM N_2O, $G(N_2)$ = 3.3 ± 0.1

B ○, 0.93 ± 0.04 mM N_2O, $G(N_2)$ = 3.8 ± 0.1

□, 2.0 ± 0.1 mM N_2O, $G(N_2)$ = 3.3 ± 0.2

C ○, 8.3 ± 0.5 mM N_2O, $G(N_2)$ = 3.8 ± 0.1

TABLE III-5

Yields of N_2 from Water Samples Containing N_2O at 81 ± 1°C

$[N_2O]$ mM	Yield N_2 μmoles/ml	Dose 10^{18} eV/ml
19.3	0.012	0.0
18.7	0.057	0.560
18.7	0.088	1.12
40	0.061	0.560
39.3	0.11	1.12
40.0*	0.10	1.05
40.0+	0.096	1.02
50.7	0.015	0.0
73.3	0.099	0.912

* This sample contained 0.1 ml of methanol in a sample vol. of 4.3 ml.

+ This sample contained 0.001 ml n-hexane in a sample vol. of 4.1 ml.

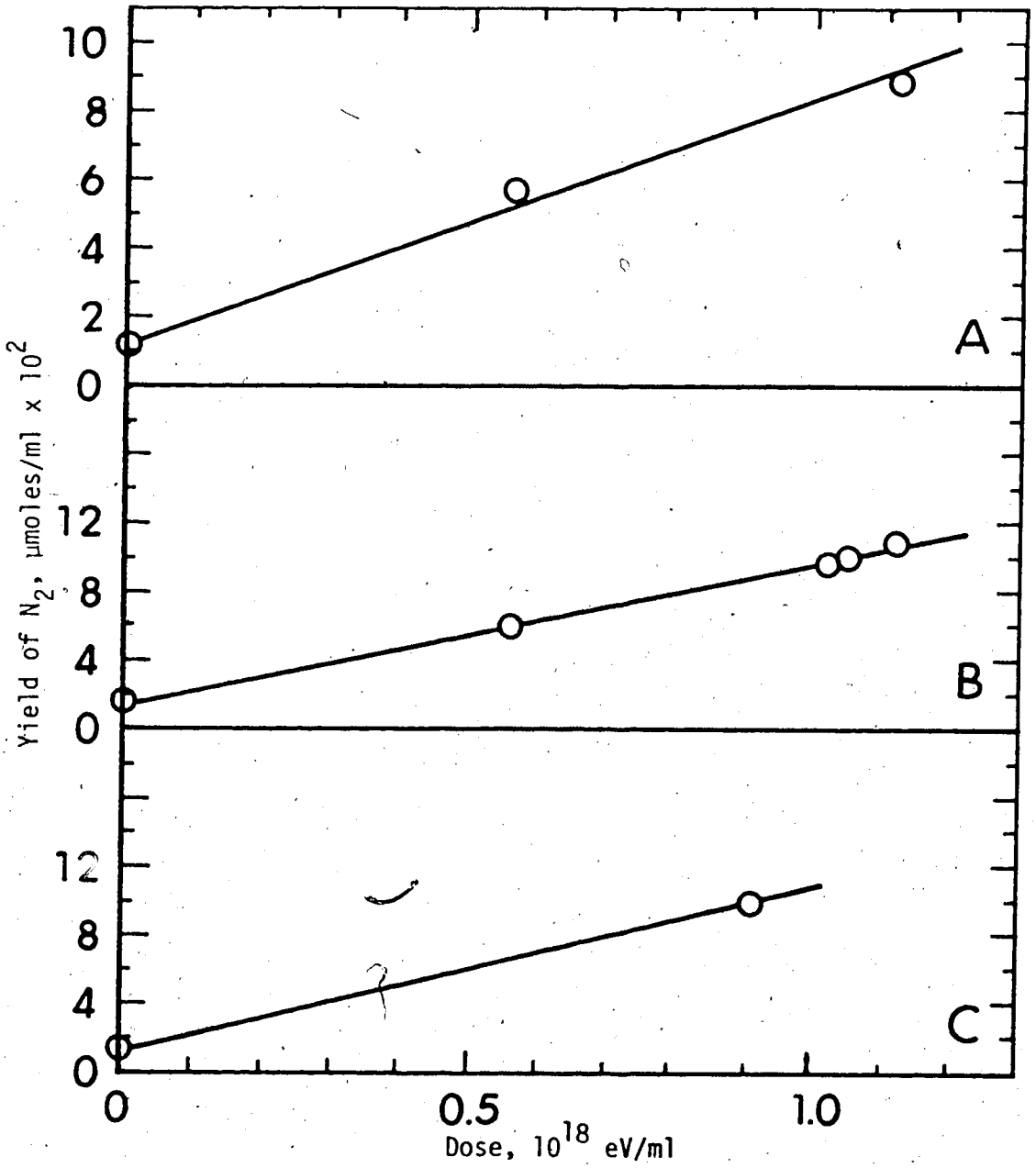

FIGURE III-6 Nitrogen yields as a function of dose at 81 ± 1°C (H_2O).

A ○, 19 ± 1 mM N_2O, $G(N_2)$ = 4.6 ± 0.2

B ○, 40 ± 2 mM N_2O, $G(N_2)$ = 4.9 ± 0.05

C ○, 73 ± 3 mM N_2O, $G(N_2)$ = 5.6 ± 0.2

Tables III-6 and III-7 and Figures III-7 and III-8 show results from irradiation of water samples at 142 ± 2°C. The N_2O concentration range studied was from 0.21 mM to 33 mM and $G(N_2)$ varied from 4.6 to 6. As shown in Table III-7, the addition of 10^{-3} ml of methanol to a 33.3 mM (N_2O) sample produced a three-fold increase in the yield of N_2. Adding 10^{-3} ml of n-hexane to another sample had no effect on the N_2 yield.

TABLE III-6

Yield of N_2 from Water Samples Containing N_2O at 142 ± 2°C

$[N_2O]$ mM	Yield N_2 µmoles/ml	Dose 10^{18} eV/ml
0.21	0.016	0.0
0.21	0.045	0.344
0.22	0.042	0.340
0.21	0.051	0.511
0.78	0.011	0.0
0.78	0.019	0.0
0.78	0.047	0.344
0.78	0.042	0.340
0.78	0.063	0.511
0.78	0.059	0.517
1.61	0.016	0.0
1.61	0.055	0.340
1.56	0.044	0.344
2.00	0.059	0.517
2.10	0.058	0.511

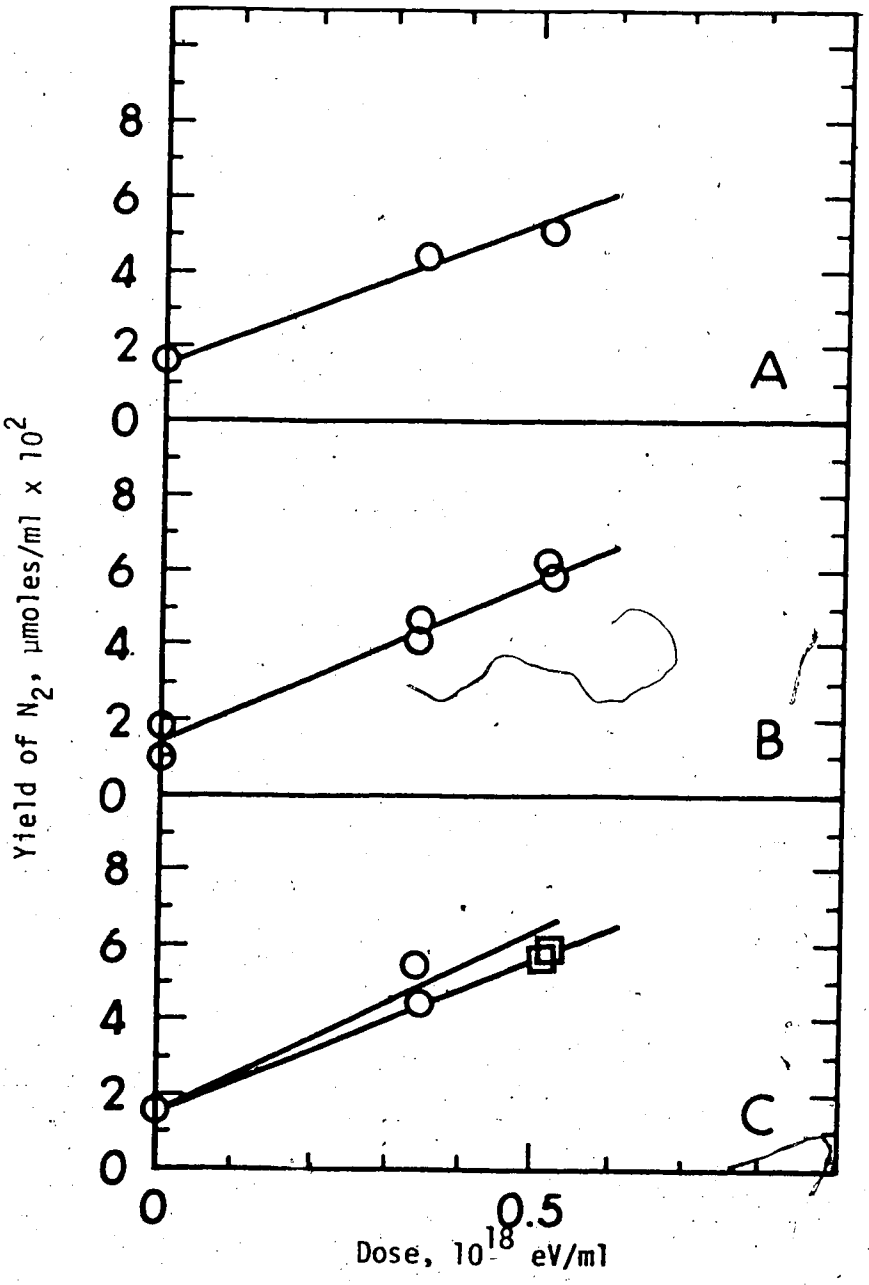

FIGURE III-7 Nitrogen yields as a function of dose at 142 ± 2°C (H_2O)

A ○, 0.22 ± 0.01 mM N_2O, $G(N_2)$ = 4.5 ± 0.3

B ○, 0.78 ± 0.03 mM N_2O, $G(N_2)$ = 5.2 ± 0.3

C ○, 1.61 ± 0.1 mM N_2O, $G(N_2)$ = 5.8 ± 0.2

□, 2.1 ± 0.1 mM N_2O, $G(N_2)$ = 5.8 ± 0.2

TABLE III-7

Yields of N_2 from Water Samples Containing N_2O at 142 ± 2°C

$[N_2O]$ mM	Yield N_2 µmoles/ml	Dose 10^{18} eV/ml
6.7	0.0095	0.0
7.2	0.037	0.344
6.7	0.081	0.689
16.1	0.0083	0.0
15.6	0.012	0.0
15.6	0.048	0.344
16.1	0.063	0.344
15.6	0.061	0.689
32.2	0.053	0.344
33.3*	0.21	0.479
33.3+	0.064	0.638
32.2	0.080	0.689

* This sample contained 10^{-3} ml of methanol in a sample vol. of 4.3 ml.

+ This sample contained 10^{-3} ml of n-hexane in a sample vol. of 5.5 ml.

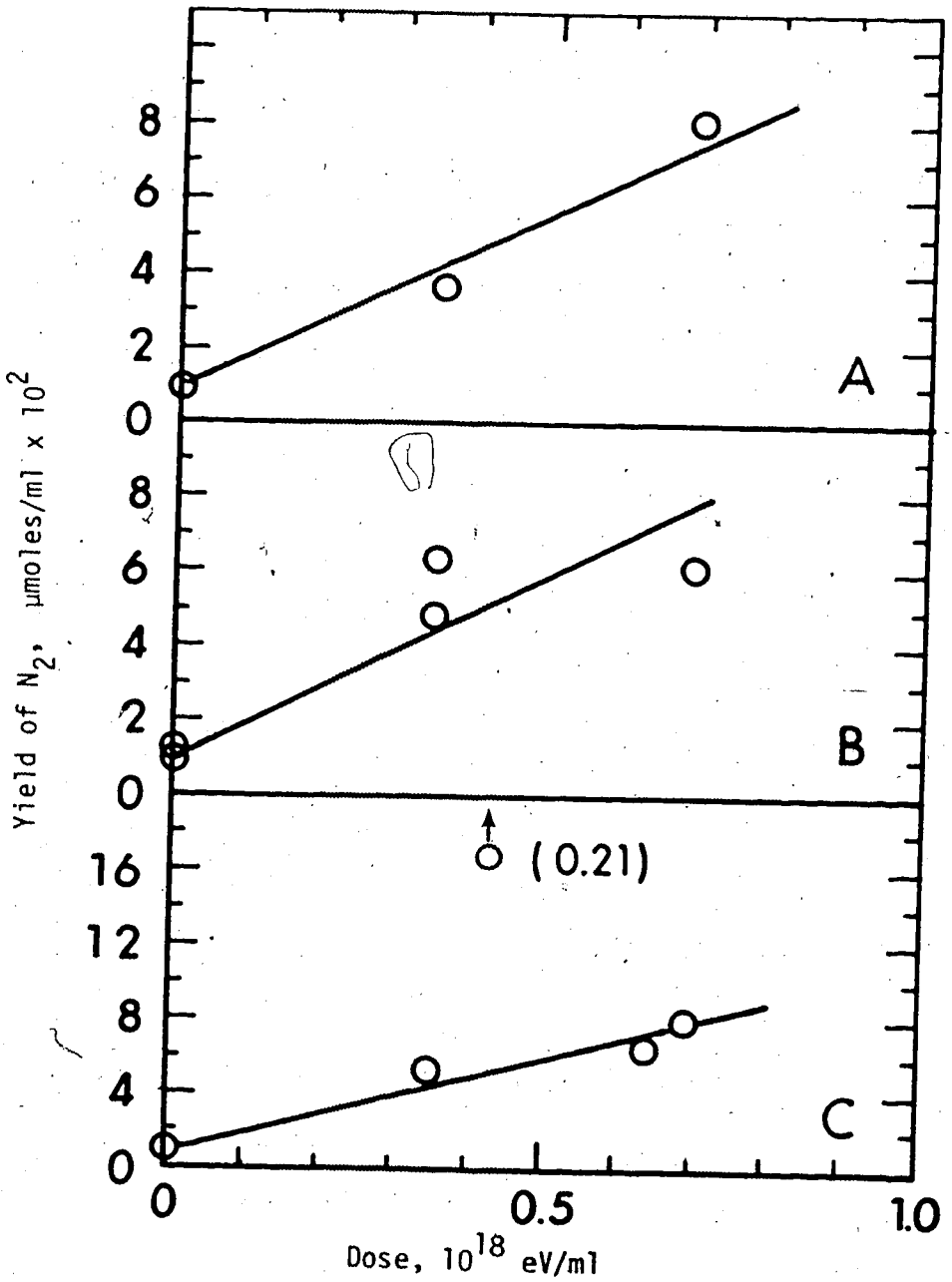

FIGURE III-8 Nitrogen yields as a function of dose at 142 ± 2°C (H_2O)

A ○, 6.7 ± .5 mM N_2O, $G(N_2) = 5.6 \pm 0.3$
B ○, 15.6 ± 1 mM N_2O, $G(N_2) = 6 \pm 0.5$
C ○, 33 ± 2 mM N_2O, $G(N_2) = 5.9 \pm 0.4$

C. Product Yields from the Radiolysis of D_2O-N_2O Mixtures

Deuterium oxide samples containing N_2O were irradiated at a dose rate of 3×10^{17} eV/g/min at 23°C, 81 ± 1°C, and 142 ± 2°C.

The Tables and Figures showing the results from the radiolysis of D_2O-N_2O mixtures are similar to those for the radiolysis of water-N_2O mixtures. The Ostwald solubility coefficients for N_2O in D_2O are not known and for this study are assumed to be the same as those for N_2O in water.

Tables III-8 and III-9 and Figures III-9 and III-10 show the results from the irradiation of D_2O-N_2O mixtures at 23°C. Over the dose range studied the yield of N_2 is linear with dose and the value of $G(N_2)$ is obtained from the slope. The N_2O concentration was changed from 0.23 mM to 133 mM and the $G(N_2)$ values obtained are between 2.8 and 4.7.

TABLE III-8

Yields of N_2 from D_2O Samples Containing N_2O at 23°C

$[N_2O]$ mM	Yield N_2 μmoles/ml	Dose 10^{18} eV/ml
0.25	0.018	0.0
0.28	0.043	0.574
0.27	0.065	0.860
1.08	0.020	0.0
0.82	0.048	0.574
0.97	0.064	0.860
1.03	0.078	1.150
4.10	0.061	0.860
4.36	0.112	1.720
14.9	0.013	0.0
16.4	0.126	1.718
31.8	0.112	1.150
28.7	0.049	0.573

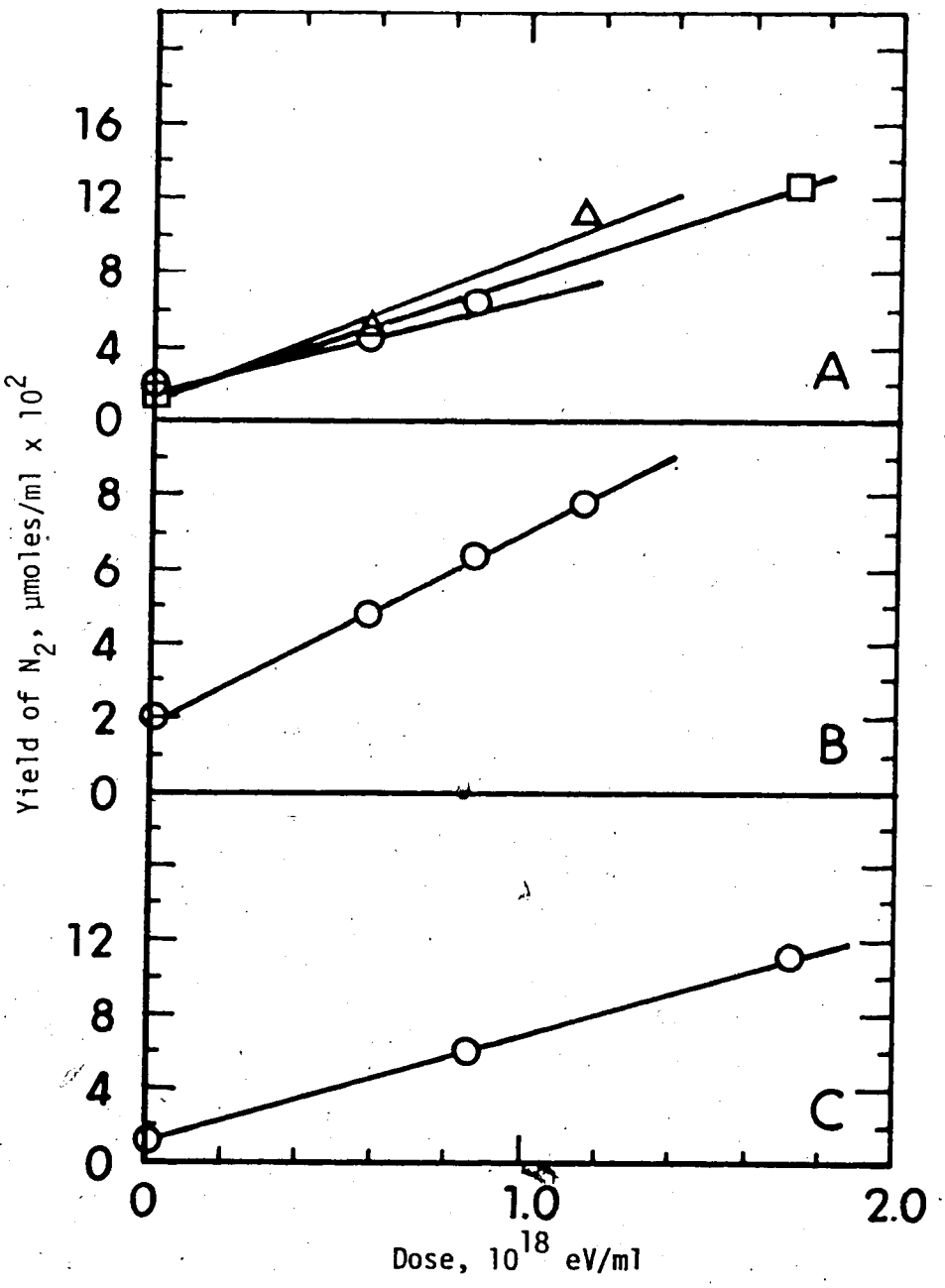

FIGURE III-9 Nitrogen yields as a function of dose at 23°C (D_2O)

A ○, 0.27 ± 0.02 mM N_2O, $G(N_2) = 2.8 \pm 0.1$
□, 16 ± 1 mM N_2O, $G(N_2) = 4.0 \pm 0.2$
△, 30 ± 2 mM N_2O, $G(N_2) = 4.4 \pm 0.2$

B ○, 0.97 ± 0.15 mM N_2O, $G(N_2) = 3.1 \pm 0.05$

C ○, 4.2 ± 0.2 mM N_2O, $G(N_2) = 3.4 \pm 0.05$

TABLE III-9

Yields of N_2 from D_2O Samples Containing N_2O at 23°C

$[N_2O]$ mM	Yield N_2 µmoles/ml	Dose 10^{18} eV/ml
61.5	0.012	0.0
61.5	0.061	0.580
61.5	0.079	1.172
61.5	0.149	1.760
61.5	0.231	2.900
133.3	0.011	0.0
117.9	0.082	0.870
112.8	0.157	1.740
107.7	0.224	2.900

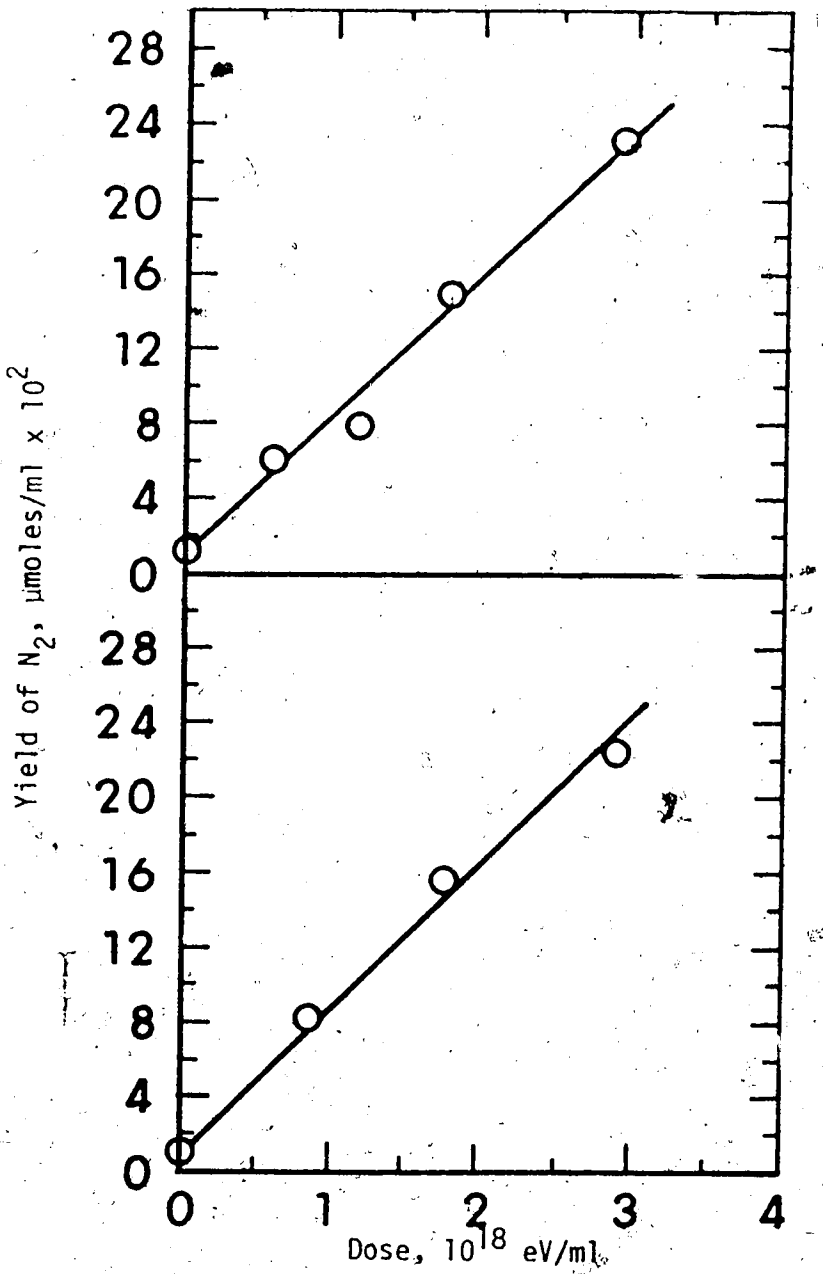

FIGURE III-10 Nitrogen yields as a function of dose at 23°C (D_2O)

A ○, 62 ± 2 mM N_2O, $G(N_2)$ = 4.5 ± 0.05

B ○, 118 ± 5 mM N_2O, $G(N_2)$ = 4.7 ± 0.1

Tables III-10 and III-11 along with Figures III-11 and III-12 show the results from irradiated D_2O samples at 81 $\pm$ 1°C. The N_2O concentration was varied from 0.25 mM to 73 mM and the values of $G(N_2)$ are between 3.4 and 6.8.

TABLE III-10

Yields of N_2 from D_2O Samples Containing N_2O at 81 ± 1°C

$[N_2O]$ mM	Yield N_2 μmoles/ml	Dose 10^{18} eV/ml
0.25	0.015	0.0
0.29	0.033	0.369
0.33	0.054	0.608
1.00	0.018	0.0
0.93	0.040	0.369
0.93	0.062	0.553
2.00	0.021	0.203
2.13	0.038	0.369
2.47	0.052	0.553
8.67	0.006	0.0
8.67	0.048	0.369
8.67	0.051	0.553
8.00	0.083	0.737

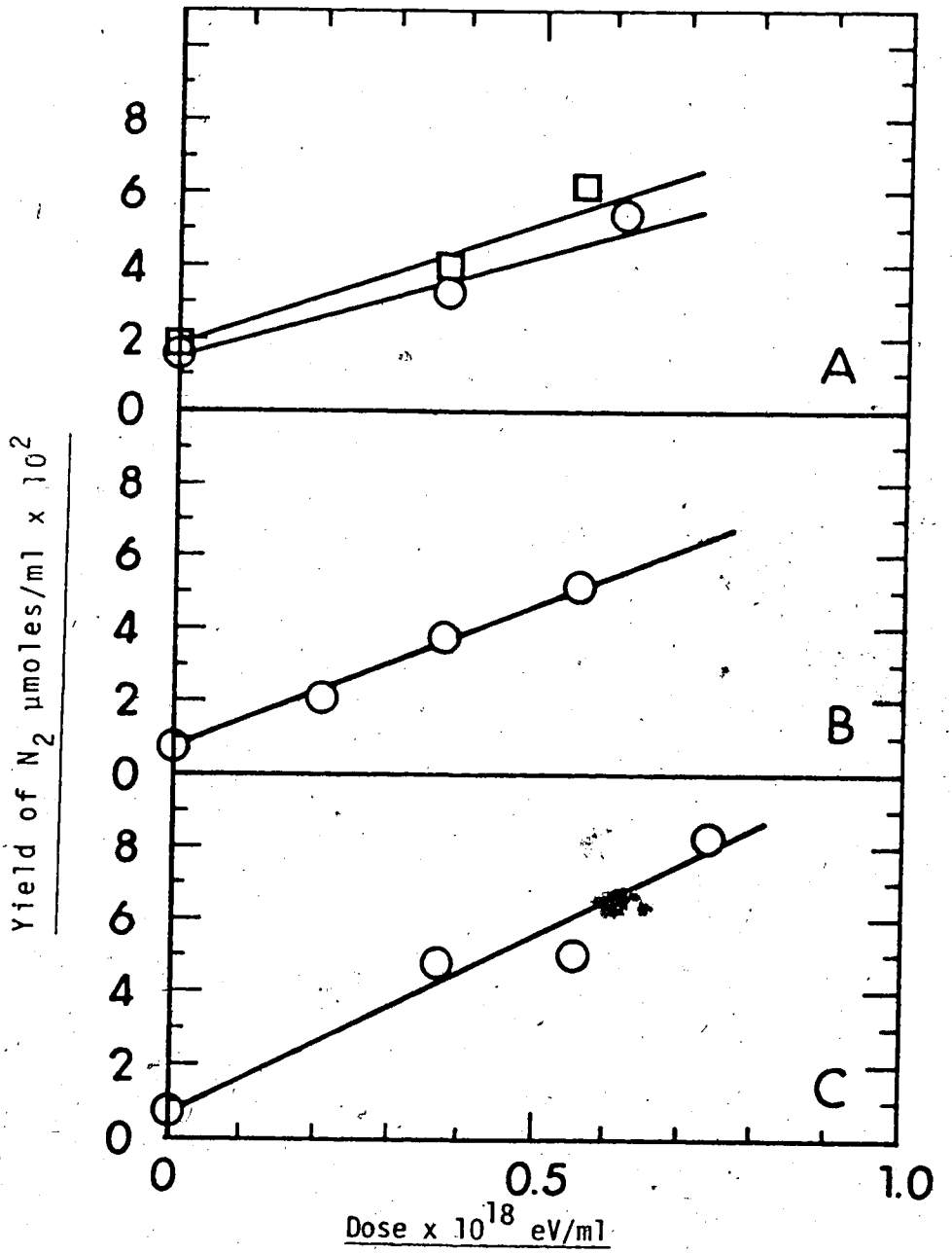

FIGURE III-11 Nitrogen yields as a function of dose at 81 ± 1°C (D_2O)

A ○ 0.29 ± 0.03 mM N_2O, $G(N_2)$ = 3.4 ± 0.3
□ 0.93 ± 0.05 mM N_2O, $G(N_2)$ = 4.1 ± 0.4
B ○ 2.2 ± 0.2 mM N_2O, $G(N_2)$ = 3.5 ± 0.1
C ○ 8.4 ± 0.5 mM N_2O, $G(N_2)$ = 5.8 ± 0.2

TABLE III-11

Yield of N_2 from D_2O Samples Containing N_2O at 81 ± 1°C

$[N_2O]$ mM	Yield N_2 μmoles/ml	Dose 10^{18} eV/ml
18.0	0.010	0.0
18.7	0.043	0.369
38.7	0.015	0.0
38.7	0.049	0.369
38.7	0.088	0.737
73.3	0.042	0.255
73.3	0.062	0.369
73.3	0.070	0.492
73.3	0.088	0.565
73.3	0.095	0.730

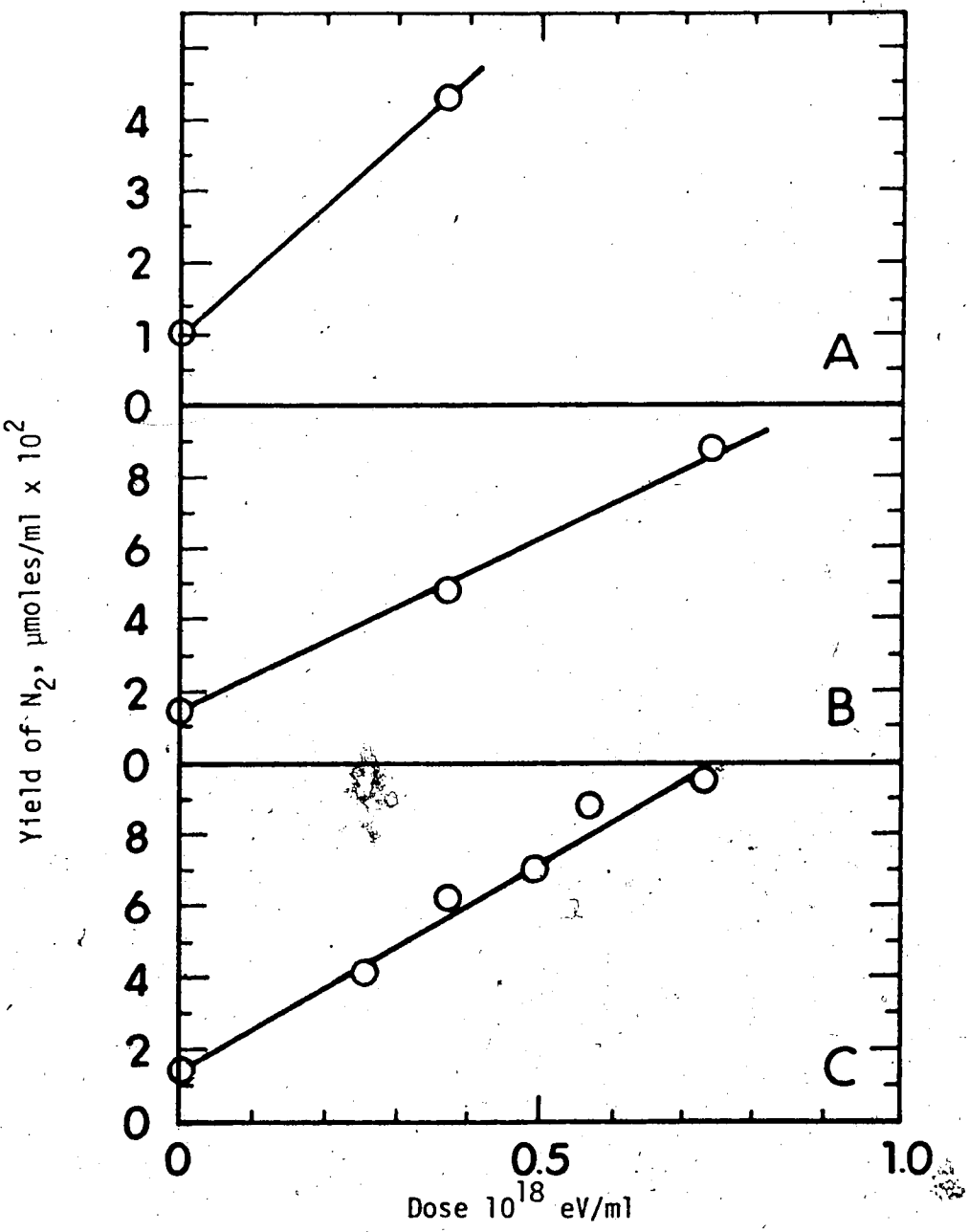

FIGURE III-12 NItrogen yields as a function of dose at 81 ± 1°C (D_2O)

A ○, 18 ± 1 mM N_2O, $G(N_2)$ = 5.4 ± 0.3
B ○, 39 ± 2 mM N_2O, $G(N_2)$ = 5.8 ± 0.2
C ○, 73 ± 3 mM N_2O, $G(N_2)$ = 6.8 ± 0.2

Tables III-12 and III-13 and Figures III-13 and III-14 show the results of irradiations at 142 ± 2°C. The N_2O concentration range studied was from 0.21 mM to 32 mM and $G(N_2)$ varied from 5 to 6.9.

TABLE III-12

$G(N_2)$ from D_2O Samples Containing N_2O at 142 ± 2°C

$[N_2O]$ mM	Yields N_2 µmoles/ml	Dose 10^{18} eV/ml
0.21	0.012	0.0
0.24	0.043	0.344
0.78	0.018	0.0
0.78	0.049	0.344
0.78	0.062	0.517
1.78	0.007	0.0
1.78	0.038	0.344
1.89	0.059	0.517

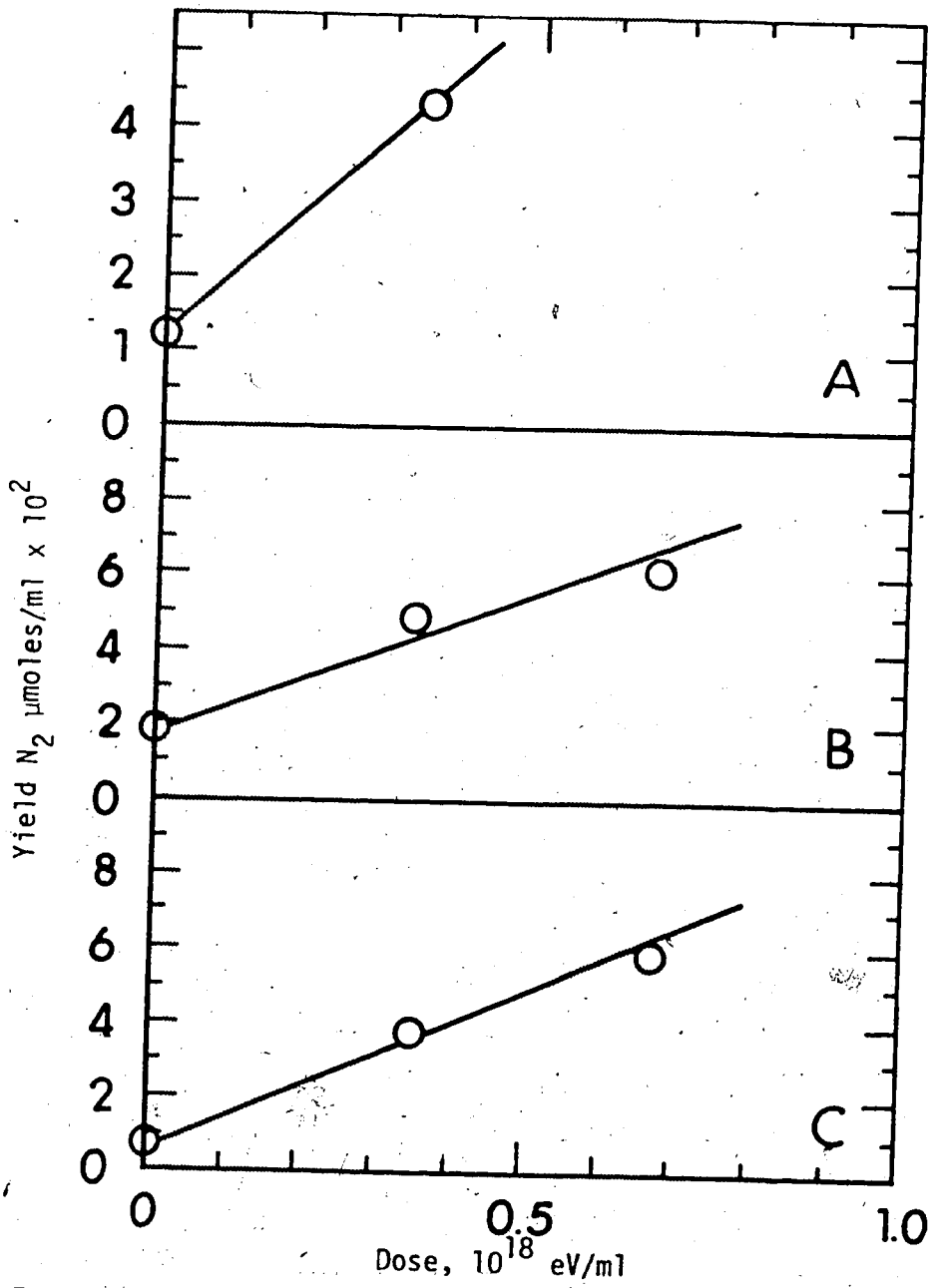

FIGURE III-13 Nitrogen yields as a function of dose at 142 ± 2°C (D_2O)

A ○ ; 0.22 ± 0.02 mM N_2O, $G(N_2)$ = 5.4 ± 0.5
B ○ , 0.78 ± 0.03 mM N_2O, $G(N_2)$ = 5 ± 0.5
C ○ , 1.84 ± 0.06 mM N_2O, $G(N_2)$ = 5.1 ± 0.3

TABLE III-13

Yield of N_2 from D_2O Samples Containing N_2O at 142 ± 2°C

$[N_2O]$ mM	Yield N_2 µmoles/ml	Dose 10^{18} eV/ml
3.6	0.079	0.689
7.2	0.048	0.344
15.6	0.009	0.0
15.6	0.042	0.344
15.6	0.088	0.689
27.2	0.015	0.0
29.4	0.050	0.344
31.7	0.096	0.689

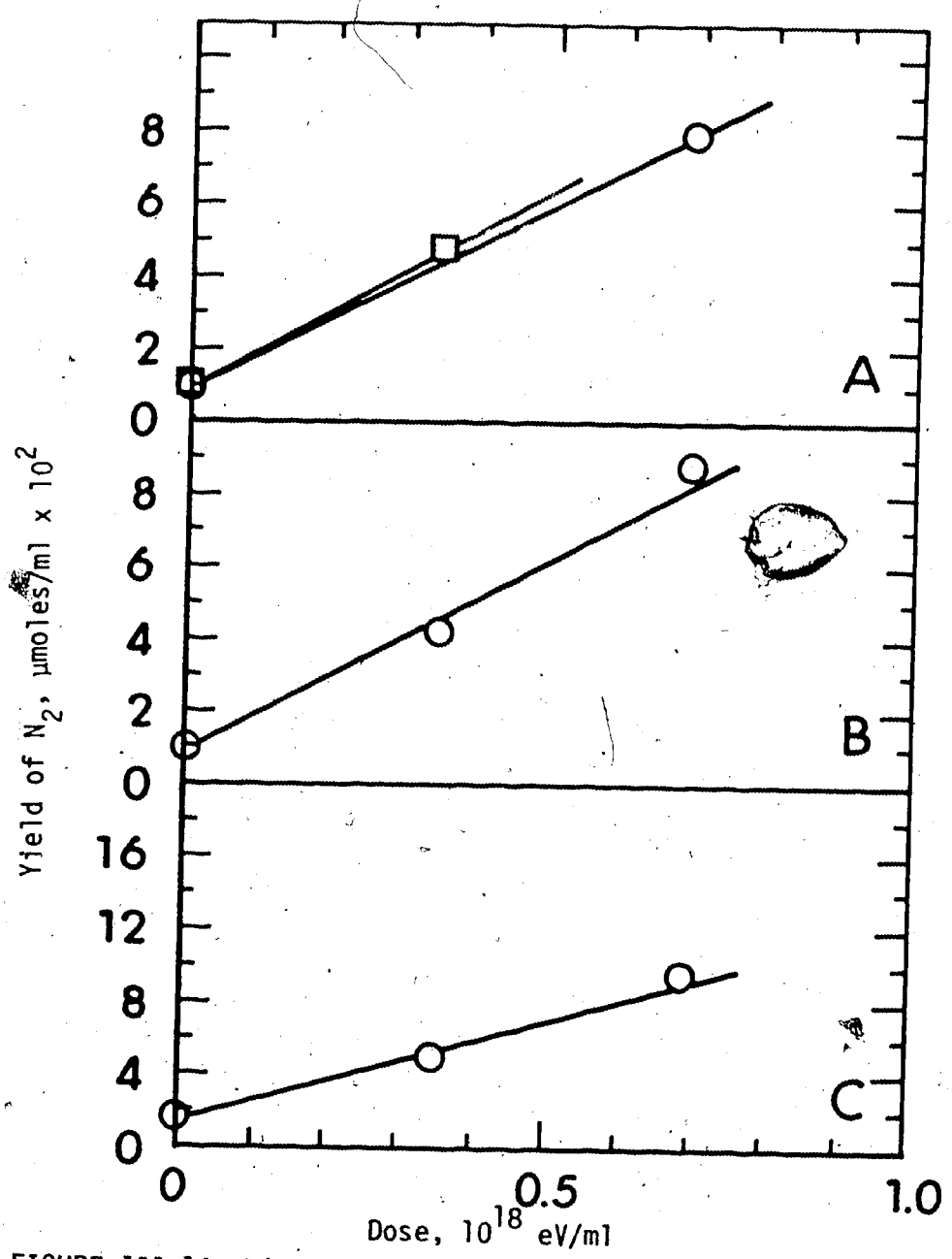

FIGURE III-14 Nitrogen yields as a function of dose at 142 ± 2°C (D_2O)

A ○, 3.6 ± 0.2 mM N_2O, $G(N_2)$ = 6.1 ± 0.3
□, 7.2 ± 0.3 mM N_2O, $G(N_2)$ = 6.9 ± 0.3
B ○, 15.6 ± 0.6 mM N_2O, $G(N_2)$ = 6.4 ± 0.4
C ○, 30 ± 3 mM N_2O, $G(N_2)$ = 6.6 ± 0.2

Table III-14 is a summary of the $G(N_2)$ values for the H_2O and D_2O solutions at various temperatures. Estimates of the random error in the $G(N_2)$ values and nitrous oxide concentrations are included in the table.

Figure III-15 contains a plot of $G(N_2)$ *versus* the log of the nitrous oxide concentrations for the three temperatures studied. The error bars on the $G(N_2)$ values are determined from the plots of nitrogen yield *versus* dose, Figures III-2 to III-14.

The lines through the data in Figure III-15 are drawn in such a way that they are analogous in shape to curves obtained in other studies (4,16). Below 10^{-2} M nitrous oxide the curves are more or less flat because a wide range of N_2O concentrations can efficiently scavenge the free ions. The increase in N_2 yield above 10^{-2} M nitrous oxide is due to the scavenging of ions in spurs.

TABLE III-14

$G(N_2)$ Values for Various Concentrations of N_2O in Water and D_2O

$[N_2O]$ mM, H_2O	$G(N_2)$ H_2O	Temp. H_2O, °C	$[N_2O]$ mM D_2O	$G(N_2)$ D_2O	Temp. D_2O, °C
0.24 ± 0.01	2.7 ± 0.1	23	0.27 ± 0.02	2.8 ± 0.1	23
0.92 ± 0.1	2.8 ± 0.05	23	0.97 ± 0.15	3.1 ± 0.05	23
3.0 ± 0.3	2.9 ± 0.1	23	4.21 ± 0.2	3.4 ± 0.05	23
6.2 ± 0.2	3.3 ± 0.1	23	16 ± 1	4.0 ± 0.2	23
15.4 ± 1	4.0 ± 0.05	23	30 ± 2	4.4 ± 0.2	23
33.3 ± 1.5	3.8 ± 0.3	23	62 ± 2	4.5 ± 0.05	23
77 ± 3	4.3 ± 0.2	23	118 ± 5	4.7 ± 0.1	23
130 ± 5	4.1 ± 0.1	23	0.29 ± 0.03	3.4 ± 0.3	81 ± 1
0.25 ± 0.01	3.3 ± 0.1	81 ± 1	0.93 ± 0.05	4.1 ± 0.4	81 ± 1
0.93 ± 0.04	3.8 ± 0.1	81 ± 1	2.2 ± 0.2	3.5 ± 0.1	81 ± 1
2.0 ± 0.1	3.3 ± 0.2	81 ± 1	8.4 ± 0.5	5.8 ± 0.2	81 ± 1
8.3 ± 0.5	3.8 ± 0.1	81 ± 1	18 ± 1	5.4 ± 0.3	81 ± 1
19 ± 1	4.6 ± 0.2	81 ± 1	39 ± 2	5.8 ± 0.2	81 ±
40 ± 2	4.9 ± 0.05	81 ± 1	73 ± 3	6.8 ± 0.2	81 ± 1
73 ± 3	5.6 ± 0.2	81 ± 1	0.22 ± 0.02	5.4 ± 0.5	142 ± 2
0.22 ± 0.01	4.5 ± 0.3	142 ± 2	0.78 ± 0.03	5 ± 0.5	142 ± 2
0.78 ± 0.03	5.2 ± 0.3	142 ± 2	1.83 ± 0.05	5.1 ± 0.3	142 ± 2
1.61 ± 0.1	5.0 ± 0.5	142 ± 2	3.6 ± 0.2	6.1 ± 0.3	142 ± 2
2.10 ± 0.1	5.8 ± 0.2	142 ± 2	7.2 ± 0.3	6.9 ± 0.3	142 ± 2
6.7 ± 0.5	5.6 ± 0.3	142 ± 2	15.6 ± 0.6	6.4 ± 0.4	142 ± 2
15.6 ± 1	6 ± 0.5	142 ± 2	30 ± 3	6.6 ± 0.2	142 ± 2
33 ± 2	5.9 ± 0.4	142 ± 2			

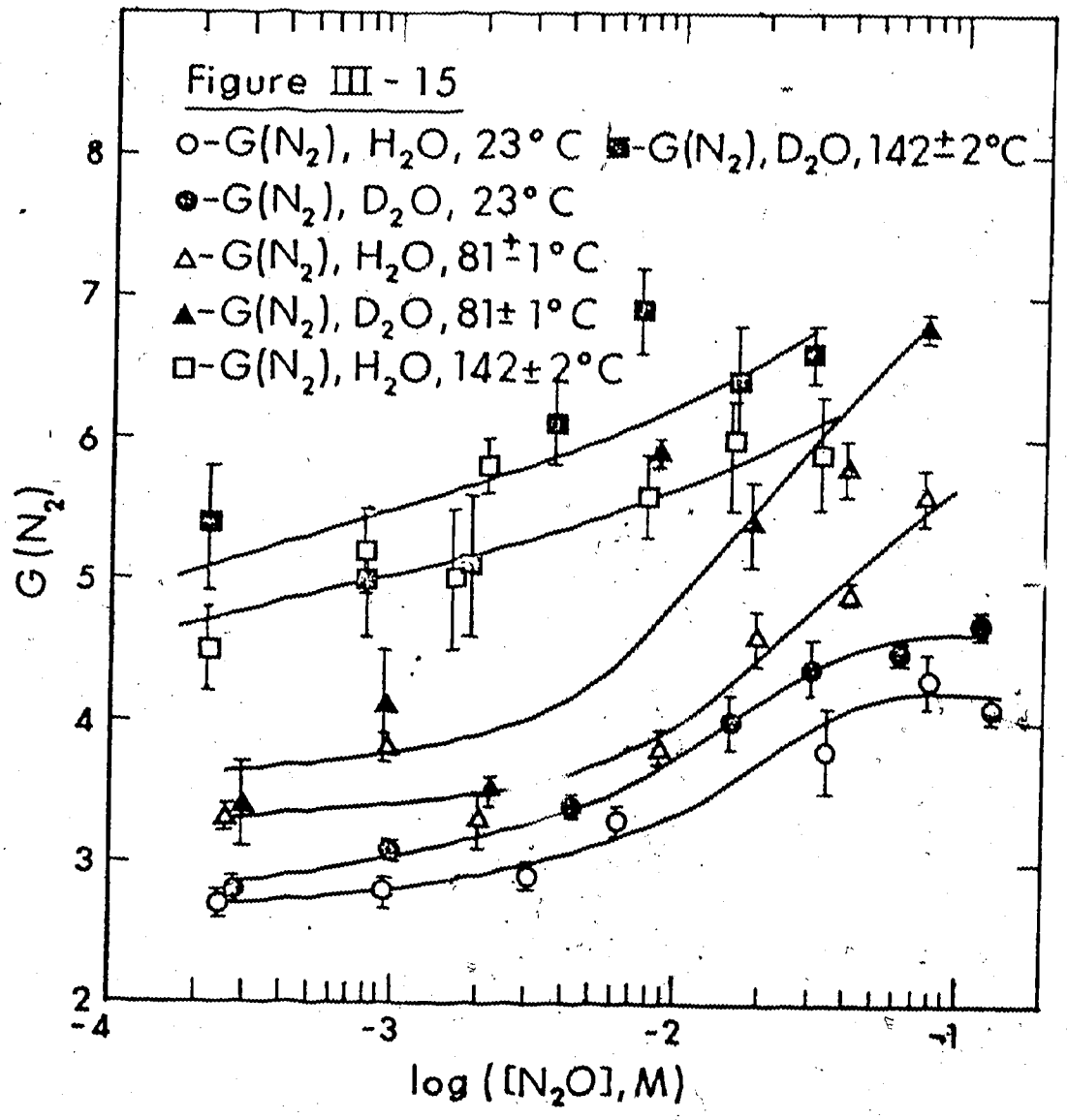

FIGURE III-15 $G(N_2)$ versus the log of the nitrous oxide concentration.

D. Radiation Sensitized Chain Reaction

Methanol and 2-propanol were used as additives to water solutions containing N_2O. When these solutions were irradiated at 573K, high yields of products were obtained, indicating the presence of a chain reaction. In each system a series of experiments was carried out where the N_2O concentration was changed and the temperature, alcohol concentration, and dose rate were kept constant. In both systems also a series of experiments was done where the alcohol concentration was changed and the N_2O concentration, temperature, and dose rate were kept constant. Another series involved changing the temperature while keeping the other conditions constant. In a final series the only experimental condition changed was the dose rate.

a. Product Yields from the Methanol System

The products obtained from the irradiation of N_2O, methanol, water solutions were nitrogen and formaldehyde. The following Tables and Figures show the results from the various experiments mentioned above.

Table III-15 contains yields of N_2 and formaldehyde for blank samples and $G(N_2)$, $G(CH_2O)$ and $G(CO)$ for some irradiated samples. The G values in the Table for unirradiated samples are calculated assuming a one minute irradiation so that they can be compared with the G values from one minute irradiated samples. The yields of N_2 from blank samples were less than 5% of those from irradiated samples and have been subtracted for all data given for the methanol system. The value of $G(CH_2O)$ from blank samples was effectively zero.

The $G(CH_2O)$ values in the methanol system were lower than the $G(N_2)$ values and carbon monoxide was considered as a possible third product that could account for the difference. However, the G(CO) values are negligible as shown in Table III-15.

TABLE III-15

Blank Sample Yields and G(CO) Values for the Methanol Syst

$[CH_3OH]$ M	$[N_2O]$ mM	Temp K	Dose 10^{17} eV/g	$G(N_2)$	G(HCHO)	G(CO)
0.6	40	573 ± 2	0.00	7	-	-
0.7	40	598 ± 2	0.00	15	0	-
0.03	38	573 ± 2	0.00	7	-	-
0.03	38	573 ± 2	0.00	2	-	-
0.5	38	573 ± 2	1.56	141	94	1
1×10^{-3}	38	573 ± 2	1.56	79	53	2
3×10^{-4}	38	573 ± 2	1.56	51	0	1
6×10^{-5}	38	573 ± 2	1.56	35	4	0

Table III-16 shows the yields of N_2 and formaldehyde from irradiations at 573K in the presence and absence of methanol and at N_2O concentrations between 4.3 and 149.3 mM. $G(N_2)$ values are between 7 and 238 and G(HCHO) values between 13 and 181.

Figure III-16 shows a plot of $G(N_2)$ and G(HCHO) versus the square root of the N_2O concentration. The yields of formaldehyde are lower than those of N_2 except for the lowest N_2O concentration studied. The line drawn through the points is calculated and will be discussed in Chapter IV.

TABLE III-16

Product Yields as a Function of $[N_2O]$ at 573 ± 2K*

$[CH_3OH]$ M	$[N_2O]$ mM	$G(N_2)$	G(HCHO)
0.0	8.9	9	-
0.0	13.2	7	-
0.0	17.5	9	-
0.0	96	7	-
0.53	4.3	9	13
0.56	8.9	25	24
0.50	21.1	39	34
0.53	35.0	86	69
0.56	45.6	115	78
0.53	70.3	157	129
0.51	96.0	188	149
0.56	122.9	215	180
0.53	149.3	238	181

*Dose rate = 1.5×10^{17} eV/g min

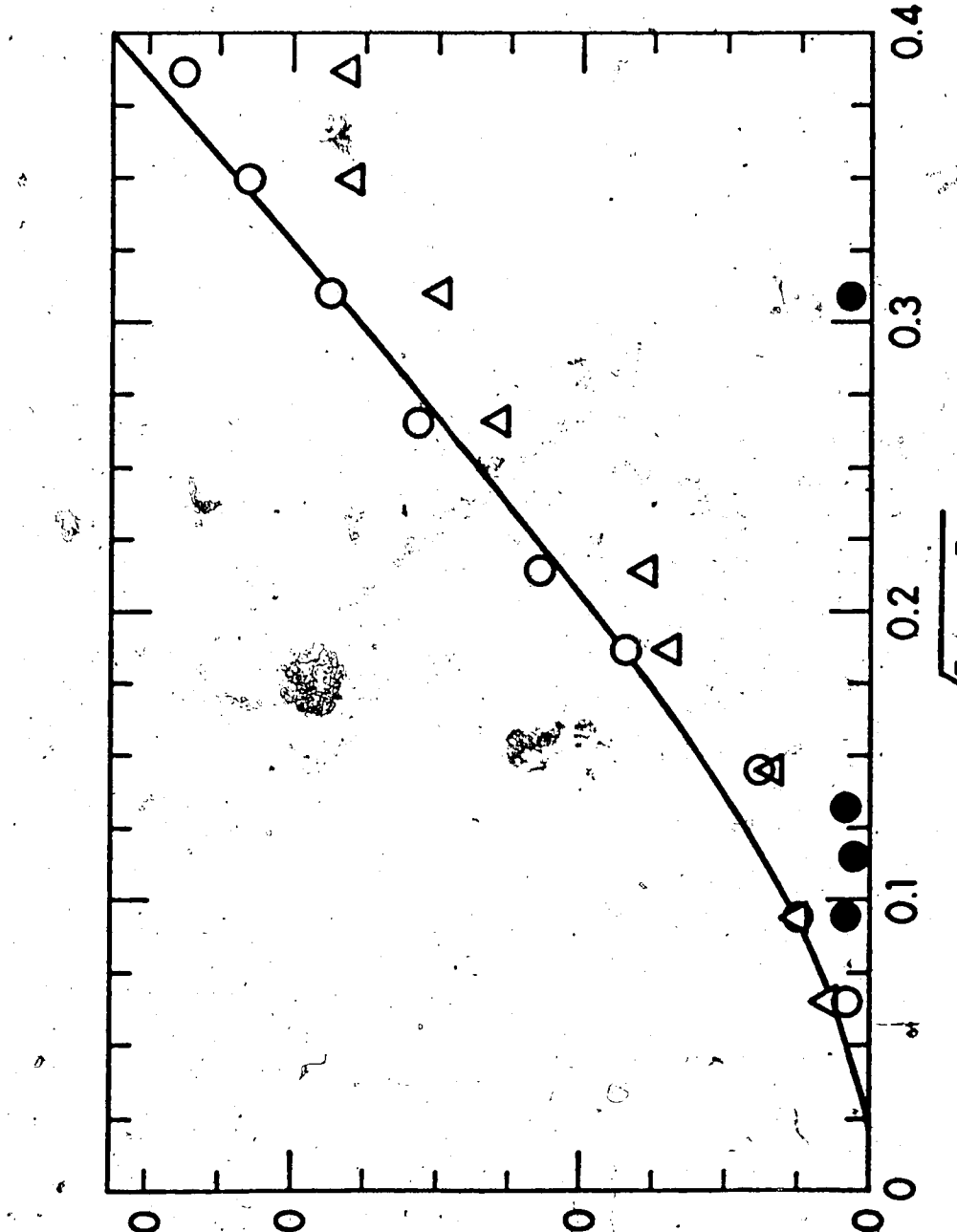

FIGURE III-16 Product yields plotted against the square root of the nitrous oxide molarity at 573K. $[CH_3OH] = 0.53 \pm 0.03$ M. ○, $G(N_2)$; △, $G(CH_2O)$. The full curve was calculated from equations (iii) and (iv) using the rate constant values given in text.

Table III-17 gives the results for the irradiation of samples containing 96 mM (N_2O) and concentrations of methanol between 0.06 and 510 mM. The irradiation temperature was 573°K and the $G(N_2)$ and G(HCHO) values are from 35 to 188 and 0 to 149 respectively. Figure III-17 is a plot of $G(N_2)$ and G(HCHO) versus methanol concentration.

TABLE III-17

Product Yields as a Function of $[CH_3OH]$ at $573 \pm 2K^{\dagger}$

$[N_2O]$ mM	$[CH_3OH]$ mM	$G(N_2)$	G(HCHO)
96	510	188	149
96	260	171	147
96	100	169	145
96	70	160	106
96	32	133	111
96	26	121	53
96	17	108	51
96	8.6	91	48
96	4.7	83	49*
96	1.3	79	53*
96	0.34	74	30
96	0.30	51	0
96	0.06	35	4

* These two values of G(HCHO) not plotted in Figure III-17 because there is no space on the graph for them.

† Dose rate = 1.5×10^{17} eV/ g min.

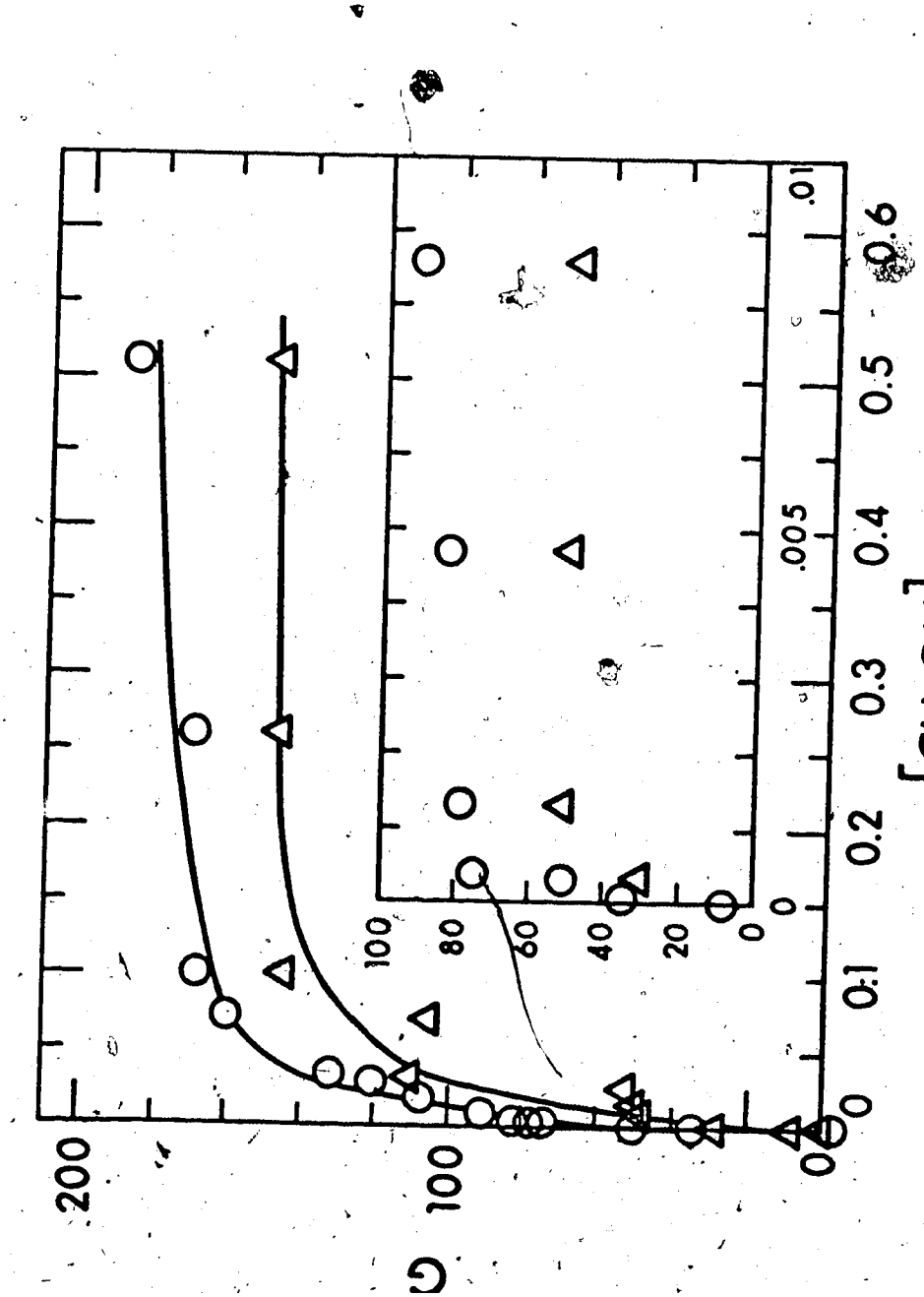

FIGURE III-17 Product yields plotted against the methanol molarity at 573K. $[N_2O] = 96 \pm 5$ mM. ○, $G(N_2)$; △, $G(CH_2O)$.

Table III-18 contains the yields of N_2 and formaldehyde as a function of dose rate at 573K. The dose rate was changed from 0.6×10^{16} to 15×10^{16} eV/g min and $G(N_2)$ values were between 158 and 567. The $G(CH_2O)$ values are slightly lower than the $G(N_2)$ values and are in the range 139 to 464.

Figure III-18 shows a plot of $G(N_2)$ and $G(CH_2O)$ versus $(\text{dose rate})^{-\frac{1}{2}}$. A line is drawn through the points for mechanistic reasons which will be given in Chapter IV.

TABLE III-18

Product Yields as a Function of Dose Rate at 573 ± 2K*

Dose 10^{16} eV/g min	(Dose rate)$^{-\frac{1}{2}}$ 10^{-9} eV$^{-\frac{1}{2}}$/g$^{-\frac{1}{2}}$min$^{-\frac{1}{2}}$	G(N_2)	G(HCHO)
15.0	2.58	158	139
16.1	2.49	188	149
5.50	4.25	232	178
1.40	8.51	426	326
0.60	13.0	567	464

* $[N_2O]$ = 96 mM, $[CH_3OH]$ = 0.53 ± 0.03M.

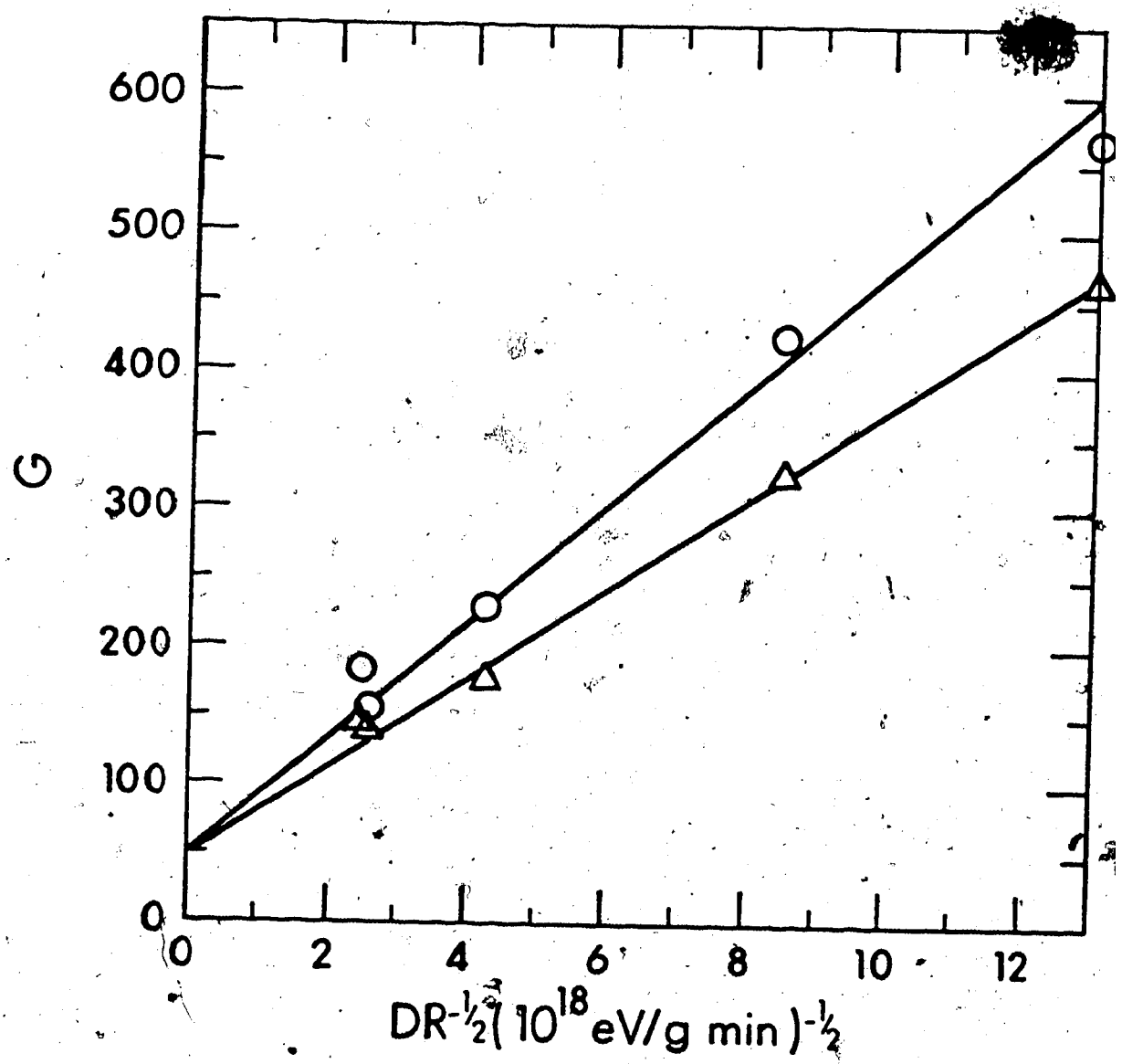

FIGURE III-18 Product yields plotted against (dose rate)$^{-\frac{1}{2}}$. $[N_2O]$ = 96 ± 5 mM, $[CH_3OH]$ = 0.53 ± 0.03 M, T = 573K. O, $G(N_2)$; Δ, $G(CH_2O)$.

Table III-19 contains data obtained from changing the irradiation temperature for samples contining 96 mM N_2O and 0.53 $\pm$ 0.03 M methanol. The temperature was changed from 498K to 573K and nitrogen yields were in the range 58 to 180. Formaldehyde yields were slightly lower varying from 53 to 149.

Figure III-19 contains an Arrhenius plot of the data in Table III-18. The semilog plot of $G(N_2)$ and $G(CH_2O)$ *versus* 1000/T(K) yields a reasonably straight line the slope of which will be discussed in Chapter IV.

TABLE III-19

Effect of Temperature on the Product Yields

$[N_2O]$ mM	$[CH_3OH]$ M	T K	$G(N_2)$	G(HCHO)
98	0.53	498 ± 2	58	53
96	0.56	523 ± 2	98	81
96	0.53	548 ± 2	154	124
96	0.51	573 ± 2	188	149

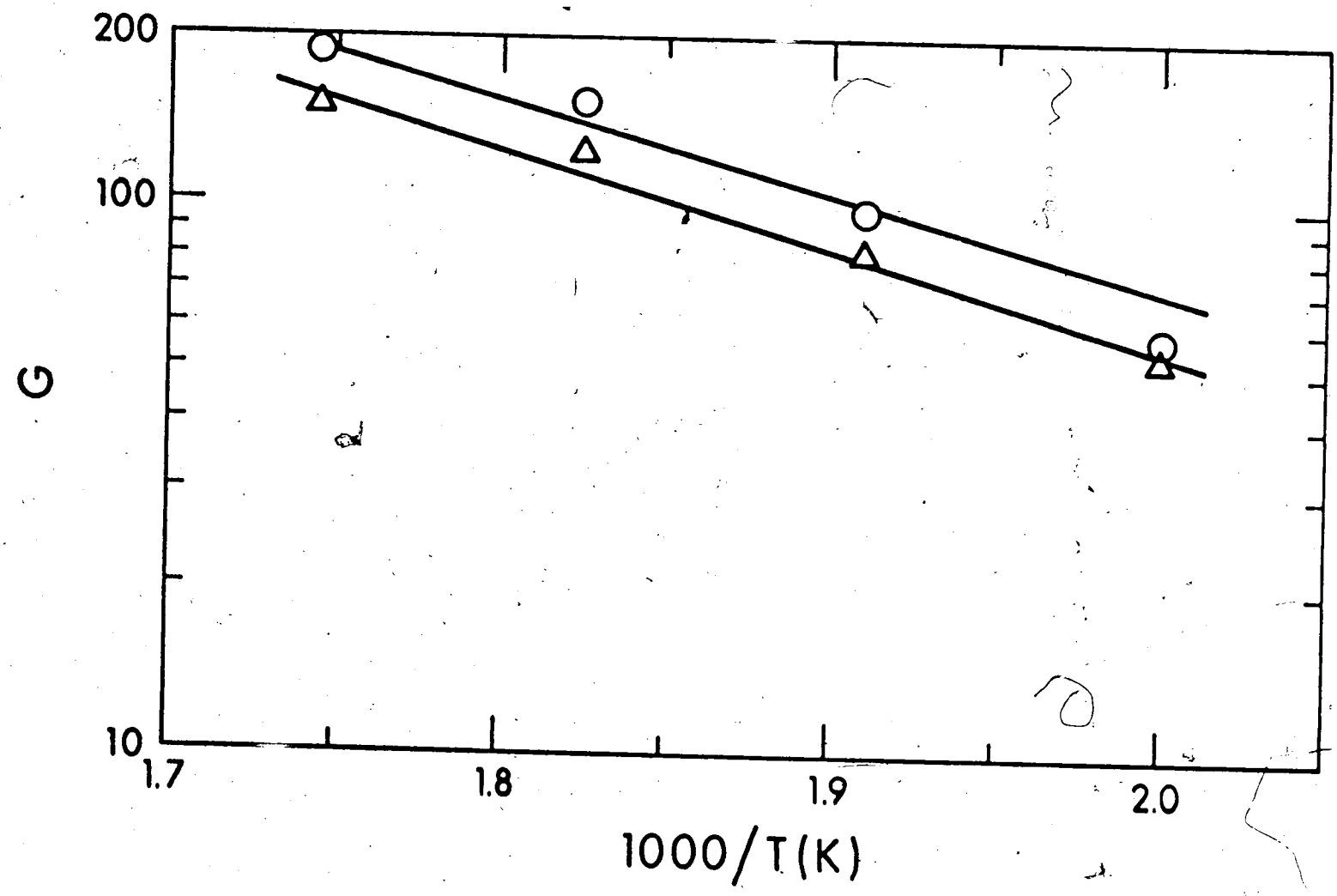

FIGURE III-19 Arrhenius plot of chain product yields. $[N_2O]$ = 95 ± 5 mM. $[CH_3OH]$ = 0.53 ± 0.03 M. ○, $G(N_2)$; △, $G(CH_2O)$.

b. Product Yields from the 2-Propanol System

The products obtained from the irradiation of N_2O, 2-propanol, water mixtures were nitrogen and acetone. The following Tables and Figures show the results from the various experiments performed.

Table III-20 contains blank ampl[illegible]elds of N_2 and acetone for 0.3 M [2-propano[illegible] mM to 91.2 mM [N_2O]. The yields were calcula[illegible]uming a one minute irradiation time and appropriate values have been subtracted for all G values shown in the following Tables for the 2-propanol system.

TABLE III-20

Blank Sample Yields for the 2-Propanol System *

$[(CH_3)_2CHOH]$	$[N_2O]$	Temp. K	Dose 10^{17} eV/g	$G(N_2)$	$G((CH_3)_2CO)$
0.3	91	583 ± 1	0.00	-	84
0.3	91	573 ± 1	0.00	11	-
0.3	77	573 ± 1	0.00	47	40
0.3	77	573 ± 1	0.00	47	0
0.3	77	573 ± 1	0.00	46	0
0.3	48	573 ± 1	0.00	-	37
0.3	0.3	573 ± 1	0.00	20	-
0.3	0.3	573 ± 1	0.00	-	0

* Dose rate = 1.4×10^{17} eV/g min.

Table III-21 gives the yields of N_2 and acetone from irradiations at 573K and 0.3 M 2-propanol concentration. The N_2O concentration was varied from 0.24 mM to 12.7 mM and $G(N_2)$ values were in the range 83 to 1367. The $G((CH_3)_2CO)$ values were equal to the $G(N_2)$ values within experimental error and varied from 138 to 1145.

Figure III-20 contains a plot of $G(N_2)$ and $G((CH_3)_2CO)$ versus the square root of the N_2O concentration. The calculated line through the points will be dealt with further in Chapter IV.

TABLE III-21

Product Yields as a Function of $[N_2O]$ at 573 ± 1 K*

$(CH_3)_2CHOH$ M	$[N_2O]$ mM	$G(N_2)$	$G((CH_3)_2CO)$
0.3	12.7	1367	-
0.3	9.1	1146	-
0.3	9.1	1078	-
0.3	5.0	828	-
0.3	2.2	422	-
0.3	1.0	231	-
0.3	0.24	83	-
0.3	9.1	-	1013
0.3	9.1	-	1083
0.3	9.1	-	1145
0.3	5.0	-	961
0.3	2.2	-	586
0.3	1.0	-	328
0.3	0.24	-	138

* Dose rate = 1.4×10^{17} eV/ g min.

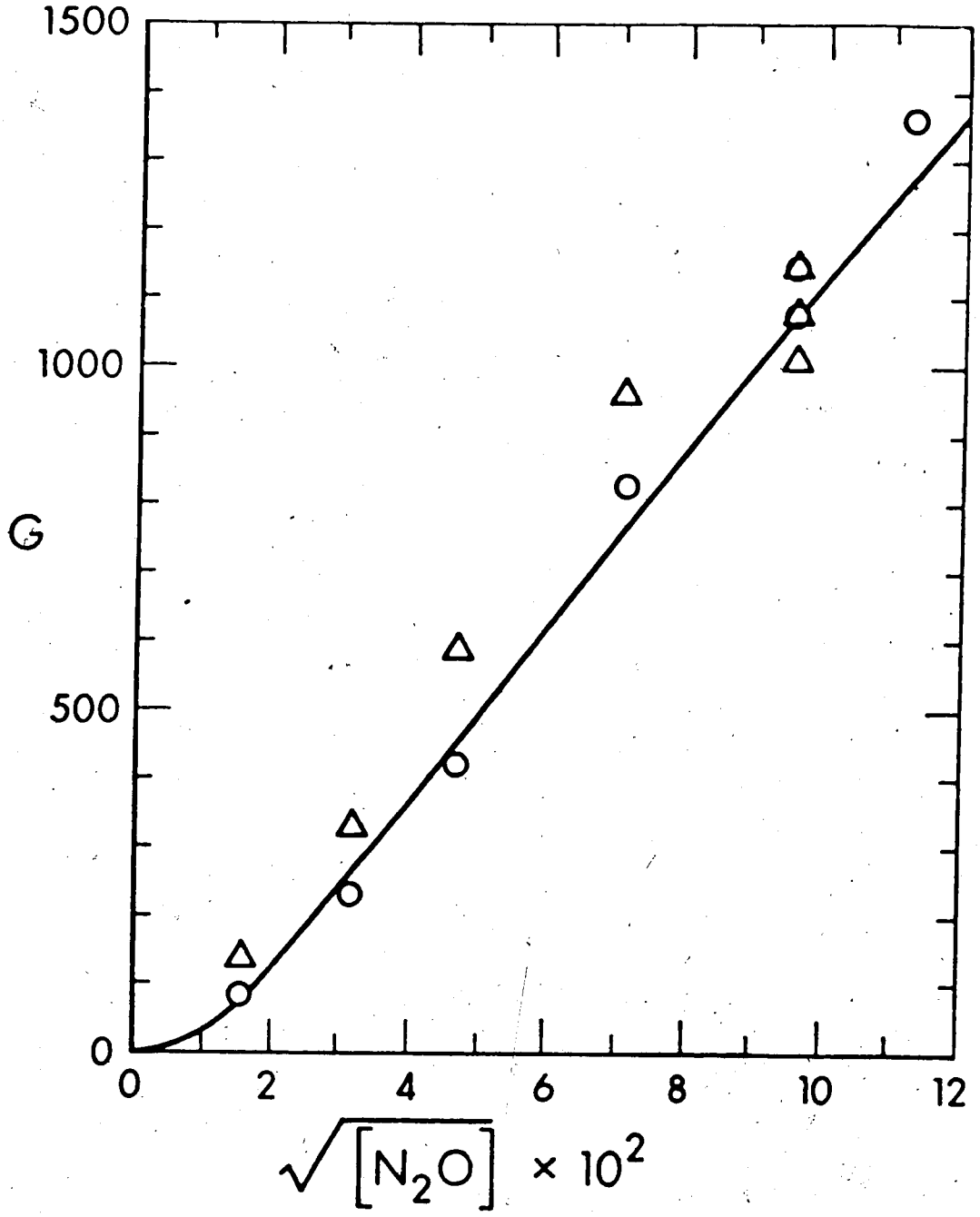

FIGURE III-20 Product yields plotted against the square root of the nitrous oxide molarity at 573K. $[(CH_3)_2CHOH]$ = 0.30 ± 0.03 M. ○, $G(N_2)$; △, G(acetone). The full curve was calculated from equation vi using the rate constant values given in the text.

Table III-22 contains the results for the irradiation of samples containing 8.7 ± 0.4 mM [N_2O] and concentrations of 2-propanol between 0.18 and 300 mM. The irradiation temperature was 573K and the $G(N_2)$ values are between 39 and 1146. The $G((CH_3)_2CO)$ values are the same as the $G(N_2)$ values within experimental error and range from 69 to 1145.

Figure III-21 is a plot of $G(N_2)$ and $G((CH_3)_2CO)$ and the square root of the 2-propanol concentration. The calculated line through the points is drawn for mechanistic reasons given in Chapter IV.

TABLE III-22

Product Yields as a Function of 2-Propanol Concentration at 573 ± 1 K*

$[N_2O]$ mM	$[(CH_3)_2CHOH]$ mM	$G(N_2)$	$G((CH_3)_2CO)$
9.1	300	1078	-
9.1	300	1146	-
9.1	90	539	-
9.1	18	194	-
9.1	10	169	-
9.1	1.8	86	-
9.1	0.96	67	-
9.1	0.18	39	-
9.1	300	-	1013
9.1	300	-	1083
9.1	300	-	1145
8.4	40	-	358
8.4	20	-	134
8.4	4	-	69

* Dose rate = 1.4×10^{17} eV/g min.

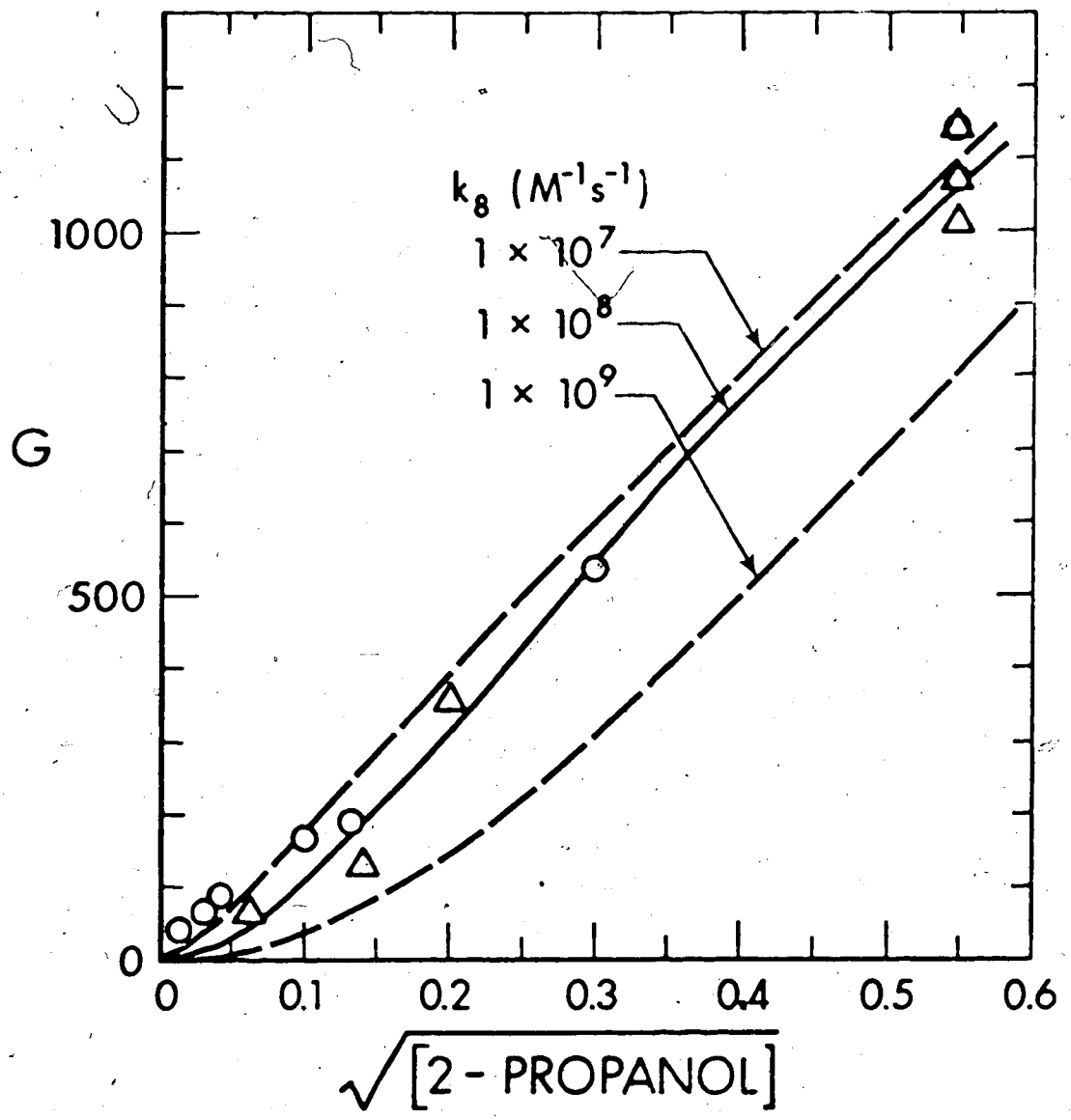

FIGURE III-21 Product yields plotted against the square root of the 2-propanol molarity at 573K. $[N_2O]$ = 8.7 ± 0.4 mM. ○, $G(N_2)$; △, G(acetone). The full curve was calculated from equations x and xi using the rate constant values given in Text, with $k_8 = 1 \times 10^8$ ℓ/mol s. The dashed curves show the effect of assuming $k_8 = 1 \times 10^7$ or 1×10^9 ℓ/mol s.

Table III-23 shows yields of N_2 and acetone as a function of dose rate at 573K. The dose rate was varied in the limits (0.518 - 13.6) x 10^{16} eV/g min and $G(N_2)$ values were between 1078 and 2823. The $G((CH_3)_2CO)$ values are slightly lower than the $G(N_2)$ values and are in the range 1013 to 2387.

Figure III-22 shows a plot of $G(N_2)$ and $G((CH_3)_2CO)$ *versus* (dose rate)$^{-\frac{1}{2}}$. The data indicate that the relationship between the quantities is not linear and the initial slope is therefore used in the calculations in Chapter IV.

TABLE III-23

Product Yields as a Function of Dose Rate at 573 ± 1 K*

Dose Rate 10^{16} eV/g min	(Dose Rate)$^{-\frac{1}{2}}$ 10^{-9} g$^{\frac{1}{2}}$min$^{\frac{1}{2}}$/eV$^{\frac{1}{2}}$	$G(N_2)$	$G((CH_3)_2CO)$
13.6	2.71	1146	-
13.6	2.71	1078	-
13.6	2.71	-	1013
13.6	2.71	-	1145
4.77	4.59	-	1445
1.19	9.17	2638	-
1.19	9.17	-	2386
0.518	13.9	2823	-
0.518	13.9	-	2387

* $[N_2O]$ = 8.7 ± 0.4 mM, [2-propanol] = 0.3 M.

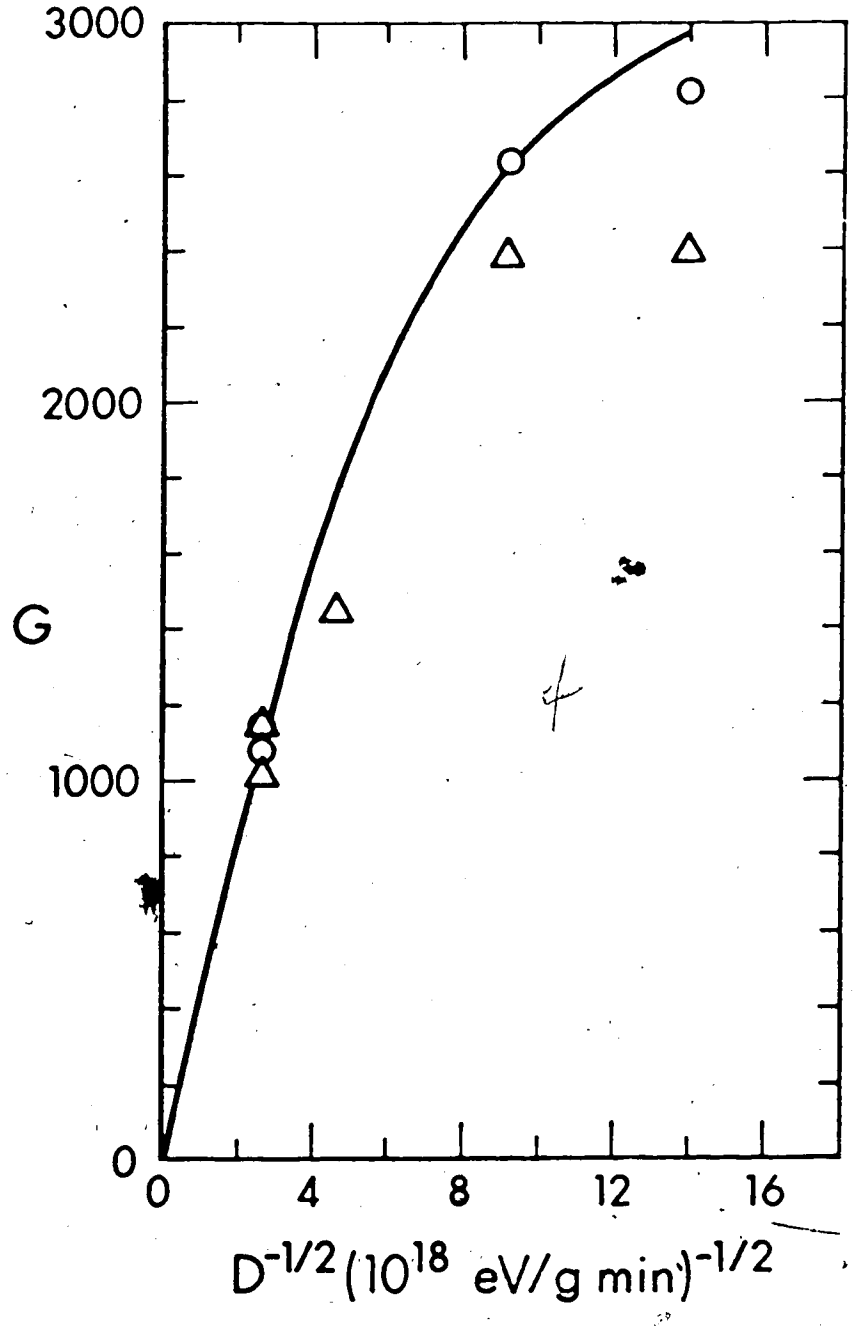

FIGURE III-22 Product yields plotted against (dose rate)$^{-\frac{1}{2}}$. $[N_2O]$ = 8.7 ± 0.4 mM, $[(CH_3)_2CHOH]$ = 0.30 ± 0.03 M T = 573K. ○, $G(N_2)$; △, $G((CH_3)_2CO)$.

Table III-24 contains data from changing the irradiation temperature for samples containing 8.7 ± 0.4 mM nitrous oxide and 0.3 M 2-propanol. The temperature was changed from 513K to 583K and nitrogen yields were in the range 234 to 1336. Acetone yields were the same as nitrogen yields within experimental error having values from 194 to 1419. A good Arrhenius plot is obtained from the data as shown in Figure III-23.

TABLE III-24

Effect of Temperature on the Product Yields

$[N_2O]$ mM	$[(CH_3)_2CHOH]$ M	T K	$G(N_2)$	$G((CH_3)_2CO)$
9.1	0.3	513	234	-
9.1	0.3	513	-	194
9.1	0.3	523	284	-
9.1	0.3	523	-	327
9.1	0.3	533	308	-
9.1	0.3	543	388	-
9.1	0.3	543	-	423
9.1	0.3	553	-	712
9.1	0.3	563	634	-
9.1	0.3	563	-	817
9.1	0.3	573	1146	-
9.1	0.3	573	1078	-
9.1	0.3	573	-	1013
9.1	0.3	573	-	1083
9.1	0.3	573	-	1145
9.1	0.3	583	1336	-
9.1	0.3	583	-	1419
8.4	0.3	583	-	1355
8.4	0.3	583	-	1243

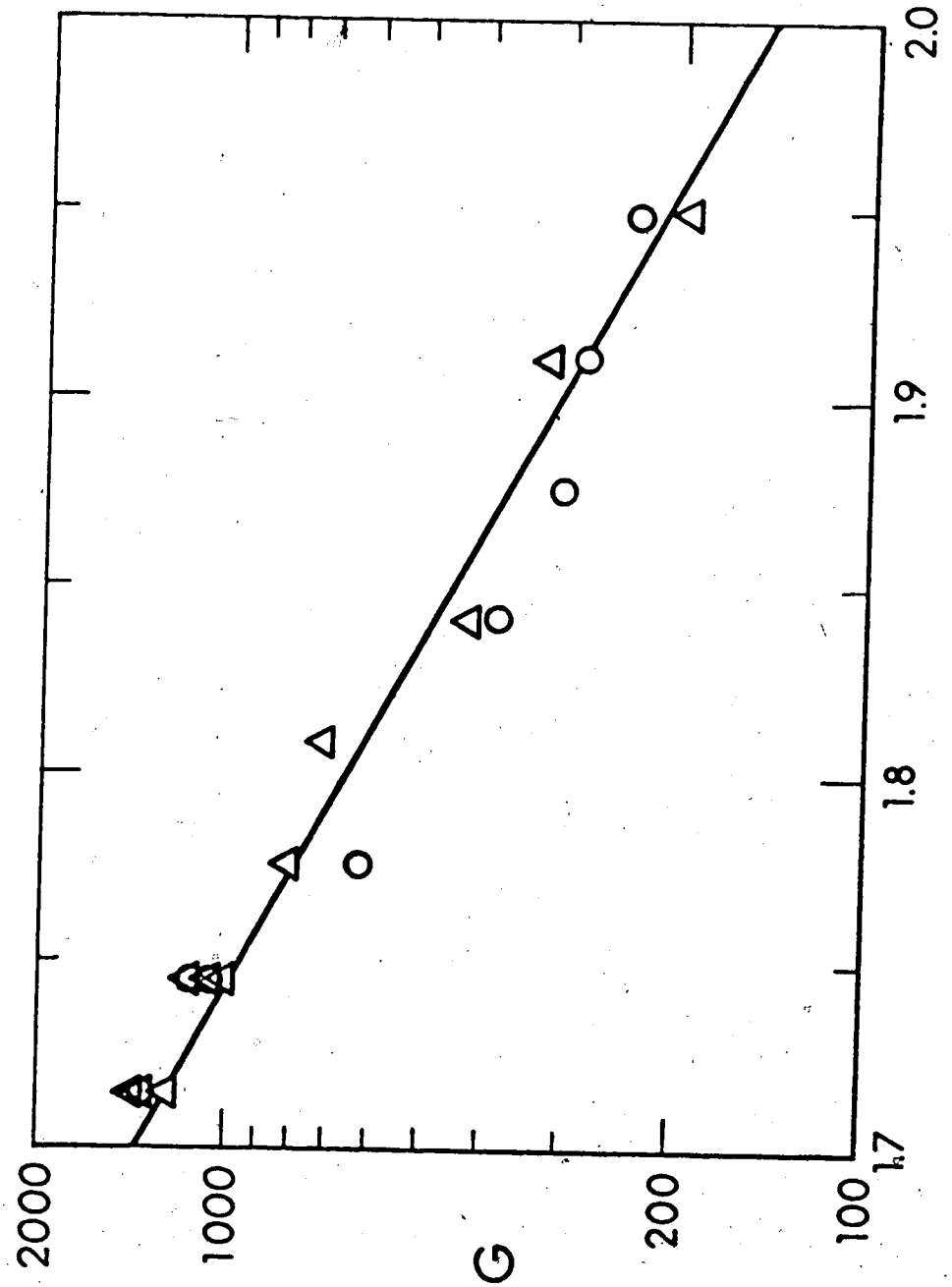

FIGURE III-23 Arrhenius plot of chain product yields.

$[N_2O]$ = 8.7 ± 0.4 mM, $[(CH_3)_2CHOH]$ = 0.30 ± 0.03 M.

○, $G(N_2)$; △, $G((CH_3)_2CO)$.

Table III-25 contains nitrogen yields at 573K, from samples containing 2-propanol, acetone, and N_2O. The addition of 0.02 M acetone to a sample containing 0.02 M 2-propanol and 9.1 mM (N_2O) seems to have little effect on the nitrogen yield. Also, the addition of 0.01 M acetone to a sample containing 0.3 M 2-propanol and 9.1 mM (N_2O) produces no measurable change in the nitrogen yield. The yield of N_2 is reduced to less than half its original value when 0.3 M acetone is added to a 0.3 M ($(CH_3)_2CHOH$), 91 mM (N_2O) sample. A sample containing 91.2 mM N_2O and 0.02 M acetone gives a yield of N_2 which is equal to the blank sample yield within experimental error.

TABLE III-25

Effect of Adding Acetone to the 2-Propanol System

$[(CH_3)_2CHOH]$ M	$[(CH_3)_2CO]$ M	$[N_2O]$ mM	Dose 10^{17} eV/g	$G(N_2)$
0.02	0.00	3.8	1.397	194
0.02	0.02	3.8	1.337	277
0.30	0.00	3.8	1.337	1049
0.30	0.01	3.8	1.337	1019
0.30	0.30	3.8	1.337	428
0.30	0.00	3.8	1.337	1050
0.00	0.02	3.8	1.337	2*
0.30	0.30	3.8	0.00	45
0.02	0.02	3.8	0.00	8.4
0.00	0.02	3.8	0.00	6

* The blank sample yield is not subtracted from this sample because it is larger than the irradiated sample yield.

IV DISCUSSION

A. Nitrous Oxide as an Electron Scavenger

Nitrous oxide has been used as an electron scavenger in a number of studies (4,6-50). The capture of an electron by N_2O produces N_2O^- which decomposes to produce N_2 and O^-. Therefore, one electron capture leads to the production of one N_2 molecule so that the N_2 yield can be equated with the electron yield.

B. Total Ionization Yields in Water and D_2O

The radiolysis of aqueous solutions of nitrous oxide at room temperature and natural pH produces yields of nitrogen which are dependent on the nitrous oxide concentration. With ~1 mM concentration the value of $G(N_2)$ is between 2.5 and 3.0 and increases to 4.0 at 100 mM. The 1 mM values are identified with the capture by nitrous oxide of all electron free ions (electrons which have diffused out of the spurs) so that the free ion yield from the γ-radiolysis of water is in the range 2.5 - 3.0. The value of $G(N_2) = 4.0$ at 100 mM nitrous oxide is taken to represent the capture of nearly all electrons produced by the irradiation. Electrons and positive ions are the primary species generated by the γ-rays and the yield of nitrogen obtained when all electrons are captured by nitrous oxide is a measure of

the total number of ion pairs produced. The number of ion pairs produced by the absorption of 100 eV of energy from the radiation is called G(total ionization).

The value of G(total ionization) in liquids cannot be determined directly as no method exists for the collection at electrodes of all ions produced during irradiation. The use of electron scavengers such as nitrous oxide provide an indirect method for determining this quantity. By such means the value of G(total ionization) in water and alcohols has been estimated to be between 4 and 5 (51-53). No estimate exists for the value of G(total ionization) in D_2O but the present work indicates that it is larger than G(total ionization) in water.

C. Radiolysis of N_2O-H_2O and N_2O-D_2O Mixtures at 23°C

Figures III-1 to III-3 show the nitrogen yields obtained from water-N_2O mixtures and III-8 and III-9 show the yields from the N_2O-D_2O system. The yields are presented as μmoles/ml plotted against dose in eV/ml for three reasons.

(1) The G values calculated from the slopes of the lines are more accurate than G values calculated from single points.

(2) A straight line shows that the G value is independent of dose.

(3) The plot indicates whether or not the best straight line through the points has an intercept equal to the measured blank sample yield.

Figures III-2A and III-2B satisfy these requirements quite well. Figures III-3A, III-3B, and III-3C indicate dose independent G values and intercepts that agree with experimental blanks. Figure III-4B contains a number of points and gives a good straight line and intercept.

The N_2 yields from the D_2O system at 23°C in Figure III-9A show considerable scatter; however, the points in Figure III-3B, III-9C, III-10A and III-10B satisfy the above criteria very well.

The $G(N_2)$ value for H_2O and D_2O as a function of log (nitrous oxide concentration) at 23°C are shown in Figure III-15. At a concentration of ~1 mM in water the $G(N_2)$ value is 2.8 indicating a free ion yield of 2.8 in neutral water at room temperature. Previous values obtained are: 2.45 (6), 2.65 (54), 2.65 (55), 2.7 (4) and 2.80 (10).

[illegible]00 mM nitrous oxide the yield increases to abo[illegible] dicating that G(total ionization) is $\geq$4.2 in [illegible]er. Previously a value of $G(N_2)$ of 4.0 was obtain[illegible]ter conta[illegible]ng 10% ethanol and 100 mM $[N_2O]$ (4.

The $G(N_2)$ values in D_2O are about 10% higher than the H_2O values at all nitrous oxide concentrations studied. Dainton and Peterson (8) found that the yield of nitrogen from D_2O was 12-15% higher than from H_2O at 16 mM nitrous oxide. Results obtained using SF_6 as an electron scavenger agree with those obtained with nitrous oxide in both water and D_2O for scavenger concentration up to ~2 mM (56). This was the highest SF_6 concentration studied because its solubility is not high enough, in water and D_2O, to make more concentrated solutions by the technique used.

The higher free ion yield in deuterio compounds as compared to the yield in protio compounds seems to be a general effect (57-59). The value of $(G^D_{fi} - G^H_{fi})$ for water and dimethylsulfoxide is 0.3 - 0.5, and for ammonia at -15°C it is 0.3 (58,59). Previously it was thought that this isotope effect was due to a wider initial distribution of electrons in the spurs (58). The present study implies that the difference is due to an isotope effect in the total ionization yield, as the 100 mM nitrous oxide $G(N_2)$ value is 10% larger in D_2O than in H_2O at 23°C (Figure III-15).

D. Radiolysis of N_2O - H_2O and N_2O - D_2O Mixtures at 81 ± 1°C

The nitrogen yields obtained from the radiolysis of

N_2O - H_2O and N_2O - D_2O mixtures at 81 ± 1°C are shown in Figures III-5, III-6, III-11, and III-12. Figures III-5B, III-5C, III-6A and III-6B contain a sufficient number of points to show that the yields of nitrogen in water are independent of dose over the range used. The $G(N_2)$ values from both H_2O and D_2O at 81 ± 1°C (Figure III-15) show much more experimental scatter than the 23°C yields. The system is reproducible enough, however, to draw two conclusions. First the yields at 81 ± 1°C are higher than the 23°C yields at all nitrous oxide concentrations studied. Secondly, the $G(N_2)$ values from D_2O are higher than those obtained from H_2O. The same trends were observed using SF_6 as a scavenger at 106°C (56).

It is difficult to understand the absolute values of $G(N_2)$ obtained from H_2O - N_2O and D_2O - N_2O solutions irradiated at 81 ± 1°C. The value found at a nitrous oxide concentration of ~75 mM is 5.6 in H_2O and 6.8 in D_2O (Figure III-14). These yields are difficult to interpret as the G(total ionization) is likely to be in the range 4-5. The most probable explanation is that chain reactions caused by small amounts of impurities in the water and D_2O are responsible for the usually high yields. This explanation requires that the impurities be more reactive than methanol and n-hexane, as adding 0.1 ml of methanol or 10^{-3} ml of n-hexane produced no measurable effect on the nitrogen yields from

samples containing 40 mM nitrous oxide. Table III-5 and Figure III-6B.

E. Radiolysis of N_2O - H_2O and N_2O - D_2O Mixtures at 142 ± 2°C

Figures III-7 and III-8 show that at 142 ± 2°C the yield of N_2 from the radiolysis of H_2O - N_2O solutions are dose independent for the range studied. The same conclusion can be drawn about the D_2O - N_2O results shown in Figure III-13 and III-14. When the yields are plotted against log (nitrous oxide concentration) as shown in Figure III-15 it is clear that the $G(N_2)$ values are higher in both liquids at 142 ± 2°C than at 81 ± 1°C. Also the nitrogen yields at 142 ± 2°C are higher in D_2O solution than in water. It was found using SF_6 as an electron scavenger (56) that the F^- ion yields from D_2O were larger by about 10% than those from H_2O at radiolysis temperatures from 20°C to 300°C. Yields of nitrogen from a sample containing 10^{-3} ml of methanol (Table III-7) increased the yields at 142 ± 2°C by a factor of about 3 as compared to a sample containing no methanol. Addition of 10^{-3} ml of n-hexane had no measurable effect but this is not surprising as methanol is more easily oxidized than n-hexane. There is a strong possibility that the high yields of nitrogen from both H_2O and D_2O at 142 ± 2°C are due to a chain process resulting from

the presence of small amounts of impurity.

F. Chain Reaction Mechanism

The following set of reactions is consistent with the results from the N_2O - water - methanol and N_2O - water -2-propanol systems.

$$H_2O \xrightarrow{\sim\sim} H, OH \quad (30)$$

$$H, OH + HCR_2OH \longrightarrow H_2,\ H_2O + \cdot CR_2OH \quad (31)$$

$$N_2O + \cdot CR_2OH \longrightarrow N_2 + \cdot OCR_2OH \quad (32)$$

$$\cdot OCR_2OH + H_2O \longrightarrow HOCR_2OH + OH \quad (33)$$

$$\cdot OCR_2OH + HCR_2OH \longrightarrow HOCR_2OH + \cdot CR_2OH \quad (34)$$

$$HOCR_2OH \rightleftharpoons CR_2O + H_2O \quad (35)$$

$$2 \cdot CR_2OH \longrightarrow P_1 \quad (36)$$

$$\cdot OCR_2OH + \cdot CR_2OH \longrightarrow P_2 \quad (37)$$

$$2 \cdot OCR_2OH \longrightarrow P_3 \quad (38)$$

where HCR_2OH is either methanol in which case R = H or 2-propanol where R is CH_3. Solvated electrons are also produced in reaction (30), but they initiate chains by reacting with nitrous oxide, which forms an O^- ion that reacts with alcohol to form $\cdot CR_2OH$. The net result for chain initiation is the same whether the initiators are (e^-_{solv}, H_3O^+, OH) or (H,OH). For simplicity only the

latter are presented in the chain mechansim. Reaction (31) is well established for both methanol and 2-propanol (60) but reactions 32 to 34 are proposed for the first time. Processes similar to reaction (32) have been offered before. The reaction of nitrous oxide with a hydrogen radical (H.) has been used to explain radiation induced chain reactions in H_2O - N_2O mixtures containing hydrogen (17-19).

$$N_2O + H\cdot \longrightarrow N_2 + OH \qquad (39)$$

The gas phase rate constant for reaction 39 (k_{39}) has been found to have a value of 7.06×10^6 l/mol s at 540°C with an activation energy of 16 kcal/mol (61). This indicates that at 300°C the value of k_{39} is 1×10^5 l/mol s.

Reaction 33 is proposed to explain the fact that the product yields in the methanol system are independent of methanol concentration for (0.05 - 0.5) M methanol (Figure III-17). This would not be true if reaction 34 were the rate determining process in this system. The kinetic analysis of the methanol system is not altered if reaction 33 is replaced by a decompositio-

$$OCR_2OH \longrightarrow CR_2O + OH \qquad (40)$$

but reaction (40) is not consistent with the results from the 2-propanol system where the $\cdot OC(CH_3)_2OH$ radical

would be expected to undergo reaction (40) as well. The 2-propanol results show a dependence of the yields on the 2-propanol concentration that is consistent with reaction (34) being important in the propagation and not reaction (40) (Figure III-[illegible]). Reaction 33 is probably endothermic in the gas phase by at least 18 kcal/mol. The reason for this conclusion is that the bond dissociation energy for the HO-H bond is 119 kcal/mol and the CH_3O-H and iso-C_3H_7O-H bonds have values of 100 and 102 kcal/mol respectively (62). The H-OCH_2OH bond dissociation energy is not likely to be greater than 100 kcal/mol as the electron withdrawing OH group will tend to reduce the bond strength.

In water solution the $HOC(CH_3)_2OH$ dissociates readily (reaction 35) but $HOCH_2OH$ does not. The value of

$$K_{eq} = \frac{(HOCR_2OH)}{(R_2CO)} \qquad (ii)$$

the constant is 2×10^3 for formaldehyde and 2×10^{-3} for acetone at room temperature (63). Reaction (33) may be much more energetically favored in the aqueous methanol system at 300°C than in the gas phase, as the $HOCH_2OH$ species is likely to be a stable product. Reaction energetics can be greatly affected by solvation, although no direct information is available about (33).

G. Analysis of the N_2O-Methanol-Water System

A steady state treatment of the above set of reactions, assuming that reactions (32) and (33) are important propagation processes, that reaction (34) is unimportant, and that termination is by (36) and (37) leads to a third order equation (see appendix A for derivation).

$$k_{37}k_{36}[\cdot CH_2OH]^3 + (k_{32}k_{37}[N_2O] + k_{33}k_{36})[\cdot CH_2OH]^2 - k_{37}I[\cdot CH_2OH] - k_{33}I = 0 \qquad \text{(iii)}$$

where $I = 10^{-2}\ D\ G(int)$ is the rate of initiation of the chain process, G(int) is the G value for initiation, assumed equal to 5 for this work, and D is the dose rate. Equation (iii) can be solved for the $[\cdot CH_2OH]$ by an iterative method using a computer if values can be assigned to the rate constants. The value of k_{36}, the rate constant for the recombination of two $\cdot CH_2OH$ radicals is 1.2×10^9 l/ml s in water at room temperature (64). The rate constant for a diffusion controlled reaction in water has a value of $\sim 0^9$ l/mol s at room temperature (65) so one can conclude that reaction 36 is diffusion controlled at 25°C. The coefficient of viscosity of water changes by a factor of 10 between 25°C and 300°C so it follows that 1×10^{10} l/mol s is a good

radicals is assumed to have a value $k_{37} = 1 \times 10^{10}$ l/mol s.

The magnitudes of k_{32} and k_{33} are determined from the experimental data. The line drawn through the data in Figure III-16 is calculated using $k_{32} = 2.48 \times 10^4$ l/mol s and $k_{33} = 1.51 \times 10^3\ s^{-1}$. First the $[\cdot CH_2OH]$ is determined using equation (iii) and then the $G(N_2)$ value is obtained from equation (iv).

$$G(CH_2O) = G(N_2) = \frac{k_{32}[N_2O][\cdot CH_2OH]}{10^{-2}\ D} \qquad \text{(iv)}$$

where D is the dose rate $\sim 1.6 \times 10^{17}$ eV/g min. The calculated curve and the data in Figure III-16 have a complex shape but can be understood by examining the sequence of reactions 32-37. If one considers reaction (37) to be the only mode of termination at higher nitrous oxide concentration ~0.17 M, one may derive the following expression (see Appendix A for derivation).

$$G(CH_2O) = G(N_2) = \left(\frac{G(int)}{(10^{-2}D)}\right)^{\frac{1}{2}}\left(\frac{k_{32}k_{33}}{k_{37}}\right)^{\frac{1}{2}}[N_2O]^{\frac{1}{2}} \qquad \text{(v)}$$

Equation (v) predicts that $G(N_2)$ plotted against the square root of the nitrous oxide concentration should give a straight line through the origin. From Figure III-16 is appears that one would have to study higher N_2O concentrations to see such an effect. It was found that the curve calculated with equations (iii) and (iv)

agreed with equation (v) for nitrous oxide concentrations $\geq$ 1 M (Figure IV-1).

At low nitrous oxide concentrations, ~0.01 M, there is a curvature of the data back towards the origin. For small concentrations of N_2O, reaction (32) will occur at a lower rate so that the concentration of $\cdot CH_2OH$ is increased and termination by reaction (36) is more probable. A steady state treatment considering reaction (36) as the only mode of termination leads to equation (vi) (see Appendix A for derivation).

$$G(CH_2O) = G(N_2) = \frac{k_{32}}{\sqrt{k_{36}}} \times \frac{[N_2O](G(int))^{\frac{1}{2}}}{(10^{-2}D)} \qquad (vi)$$

The bending of the experimental data for $(N_2O)^{\frac{1}{2}} < 0.1\ M^{\frac{1}{2}}$ in Figure III-16 indicates a first order dependence on N_2O concentration in this region in agreement with equation (vi). The change from square root dependence to first order dependence shows also in the theoretical curve obtained by using equations (iii) and (iv) (Figure III-16). This means that the more general formulation, equation (iii), describes the system reasona well over the entire range of N_2O concentrations.

Figure III-17 shows a plot of $G(N_2)$ and $G(CH_2O)$ against the methanol concentration. The plot demonstrates that the system is not sensitive to the methanol concentration over a concentration range (0.5 → 0.005) M

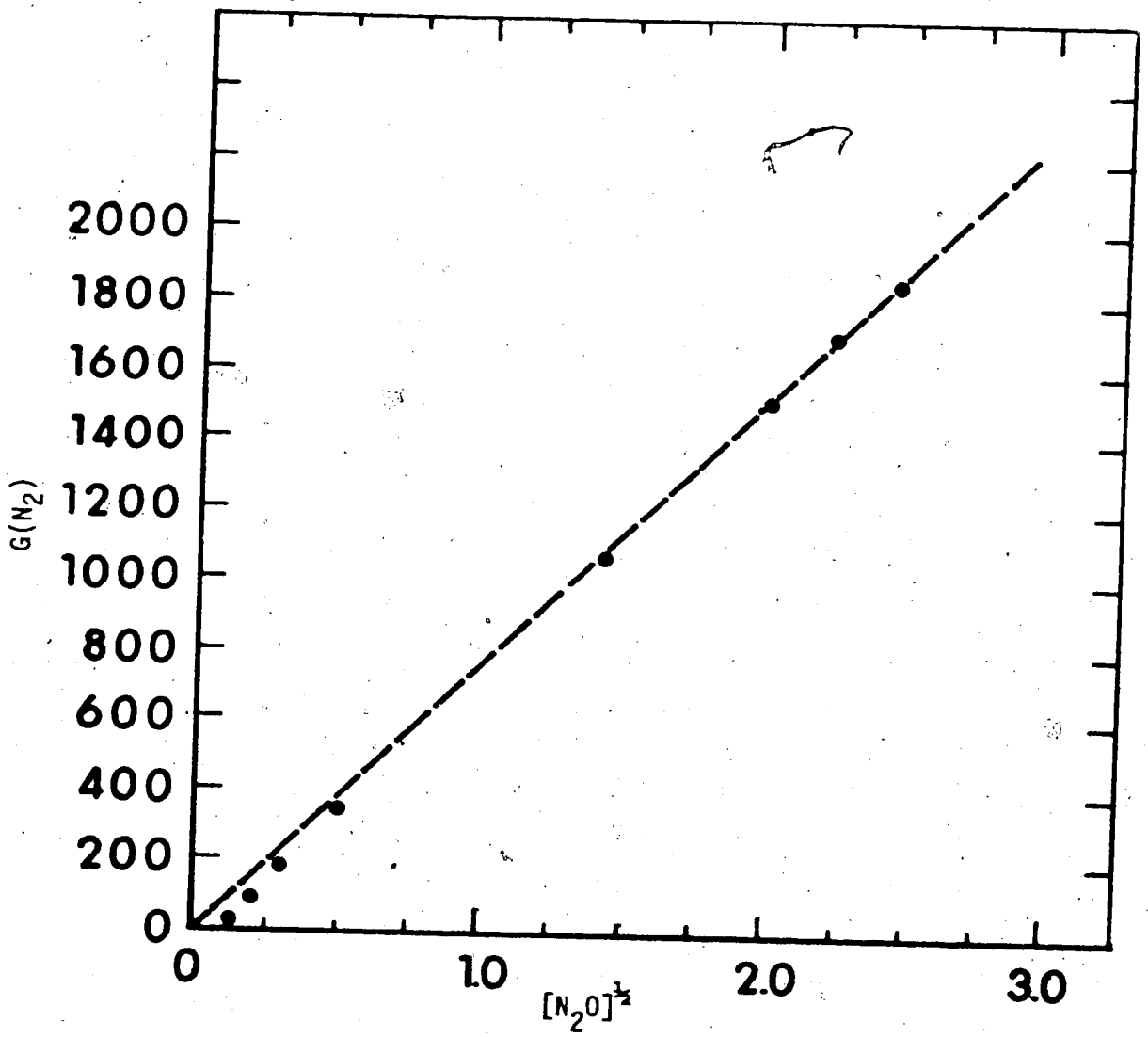

FIGURE IV-1. Calculated $G(N_2)$ values.

•, calculated using equations (iii) and (iv) with values of rate constants given in text. ----, line calculated using equation (v).

and this result is the reason why reaction 34 was considered to be unimportant in the methanol system. The study of the variation of the nitrous oxide concentrations (Figure III-16) was carried out using 0.53 ± 0.03 M methanol, the region where the yields are independent of the methanol concentration.

Figure III-18 contains a plot of $G(N_2)$ and $G(CH_2O)$ against $D^{-\frac{1}{2}}$ for a methanol concentration of 0.05 M and 96 mM nitrous oxide. As mentioned above these are the conditions where equation (v) applies. The linear dependence of $G(N_2)$ and $G(CH_2O)$ on $D^{-\frac{1}{2}}$ predicted by equation (v) is born out by experiment (Figure III-18). However, an intercept of 50 G units is obtained from the experimental data and equation (v) predicts an intercept of zero. This discrepancy is not understood.

Arrhenius plots for nitrogen and formaldehyde are given in Figure III-19. The conditions for the temperature study were 96 mM nitrous oxide and 0.53 ± 0.03 M methanol, so equation (v) is applicable. Therefore the slope of the line, which is the same for N_2 as for CH_2O, gives $1/2E_{32} + 1/2E_{33} - 1/2E_{37} = 8$ kcal/mol. Reaction (37) is assumed to be diffusion controlled so that its activation energy is about 3 kcal/mol. Setting E_{37} to 3 kcal/mol gives $E_{32} + E_{33} = 19$ kcal/mol. It is not possible from the present work to determine individual values for E_{32} and E_{33}.

The yield of N_2 under all conditions studied was higher than the yield of formaldehyde (Figure III-16, III-17, III-18 and III-19), while the mechanism predicts that the N_2 and CH_2O yields should be the same. Radiolysis of water containing nitrous oxide in the absence of methanol at 300°C yielded a $G(N_2)$ of ~9, Table III-16 and Figure III-16. This could account for some of the difference between the N_2 and CH_2O yields from samples containing methanol. The remaining difference is most likely due to the consumption of CH_2O by reaction. A sample containing 9×10^{-5} M CH_2O and 97 mM N_2O was irradiated at 300°C. All the formaldehyde was consumed and 87 G units of N_2 and 7 G units of CO were produced. The consumption of CH_2O represents $G(-CH_2O) = 35$, so about 2 molecules of N_2 result from the consumption of one CH_2O molecule. No further study was done on the system but this was considered sufficient evidence that formaldehyde can be consumed by a chain reaction in this system. To explain the difference between the N_2 and formaldehyde yields requires that 8% of the initial CH_2O formed reacts further to produce nitrogen. If formaldehyde is in fact reacting to produce nitrogen, the real values of k_{32} and k_{33} would be less than those reported here.

H. Analysis of the N_2O-2-Propanol-Water System

If it is assumed that reactions (32) and (34) are important propagation processes, that reaction (33) is unimportant, and that termination is by (36) and (37), then a steady state treatment leads to a third order equation (see Appendix B for derivation).

$$k_{36}k_{37}[\cdot C(CH_3)_2OH]^3 + (k_{32}k_{37}[N_2O] + k_{34}k_{36}[HC(CH_3)_2OH])[\cdot C(CH_3)_2OH]^2 - k_{37}I[\cdot C(CH_3)_2OH] - k_{34}I[HC(CH_3)_2OH] = 0 \qquad \text{(vii)}$$

The value of k_{36}, the rate constant for the recombination and disproportionation of two $\cdot C(CH_3)_2OH$ radicals, is 0.7×10^9 l/mol s in water at room temperature (64). A good estimate for k_{36} at 300°C is 1×10^{10} l/mol s as discussed in the previous section. A value of 1×10^{10} l/mol s is assumed for k_{37} at 300°C.

The line drawn through the data in Figure III-20 is calculated using $k_{32} = 2.9 \times 10^6$ l/mol s and $k_{34} = 8.7 \times 10^3$ l/mol s. There is considerable scatter in the experimental data in Figure III-20 but the points indicate that $G(N_2)$ and $G((CH_3)_2CO)$ vary linearly with the square root of the N_2O concentration for $[N_2O]^{\frac{1}{2}} \geq 0.06$. This can be understood by realizing that for high concentrations of N_2O the $[\cdot C(CH_3)_2OH]$ will be small so it is reasonable to neglect the contribution of reaction

(36) to termination under these conditions. A steady state treatment assuming that reaction 37 is the only mode of termination leads to equation (viii) (Appendix B)

$$G(N_2) = G((CH_3)_2CO) = (G_{int})^{\frac{1}{2}}\left(\frac{k_{32}k_{34}}{k_{37}}\right)^{\frac{1}{2}} \frac{[N_2O]^{\frac{1}{2}}(HC(CH_3)_2OH]^{\frac{1}{2}}}{(10^{-2}\ D)^{\frac{1}{2}}} \qquad \text{(viii)}$$

For a constant 2-propanol concentration equation (viii) predicts a linear dependence of $G(N_2)$ and $G((CH_3)_2CO)$ on the square root of the N_2O concentration.

At low N_2O concentration the $\cdot C(CH_3)_2OH$ concentration will be increased and termination by reaction (36) will be more important. Considering the extreme case where reaction (36) is the only mode of termination leads to the expression

$$G(N_2) = G((CH_3)_2CO) = (G_{int})^{\frac{1}{2}} \frac{k_{32}}{(k_{36})^{\frac{1}{2}}} \frac{[N_2O]}{(10^{-2}\ D)^{\frac{1}{2}}} \qquad \text{(ix)}$$

The data in Figure III-20 appear to show a first order dependence on the N_2O concentration for $[N_2O]^{\frac{1}{2}} \leq \sim 0.02$ $M^{\frac{1}{2}}$, in agreement with equation (ix). The calculated curve obtained using the general equation (vii) fits the data reasonably well at all nitrous oxide concentrations studied (Figure III-20).

If one considers reactions (37) and (38) to be the important termination reactions and propagation by 32 and 34, then equation (x) can be derived (Appendix C).

$$k_{37}k_{38}[\cdot OC(CH_3)_2OH]^3 + (k_{32}k_{38}[N_2O] + k_{34}k_{37}[HC(CH_3)_2OH][\cdot OC(CH_3)_2OH]^2$$

$$+ k_{37}I[\cdot OC(CH_3)_2OH] - k_{32}I[N_2O] = 0 \qquad (x)$$

The line through the data in Figure III-21 was obtained by solving equation (x) for the $[\cdot OC(CH_3)_2OH]$ and using equation (xi) to calculate $G(N_2)$ and $G((CH_3)_2CO)$.

$$G(N_2) = G((CH_3)_2CO) = \frac{k_{34}[\cdot OC(CH_3)_2OH][HC(CH_3)_2OH]}{10^{-2}\ D} \qquad (xi)$$

To fit the data at low 2-propanol concentrations it was necessary to assume that $k_{38} = 1 \times 10^8$ l/mol s. At higher 2-propanol concentrations reaction 34 will proceed at a higher rate so that the concentration of the $\cdot OC(CH_3)_2OH$ radical concentration will be reduced and termination by reaction (37) becomes more probable. As mentioned above, assuming that reaction (37) is the only termination reaction leads to equation (ix) so that a square root dependnece of $G(N_2)$ and $G((CH_3)_2CC)$ on the 2-propanol concentration is predicted. The $G(N_2)$ and $G((CH_3)_2CO)$ values in Figure III-21 show such a square root dependence for $[\text{2-propanol}]^{\frac{1}{2}} \geq 0.1$.

At lower 2-propanol concentration the $[\cdot OC(CH_3)_2OH]$ will be increased and termination by reaction (38) becomes more probable. If one assumes that reaction 38 is the only mode of termination then reaction (38) can be derived.

$$G(N_2) = G((CH_3)_2CO) = \frac{k_{34}}{(k_{38})^{\frac{1}{2}}} \frac{G(int)^{\frac{1}{2}}[HC(CH_3)_2OH]}{(10^{-2}\ D)^{\frac{1}{2}}} \qquad \text{(xii)}$$

The bending of the experimental data at [2-propanol]$^{\frac{1}{2}} \leq$ 0.1 $M^{\frac{1}{2}}$ (Figure III-21) is most likely due to a change to first order dependence on 2-propanol concentration as predicted by equation (xii). The calculated curve obtained from equations (x) and (xi) fits the data reasonably well for all 2-propanol concentrations studied (Figure III-21).

It should be pointed out that the 2-propanol concentration study involved a high enough N_2O concentration that equation (viii) is applicable at higher 2-propanol concentrations (Figures III-20 and III-21). The N_2O concentration was varied while keeping the 2-propanol concentration large enough that equation (viii) applies at higher N_2O concentrations (Figures III-20 and III-21). The plot of $G(N_2)$ and $G((CH_3)_2CO)$ against the square root of the N_2O concentration (Figure III-20) is curved at the bottom because of a change from termination mainly by reaction (37) at high N_2O concentration to termination mainly by 36 at low N_2O concentration. The plot of $G(N_2)$ and $G((CH_3)_2CO)$ versus the square root of the 2-propanol concentration (Figure III-21) is curved at the bottom because of a change from termination mainly by reaction 37 at high 2-propanol concentration to termination by reaction (37) at lower 2-propanol con-

centration.

Figure III-22 shows the dependence of $G(N_2)$ and $G((CH_3)_2CO)$ on the dose rate. The study was carried out using 8.7 $\pm$ 0.4 mM nitrous oxide and 0.3 M 2-propanol. These are conditions where equation (viii) is applicable, as discussed above, so that a linear dependence of both $G(N_2)$ and $G((CH_3)_2CO)$ on the reciprocal of the square root of the dose rate is predicted. The data in Figure III-22 indicate a curvature for lower dose rates but a reasonable linear dependence for higher dose rates.

The temperature study was performed using conditions where equation (viii) is applicable, 8.7 $\pm$ 0.4 mM nitrous oxide and 0.3 M 2-propanol. The mechanism predicts that $G(N_2)$ and $G((CH_3)_2CO)$ should show the same temperature behavior. The data in Figure III-23 indicate that this is the case, as $G(N_2)$ and $G((CH_3)_2CO)$ yield the same Arrhenius plot. The slope of the line in Figure III-23 yields $1/2E_{32} + 1/2E_{34} - 1/2E_{37} = 15$ kcal/mol. Assigning E_{37} a value of 3 kcal/mol gives $E_{32} + E_{34} = 33$ kcal/mol. As in the methanol system it is not possible to determine individual values for the activation energies.

I. Effect of Adding Acetone to the 2-Propanol System

In Table III-25 the results obtained by adding acetone to the 2-propanol system are presented. Acetone

is a good electron scavenger with a rate constant for reaction with hydrated electrons of ~6 x 10^9 l/mol s at room temperature (66). The reaction of N_2O with hydrated electrons at room temperature has a rate constant of 10^{10} l/mol s (16). If the mechanism were ionic one would expect that 0.02 M acetone would be sufficient to reduce the chain length substantially in a sample containing 3.8 mM N_2O, and the first two samples listed in Table III-25 indicate that this is not the case. Even the addition of 0.3 M acetone only reduced the yield of N_2 from about 1000 to 428 (Table III-25). These results support the hypothesis that the chain process responsible for the high yields of N_2 and acetone in this system is a free-radical chain.

J. Concluding Remarks Concerning the Chain Mechanism

The high yields of products from both aqueous alcohol systems containing N_2O are explained by a radiation induced chain process. The proposed mechanism involves the transfer of an oxygen atom from N_2O to a $\cdot CR_2OH$ radical, producing an $\cdot OCR_2OH$ radical. The system containing methanol shows different kinetic behavior than the 2-propanol system because in the methanol system the $\cdot OCR_2OH$ reacts with water while in the 2-propanol solution the reaction is with the alcohol. The mechanism proposed for the methanol system is supported by: a

dependence of the G values on the square root of the N_2O concentration, G values that are independent of the methanol concentration, linear dependence of the G values on $D^{-\frac{1}{2}}$, and an Arrhenius plot which gives the same slope for both $G(N_2)$ and $G(CH_2O)$. The support for the mechanism used to explain results from the 2-propanol system can be described roughly as: a linear dependence of $G(N_2)$ and $G((CH_3)_2CO)$ on the square root of both the N_2O and the 2-propanol concentrations, a linear dependence of the G values on $D^{-\frac{1}{2}}$ for large dose rates, and the same Arrhenius parameters for both $G(N_2)$ and $G((CH_3)_2CO)$.

REFERENCES

1. J. W. T. Spinks and R. J. Woods. 'An Introduction to Radiation Chemistry', Wiley, New York (1964).
2. A. Mozumder and J. L. Magee. Model of Tracks of Ionizing Radiation for Radical Mechanisms, Radiat. Res. 29, 203 (1966).
3. I. G. Draganic and Z. D. Draganic. 'The Radiation Chemistry of Water', Academic Press, New York (1971).
4. J. C. Russell and G. R. Freeman. J. Chem. Phys., 48, 90 (1968).
5. K. M. Bansal and G. R. Freeman, Radiation Res. Rev., 3, 209 (1971).
6. F. S. Dainton and D. B. Peterson. Nature, London, 186, 878 (1960).
7. F. S. Dainton and S. A. Sills, Nature, London, 186, 879 (1960).
8. F. S. Dainton and D. B. Peterson. Proc. Roy. Soc., London, Ser. A, 267, 443 (1962).
9. F. S. Dainton and W. S. Watt. Proc. Roy. Soc. London, Ser. A, 275, 447 (1963).
10. J. T. Allan and C. M. Beck. J. Am. Chem. Soc., 86, 1483 (196 .
11. G. Scholer and M. Simic. J. Phys. Chem., 68(7), 1731 (1964).

12. F. S. Dainton and S. R. Logan, Trans. Faraday Soc., 61, 715 (1965).

13. G. V. Buxton and F. S. Dainton, Proc. Roy. Soc., London, Ser. A, 287, 427 (1965).

14. D. C. Walker. Can. J. Chem., 44, 2226 (1966).

15. D. C. Walker. Can. J. Chem., 45, 807 (1967).

16. D. A. Head and D. C. Walker. Can. J. Chem., 45, 2051 (1967).

17. C. H. Cheek and J. W. Swinnerton, J. Phys. Chem., 68, 1429 (1964).

18. F. S. Dainton and D. C. Walker. Proc. Roy. Soc., London, Ser. A, 285, 339 (1965).

19. C. H. Cheek. J. Phys. Chem., 71, 2363 (1967).

20. G. Scholer, M. Simic and J. J. Weiss, Disc. Faraday Soc., 36, 214 (1963).

21. F. S. Dainton, A. R. Gibbs, D. S. Smithies. Trans. Faraday Soc., 62, 3170 (1966).

22. C. E. Burchill and G. P. Wollner. Can. J. Chem., 50, 11 (1972).

23. A. O. Allen, 'The Radiation Chemistry of Water and Aqueous Solutions', D. van Nostrand, Princeton, N. J. (1961).

24. C. E. Bricker and H. R. Johnson. Ind. Eng. Chem. Anal. Ed. 17, 400 (1945).

25. R. L. Shriner, R. C. Fuson and D. Y. Curtin. 'The Systematic Identification of Organic Compounds',

J. Wiley and Sons Inc. N.Y. (1956).

26. S. Berntsson. Anal. Chem., 28, 1337 (1956).

27. W. F. Linke (Ed.) 'Solubilities of Inorganic and Metal Organic Compounds', 2, 576, 794, 1229, American Chemical Society (1965).

28. W. Schröder. Chemie-Ing-Techn., 45, 603 (1973).

29. R. A. Holroyd. J. Phys. Chem., 72, 759 (1968).

30. G. Scholes and M. Simic. Nature 202, 895 (1964).

31. G. Scholes, M. Simic, G. E. Adams, J. W. Boag and B. D. Michael. Nature 204, 1187 (1964).

32. Y. Okada. J. Phys. Chem., 68, 2120 (1964).

33. S. Takao, Y. Hatano and S. Shida. J. Phys. Chem., 75, 3178 (1971).

34. R. R. Hentz and S. J. Rzad. J. Phys. Chem., 72, 1027 (1968).

35. K. Takeuchi, K. Shinsaka, S. Takao, Y. Hatano and S. Shida. Bull Chem. Soc. Japan, 44, 2004 (1971).

36. R. R. Hentz and R. J. Knight. J. Phys. Chem., 72, 4684 (1968).

37. N. H. Sagert, R. W. Robinson and A. S. Blair. Can. J. Chem., 46, 3512 (1968).

38. J. M. Warman, K. D. Asmus and R. H. Shuler. Advan. Chem. Ser., 82, 25 (1968).

39. P. J. Dyne. Can. J. Chem. 43, 1080 (1965).

40. M. G. Robinson and G. R. Freeman. J. Chem. Phys., 48, 983 (1968).

41. G. Meissner and A. Henglein. Bunginger Physik. Chem., 69, 264 (1965).

42. R. A Oiroyd. Advan. Chem. Series 82, 488 (1968).

43. B. Blackburn and A. Charlesby. Nature, 210, 1036 (1966).

44. G. R. A. Johnson and J. M. Warman. Trans. Faraday Soc., 61, 1709 (1965).

45. J. W. Warman. Nature 213, 381 (1967).

46. G. R. A. Johnson and M. Simic. J. Phys. Chem., 71, 1118 (1967).

47. L. A. Rajbenback. J. Am. Chem. Soc., 47, 242 (1967).

48. J. M. Warman. J Phys. Chem., 71, 4066 (1967).

49. N. H. Sagert and A. S. Blair. Can. J. Chem., 45, 1351 (1967).

50. W. J. Holtslander and G. R. Freeman. Can. J. Chem., 45, 1661 (1967).

51. J. C. Russell and G. R. Freeman. J. Phys. Chem., 72, 808 (1968).

52. J. C. Russell and G. R. Freeman. J. Phys. Chem., 72, 816 (1968).

53. K. N. Jha and G. R. Freeman. J. Chem. Phys., 51, 2846 (1969).

5. Haissinsky. J. Chim. Physique, 62, 1149 (1965).

55. J. Rabani and G. Stein. J. Chem. Phys., 37, 1865 (1962).

56. K. N. Jha, T. G. Ryan and G. R. Freeman. J. Phys. Chem., 79, 868 (1975).

57. F. S. Dainton, A. R. Gibbs and D. Smithies. Trans. Faraday Soc., 62, 3170 (1966).

58. T. K. Cooper, D. C. Walker, H. A. Gillis and N. V. Klassen. Can. J. Chem., 51, 2195 (1973).

59. W. A. Seddon, J. W. Fletcher, J. Jevack, and F. C. Sopchysuyn. Can. J. Chem., 51, 3653 (1973).

60. A. Kato and R. J. Cvetanovic. Can. J. Chem., 46, 235 (1968).

61. R. R. Baldwin, A. Gethin, J. Plaistowe, and R. W. Walker. J. Chem. Soc. Faraday I, 71, 1265 (1975).

62. J. G. Calvert and J. N. Pitts, 'Photochemistry', J. Wiley, New York (1966) pp.824-826.

63. Y. Ogata and A. Kawasaki, 'Chem. Carbonyl Compounds', Interscience Publishers, 2, 1-69 (1970).

64. M. Simic, P. Neta and E. Hayon, J. Phys. Chem., 73, 3794 (1969).

65. E. F. Caldin, 'Fast Reactions in Solution', J. Wiley & Sons Inc. N.Y. (1964) p.12.

66. Z. D. Draganic and I. G. Draganic, J. Phys. Chem., 75, 3950 (1971).

PART II

ELECTRON RANGES AND MOBILITIES IN HYDROCARBONS

V INTRODUCTION

A. General

Measurement of radiation induced electrical conductance in hydrocarbons makes possible the estimation of penetration ranges of low energy electrons and the measurement of the mobilities of thermal electrons in liquids. The measurement of penetration ranges and the associated energy loss processes of low energy electrons (<10 eV) has not previously been possible in liquids. Ranges and mobilities give new information about the behavior of electrons in matter.

The first X ray induced conductance experiments on dielectric liquids were carried out by Pierre Curie in 1902 (1). In the 1940's X ray induced conductance was observed in liquid nitrogen and liquid helium by Gerritsen (2). With field strengths up to 20 kV/cm ionization currents up to 40 picoamps were obtained. The current was directly proportional to the voltage in liquid nitrogen at 77K but in liquid helium between 1 and 4K the curves showed a tendency towards saturation.

Gamma radiation induced conductance in liquid hydrocarbons was studied by Freeman (3-5). Field strengths up to 70 kV/cm and dose rates of 10^{15} eV/cm^3 were used. Conductances measured were between 10^{-9} and

10^{-12} mho and showed a sharp sensitivity to impurities in the liquids. Two liquids, n-hexane and cyclohexane were studied and the effect of a number of additives was examined. The influence of dose rate, temperature, and liquid viscosity was determined and the results were interpreted by means of the Onsager theory (6).

Ionization currents produced by soft X rays were determined for a wide range of liquids by Ullmaier (7). Field strengths up to 50 kV/cm were used and ionization currents versus field strength were plotted for each liquid. The more branched hydrocarbons tended to give larger ionization currents than the straight chain hydrocarbons. For example, n-pentane gave 1.82×10^{-9} A at a dose rate of 2.14×10^{12} eV/s while 2,2,4-trimethylpentan yielded a current of 3.21×10^{-9} A for a dose rate of 2.35×10^{12} eV/s, both measured at 50 kV/cm.

Allen and Hummel (8,9) studied X ray induced conductance in n-hexane and extended the method to the determination of positive and negative ion mobilities. They obtained a free ion yield in n-hexane of 0.09 molecules/1 eV indicating that practically all electrons produced in spurs react with the positive ions before they can escape.

The influence of dielectric constant on the free ion yield produced from the γ radiolysis in liquids was examined using a conductance method (10). It was found

that the free ion yield increased with increasing dielectric constant. Normal hexane with a dielectric constant of 1.9 gave a free ion yield of 0.10. The dielectric constant of n-butyl chloride is 7.2 and the free ion yield was found to be 0.39.

The effect of temperature on positive and negative ion mobilities in liquid n-hexane was examined by Hummel, Allen and Watson (11) using irradiation by 1.5 MeV X rays. They found that the activation energy for positive and negative ion mobilities were 0.09 eV and 0.125 eV respectively. The results agreed reasonably well with those obtained earlier by photoinjection technique (12-14).

B. Mobilities of Electrons in Liquids

The mobilities of electrons in liquid rare gases were measured extensively between 1950 and 1970 (15-19) but until 1964 no estimates of electron mobilities in liquid hydrocarbons existed. The first evidence that these measurements could be made was obtained by Samuel and co-workers (20). They used pulses about 30 μs in length from a Co^{60} source and irradiated two pure liquids; n-hexane and n-octacosane. They carried out extensive purification on the liquids and obtained signals that were 10^5 times larger than had previously been observed. The results were explained by postulating that electrons in the liquid were the fast charge carriers and

had mobilities of >10 cm^2/V s at room temperature. They assumed that previous workers had failed to purify the liquid hydrocarbon sufficiently so that electrons were scavenged by impurity and became negative ions with mobilities of $\sim 10^{-3}$ cm^2/V s.

The first solid evidence that electron mobilities in liquid hydrocarbons could be quantitatively determined was obtained by Tewari and Freeman (21). When measuring ion mobilities in neopentane and neohexane they observed a sharp spike on the oscilloscope trace indicating the presence of fast charge carriers. The fast signal was not removed by adding olefin but when electron scavengers oxygen or sulfur hexafluoride were added to a sample the spike disappeared and the slow ion signal remained. The mobility of the species responsible for the fast decay could not be determined as the time constant of the measuring circuit was much too large. A further study was carried out where the speed of the circuit was increased by a factor of 1000 (22), and the signal in argon and neopentane was examined. The circuit was still too slow to measure the mobilities but the fact that argon and neopentane gave about the same signal shape showed that the signal from neopentane was due to electrons. A number of laboratories began measuring electron mobilities in liquid hydrocarbons and other liquids (23-25). Minday,

Schmidt and Davis (23) estimated that the mobility of electrons in liquid normal hexane was around 1 $cm^2/V\ s$ at room temperature. Schmidt and Allen (24) obtained a mobility of 93 cm^2/V for electrons in liquid tetramethylsilane at room temperature. Conrad and Silverman (25) determined the electron mobility in liquid n-hexane to be 0.21 - 0.23 $cm^2/V\ s$ at 23°C. A great deal of work has now been done on the determination of free ion yields and measurement of electron mobility in liquids (26-60).

C. Theory

When γ-radiation is incident on a liquid vents occurring can roughly be described with the foll equations.

$$M \rightsquigarrow [M^+ + e^-] \quad (1)$$

$$[M^+ + e^-] \longrightarrow [M] \text{ (neutralization in the spur)} \quad (2)$$

$$\longrightarrow M^+ + e^- \text{ (free ions)} \quad (3)$$

$$S + e^- \longrightarrow S^- \quad (4)$$

$$\left.\begin{array}{l} M^+ + e^- \longrightarrow M \\ M^+ + S^- \longrightarrow M+S \end{array}\right\} \left(\begin{array}{l}\text{neutralization} \\ \text{in the bulk} \\ \text{medium}\end{array}\right) \quad (5)$$

here S is an electron scavenger. When the irradiated iquid is contained between parallel plates of a conductnce cell, then applying a voltage adds an additional rocess to the above description

$$M^+, e^-, S^- \longrightarrow \text{collection at the electrodes} \quad (6)$$

When the electric field is weak the collection (reaction 6) cannot compete with spur neutralization (reaction 2) and is in competition with bulk medium neutralization (reaction 5). The collection of all free ions by this technique provides a means of measuring the free ion yield, the number of free ion pairs produced per 100 eV of energy absorbed. The yield is symbolized by G_{fi}.

There are several problems associated with this type of measurement.

1. The rate at which free ions are collected must be fast enough that the number of free ions lost by bulk medium neutralization (reaction 5) is negligible. This problem is solved by putting large voltages on the electrodes and placing them close together. The electric field strength is in units of volts/cm so both these conditions favor an increase in the field strength.

2. The dose must be large enough to give a measurable signal, but not so large as to give a high rate to reaction (5). The dose is about 1 mrad, which is only 10^{-5} as large as those used in optical measurements. In practice short pulses are used, ≤ 1 μs, so that the energy is introduced into the sample in a short time.

3. The yield of reaction (3) can be increased by the electric field. A way must be found to subtract from the total ions collected, the number of ions which have been drawn out of the spur by the electric field and collected. In order to solve this problem a plot of free ion yield versus field strength is extrapolated to zero field and the intercept is taken as the unperturbed free ion yiel

4. One must eliminate from the measurement ions which have been produced in liquid which is not between the electrodes. This problem is solved by shieldin all surfaces of the collecting electrode, except the front surface, with metal shield (a guard electrode).

D. Calculation of Free Ion Yield

The free ion yield is calculated from the number of coulombs collected, after the radiation pulse, and the number of eV of energy absorbed from the pulse by the sample. The equation used is the following

$$G_{fi}{}^{E} = \frac{Q \times 2.64 \times 10^{20}}{ALD} \qquad (i)$$

where $G_{fi}{}^{E}$ is the free ion yield in ion pairs/100 eV at field strength E, Q is the charge collected in coulombs, A is the area of the collection electrode in cm^2, and L

is the distance between the electrodes in cm, D is the dose in eV/cm^3 absorbed from the radiation by the sample between the electrodes.

E. Measurement of Electron Mobility

The electron mobility is determined by measuring the rate at which electrons are collected. In the case where all electrons are collected before they can be scavenged and converted to negative ions, the calculation is simple. Electrons which are close to the collecting electrode after the pulse are collected first, and those which are close to the other electrode are collected last. The time between the collection of the first and last electrons is the time required for electrons to drift the distance L between the electrodes. Therefore

$$v_e = L/\tau \qquad (ii)$$

where v_e is the electron drift velocity in cm/s and τ is the time in seconds between the end of the pulse and the point where the conductance signal reaches zero. The electron mobility μ_e, which is the drift velocity per unit electric field strength, is given by:

$$\mu_e = \frac{L}{\tau E} = \frac{L}{\tau V/L} = \frac{L^2}{\tau V} \qquad (iii)$$

where E is the electric field strength in volts/cm and V is the voltage applied to the electrodes.

When only a fraction of the electrons are collecte before scavenging by impurities it is necessary to use another method that includes in the calculation the total dose absorbed from the pulse. If there is no loss of electrons due to scavenging during the pulse, the current at the end of the pulse is given by:

$$i_o = v_e A C_o \qquad \text{(iv)}$$

where i_o is the current in amps and C_o is the concentration of electrons in coulombs/cm^3. The electron concentration at the end of the pulse can be related to the dose from the pulse and $G_{fi}{}^E$ by the equation:

$$C_o = \frac{10^{-2} D G_{fi}{}^E}{6.24 \times 10^{18}} \qquad \text{(v)}$$

where 6.24×10^{18} is the number of electrons/coulomb. By substituting (v) into (iv) we get

$$i_o = \frac{D G_{fi}{}^E v_e A}{6.24 \times 10^{20}} \qquad \text{(vi)}$$

To convert v_e to μ_e we must divide equation (vi) by E.

$$\frac{i_o}{E} = \frac{D G_{fi}{}^E \mu_e A}{6.24 \times 10^{20}} \qquad \text{(vii)}$$

or

$$\mu_e = \frac{i_o \times 6.24 \times 10^{20}}{D G_{fi}{}^E A E} \qquad \text{(viii)}$$

F. Previous Work on the 3-Methylpentane-2,2,4,4-tetramethylpentane Series

A conductance technique has been used to determine the free ion yields from the γ irradiation of 3-methylpentane, 2,3-dimethylbutane, 3,3-dimethylpentane, 2,2,4-trimethylpentane and 2,2,4,4-tetramethylpentane. The measurements on 2,3-dimethylbutane (28), 3-methylpentane (58) and 2,2,4-trimethylpentane (33) were at room temperature only. The yields in 3,3-dimethylpentane were for the temperature range 197 - 357K (58). Free ion yields have been obtained for 2,2,4,4-tetramethylpentane for the temperature range 212-385K (37).

The mobilities of electrons in all these liquids have also been determined by a conductance technique. The mobilities of electrons in 3-methylpentane have been determined for the temperature range 258 - 371K (58,60), while only room temperature has been studied for 2,3-dimethylbutane (28,58), 2,2,4-trimethylpentane (59) and 3,3-dimethylpentane (58). Electron mobilities in 2,2,4,4-tetramethylpentane have been determined for the temperatures 295 - 385K (37).

G. The Present Work

The present work involves the measurement of free ion yields and mobilities for the above mentioned compounds over practically their entire liquid range, from near their

melting points to above their critical temperatures. For 2,3-dimethylbutane the range of temperatures was from 160 - 510K. The temperature ranges for the other compounds are: 3,methylpentane (142 - 525K), 3,3-dimethylpentane (181 - 555K), 2,2,4-trimethylpentane (240 - 552K) and 2,2,4,4-tetramethylpentane (240 - 556K). The purpose of the study was to compare the temperature effects on electron mobilities in hydrocarbons with very different structures.

VI EXPERIMENTAL

A. Materials

(a) The following chemicals were supplied by Chemical Samples Co.: 2,3-dimethylbutane (99.9%), 3,3-dimethylpentans (99%), 2,2,4-trimethylpentane (99.9%) and 2,2,4,4-tetramethylpentane (99%). The 3-methylpentane was supplied by Aldrich Chemical Co. Inc. and was 99% pure. All of the above chemicals were further purified by the lithium aluminum hydride, sodium potassium alloy technique described below.

(b) Potassium metal was obtained from BDH Chemicals.

(c) Sodium metal (Certified) was obtained from Fisher Scientific Co.

(d) Lithium aluminum hydride was supplied by Ventron Corp.

B. Apparatus and Procedures

(a) The Vacuum System

The main manifold of the vacuum system is virtually the same as shown in Figure II-1 of part 1. The only change made was to remove all stopcocks requiri ease on the upstream side of the mercury diffusion pump.

b) e Sample Preparation Manifold

he ample preparation manifold was divided into

two parts. One part was used for treatment with lithium aluminum hydride and the other part for the sodium potassium alloy process and filling of the sample cells (Figures VI-1 and VI-2).

The first step in the sample preparation was to place about 50 ml of hydrocarbon and about 50 ml of sulfuric acid in a 250 ml volumetric flask containing a two inch Teflon stirring bar. The mixture was stirred for about 24 hours and the layers were then separated using a 500 ml separatory funnel and the hydrocarbon layer was placed in a 250 ml volumetric flask containing two pellets of potassium hydroxide. The flask was shaken for about five minutes and then the contents were allowed to settle for about one hour. The hydrocarbon was then decanted into the 250 ml round bottom flask shown in Figure VI-1, 10 g of lithium aluminum hydride was added, and the Teflon stopcock was screwed on. The contents of the flask were degassed by freeze-pump-thaw cycles and the mixture was stirred for about 24 hours. 40 ml of the liquid was then transferred to T_1, cooled by liquid nitrogen, with constant pumping. Another distillation from T_1 to T_2 was carried out for further degassing and the liquid was then distilled to T_3 (Figure VI-2) while pumping to remove gas. The liquid was then distilled on to the sodium potassium alloy (Figure VI-2), about 2 ml being left behind in T_3. The contents of the alloy trap were stirred for about 48 hours

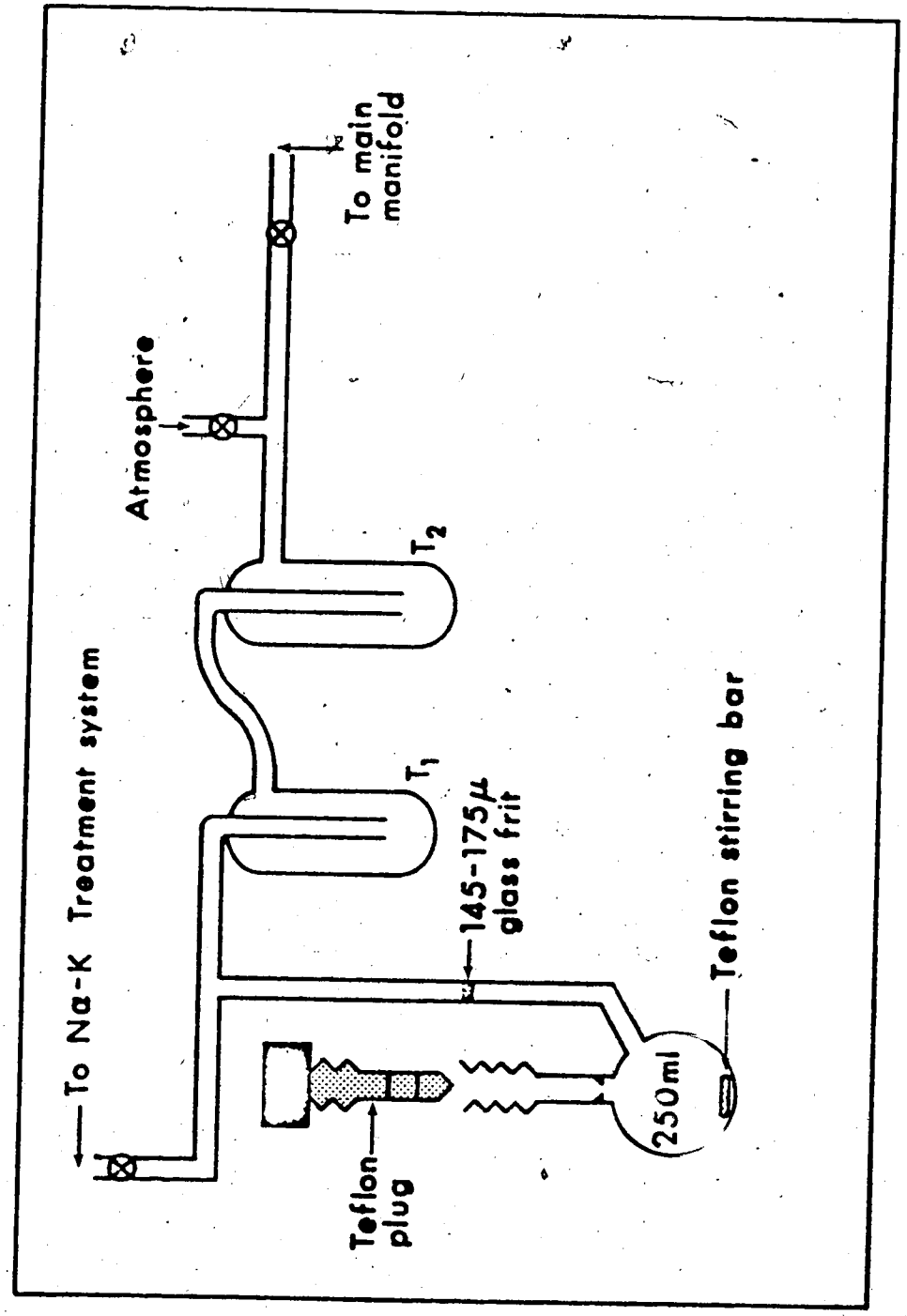

Figure VI-1 Lithium Aluminum Hydride Treatment System

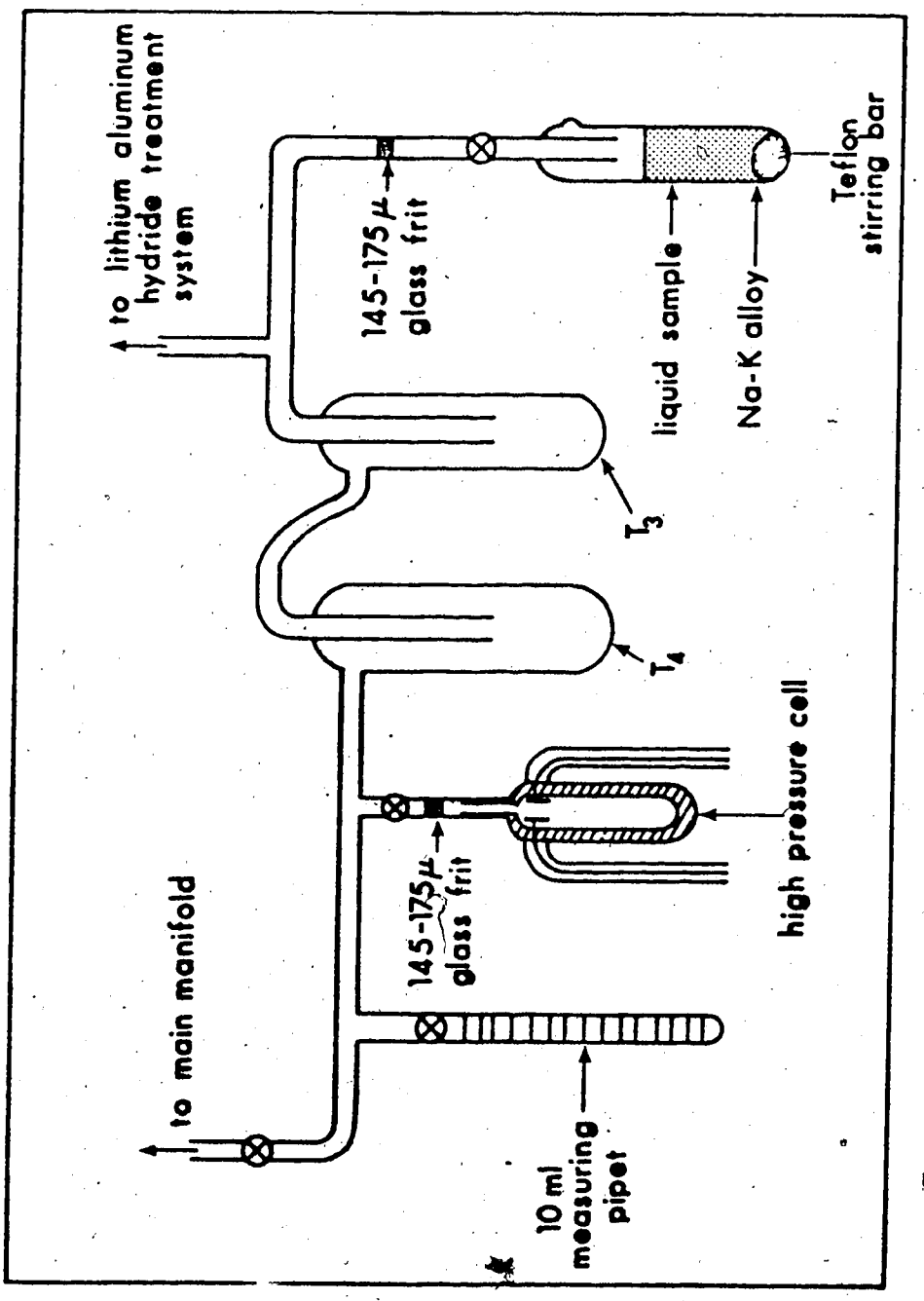

Figure VI-2 System for Na-K treatment and filling cells

and degassed about every 12 hours.

While the hydrocarbon was being pumped on the alloy the high pressure cell was attached to the rack by glass blowing. It was wrapped in heating tape and glass wool and heated to the highest temperature that would be used in the experiment. While hot it was degassed by pumping for about 20 hours and then allowed to cool to room temperature.

When the time came to do the experiment the sample cell was filled by the following procedure. About 15 ml of sample was transferred from the sodium potassium alloy to T_4 with continuous pumping. A Dewar containing liquid nitrogen was then placed around the 10 ml measuring pipet and about 9 ml of sample were distilled into it. The remaining liquid in T_4 was pumped off and the liquid in the measuring tube was degassed by thawing and pumping. The required amount of liquid was then distilled into the cell by putting a Dewar filled with liquid nitrogen around the body of the cell. The high pressure cell was then removed with a torch under continuous pumping.

(c) <u>The High Pressure Cell</u>

The high pressure cell used for the experiments is shown in Figure VI-3. The cell was constructed with Corning 7052 glass with a uranium glass graded seal used to connect the cell to the Pyrex vacuum rack. The body

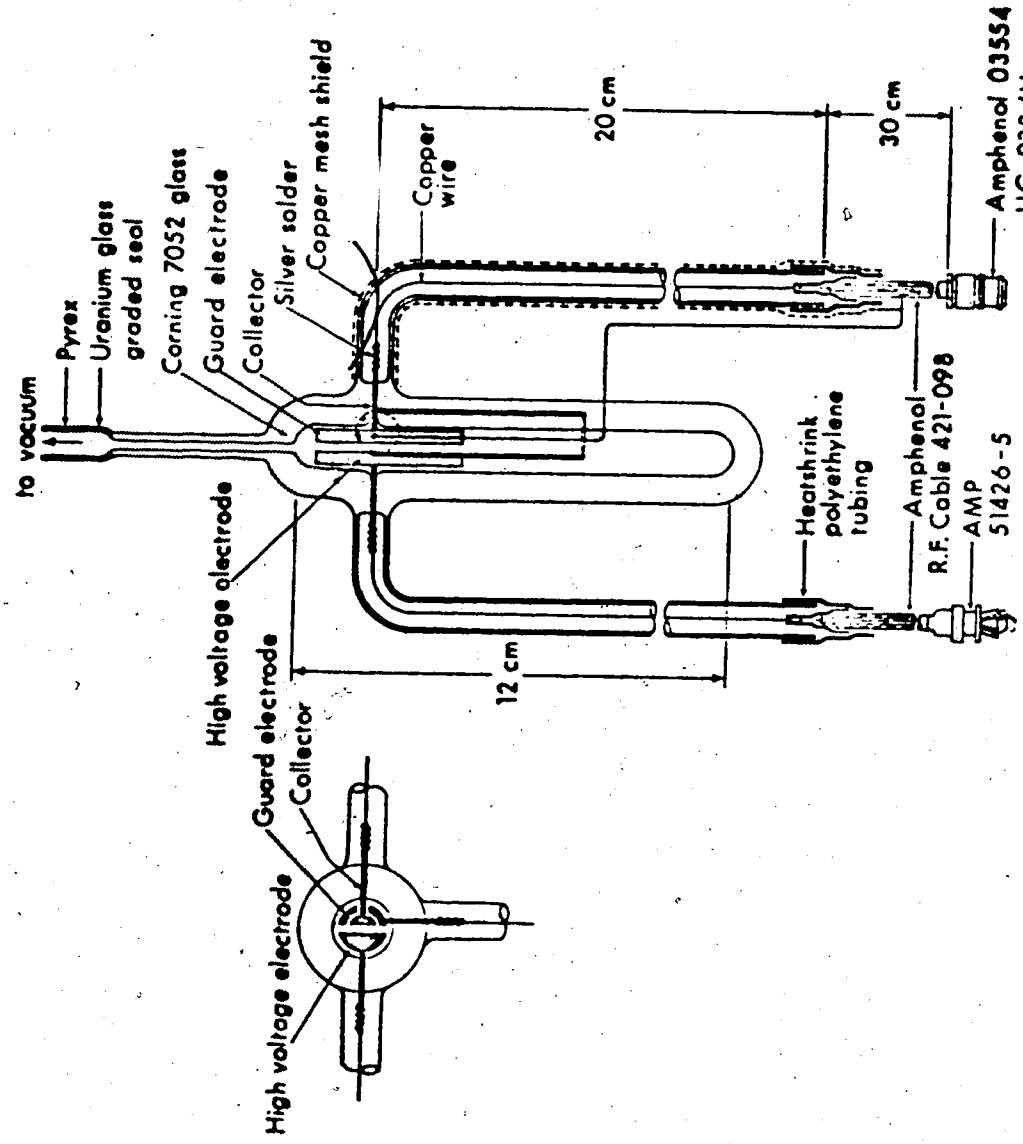

FIGURE VI-3 High Pressure Cell

of the cell was coated on the outside with Aque Dag (G. C. Electronics T.V. tube coat), with a window left in the front and back so that the liquid inside could be observed during the course of the experiment. This was important for determining at what temperature one observed the disappearance of the meniscus and the appearance and disappearance of critical opalescence. The Aqua Daz coating was grounded to the copper braid that shielded the lead to the collector electrode. This was to prevent interference from conductance in the glass. The glass side arm over the high voltage lead was not covered with Aqua Daz as it was found that the coating caused the glass to break more easily.

The distance between the electrode was measured by determining the cell constant conductionmetrically, using standard potassium chloride solutions. The conductance bridge used for this purpose is shown in FigureVI-4. The circuit was designed to maintain the guard and collector electrodes at the same A.C. potential. Over the range 1-3 KHz the cell constant was independent of frequency.

(d) Temperature Control

A box constructed of polystyrene foam was used to achieve low temperatures. A stream of cold nitrogen from a 50 l Dewar of liquid nitrogen was introduced through a port at the bottom of the box. The rate of flow of cold

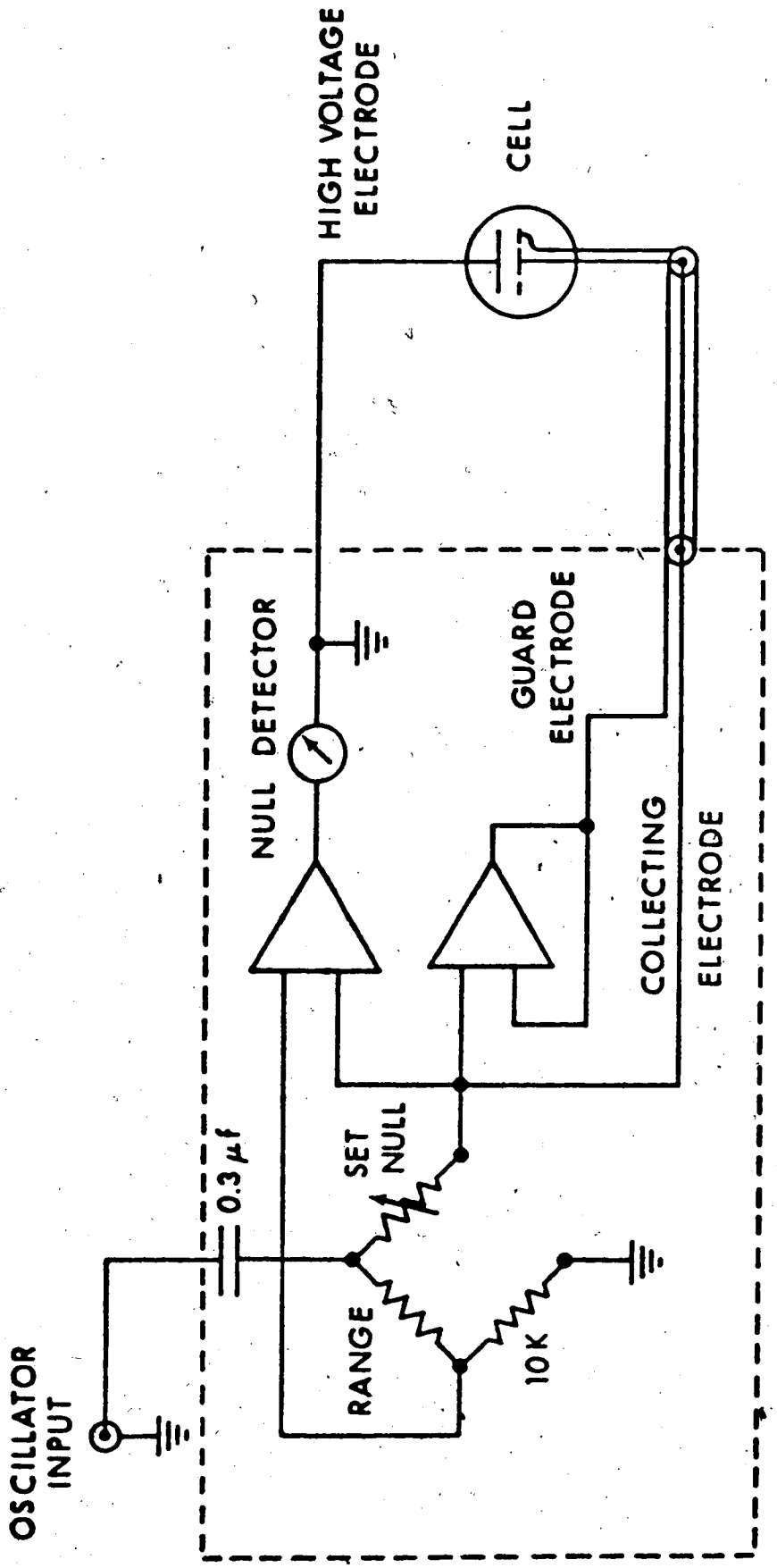

FIGURE VI-4 Circuit for measuring cell constant

nitrogen gas from the Dewar was governed by controlling the current passing through a 1 kW resistance immersed in the liquid nitrogen. The temperature around the cell was determined by two thermocouples which gave readings within 1°C of each other when the temperature was stabilized.

The apparatus used for the high temperature work is shown in Figure VI-5. The high pressure cell was positioned on asbestos supports which were glued to the wall of the clear walled Dewar. A heat gun (Master Appliance Corp. model AH0751) was fitted to a 6 cm diameter glass tube (Figure VI-5). The heating coil in the gun was connected to a LFE Corp. model 226-A21 temperature controller and the heat gun fan was powered from a normal 60 cycle outlet. Two thermocouples were placed as close as possible to the body of the cell and horizontal to the electrodes. One thermocouple was used to record the temperature and the other was connected to the temperature controller. The Faraday cage was constructed of aluminum, with copper screen in holes in the front and back walls so that one could observe the critical point. The thermocouples were calibrated by observing at what temperature the hydrocarbon went critical and correcting the experimental temperatures by comparing with the literature values for the critical temperature of that hydrocarbon. In Figure VI-5 the Dewar is represented as single walled for

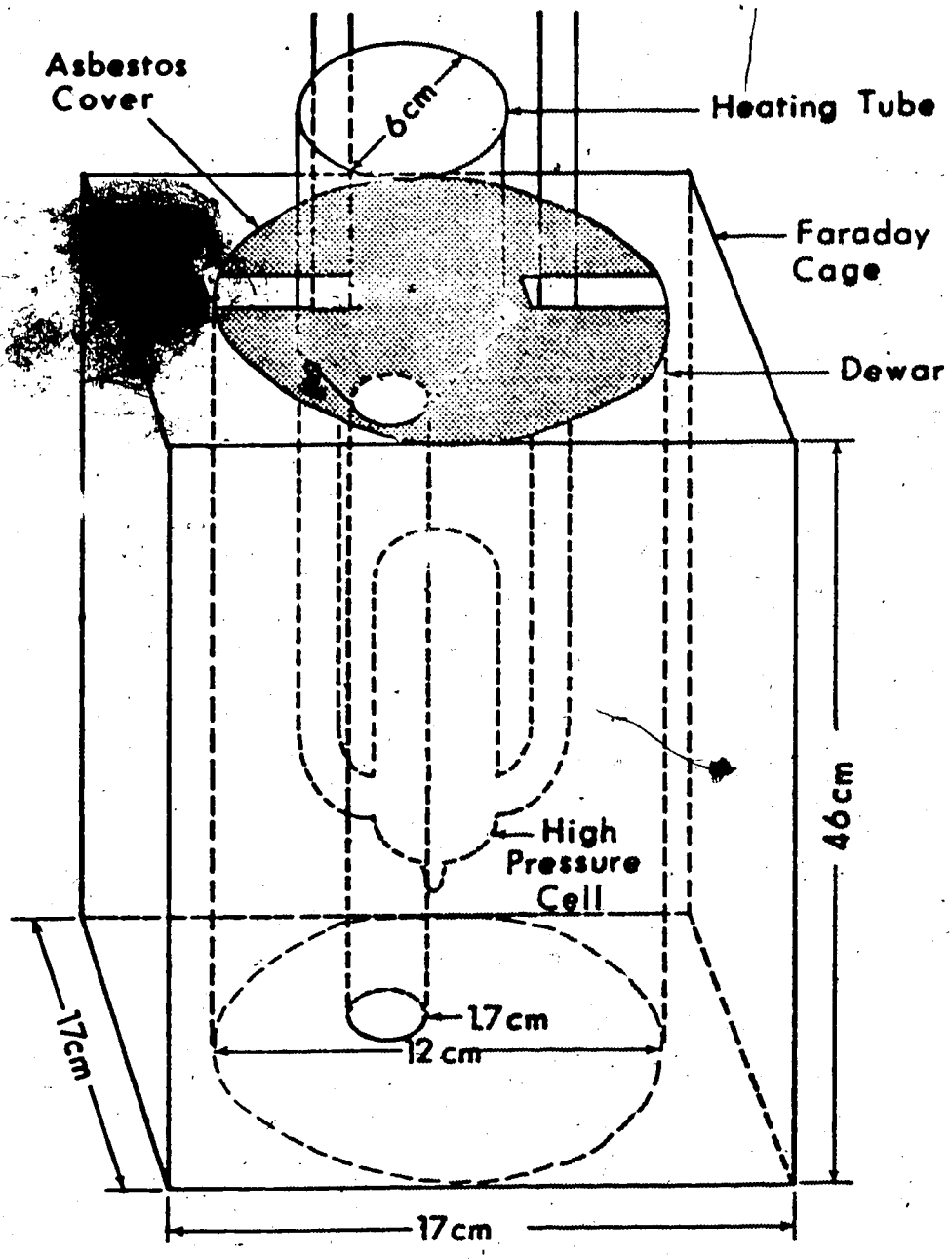

Figure VI-5 High Temperature Apparatus

convenience in drawing and the metal base of the Dewar is not shown.

(e) The Van de Graaff Accelerator

A 2.0 MeV van de Graaff Accelerator manufactured by High Voltage Engineering Corp. was used as the source of high energy electrons. The accelerator was operated at 1.70 MeV for this work and pulse lengths of 100 nanoseconds and 1.0 microseconds were used. The vacuum inside the accelerator beam pipe was of the order of 10^{-7} torr. The beam was focussed by fixing a piece of phosphorescent paper to the end of the accelerator tube. Each pulse of electrons produced a visible glow which could be viewed on closed circuit television. Steering and focussing of the beam was achieved by controlling current to electromagnets.

(f) The Gold Target

The gold target was used to indicate relative dose and to produce X rays to irradiate the sample. The target was placed at the end of the beam pipe and was insulated from ground so that the beam of 1.7 MeV electrons could cause the build up of a charge. The charge created was measured by an Ortec model 439 current digitizer and a TSI model 1535 counter was used to display the signal as picocoulombs of charge.

(g) Mobility Measurement

The circuit used to measure drift times of electrons is shown in Figure VI-6. The apparatus shown in Figure VI-4 was positioned carefully in front of the beam pipe and the signal produced from a pulse of radiation was transmitted through a low noise cable from the target room to the control room. Two amplifiers were used for making the measurements. One had a gain of 100 K and a response time of about 150 ns. The other had a gain of 5 K and a response time of about 100 ns. The exact gain of the amplifier was determined after each experiment. When the signal was large enough the fastest amplifier was always used.

(h) Charge Clearing Experiment

The method used for the charge clearing experiment was originally developed by Schmidt (27,28). The circuit used for this purpose is shown in Figure VI-7. The transient current produced by the collection of ions at the electrodes was integrated and the collected charge measured. The P.A.R. amplifier had an adjustable gain which was set to an appropriate value depending on the size of the signal. The signal was observed on the scope at the same time it was being fed into the Fabritek. When a noisy signal was obtained a large number of signals was averaged.

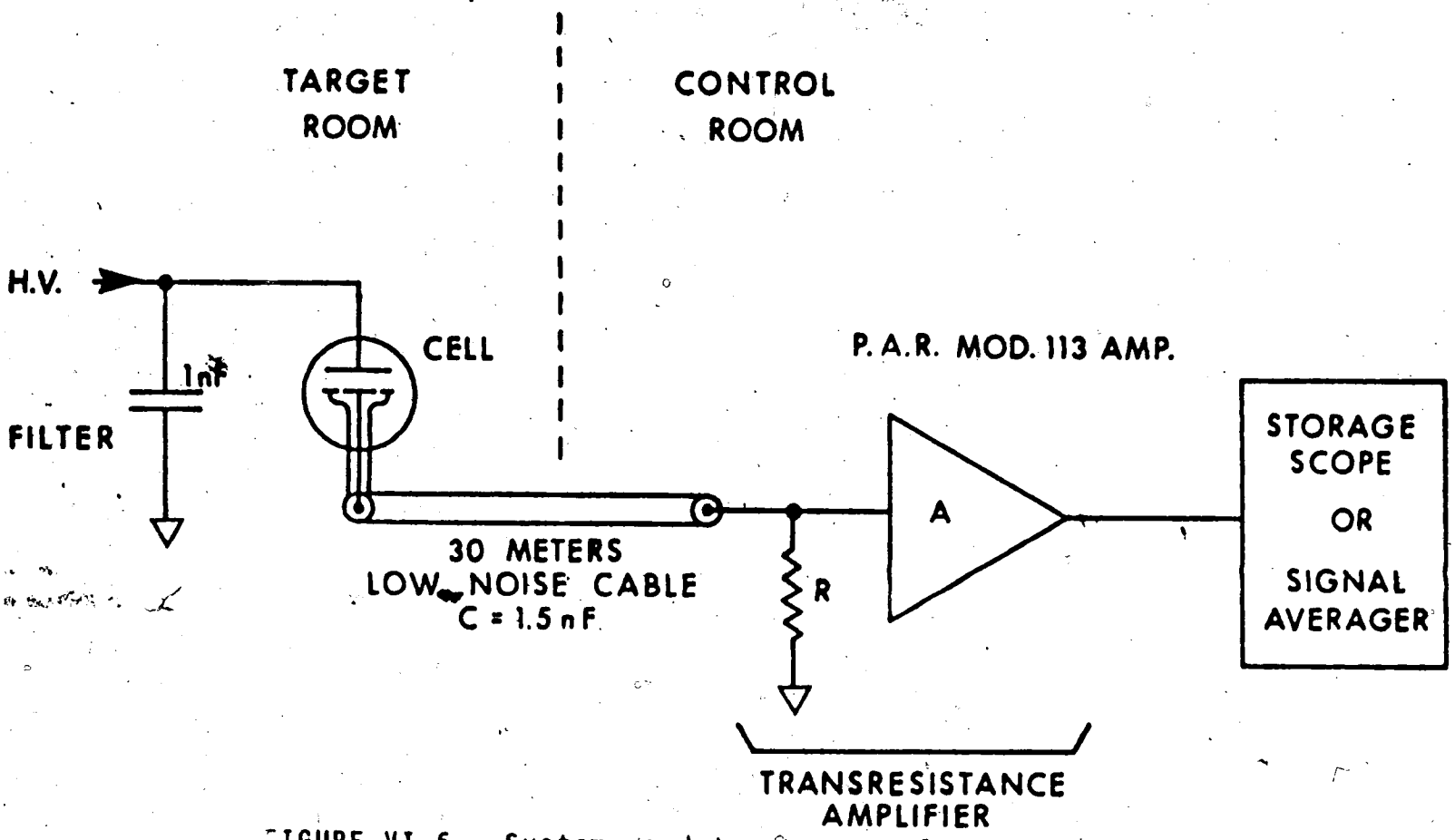

FIGURE VI-6 System used to measure electron mobilities

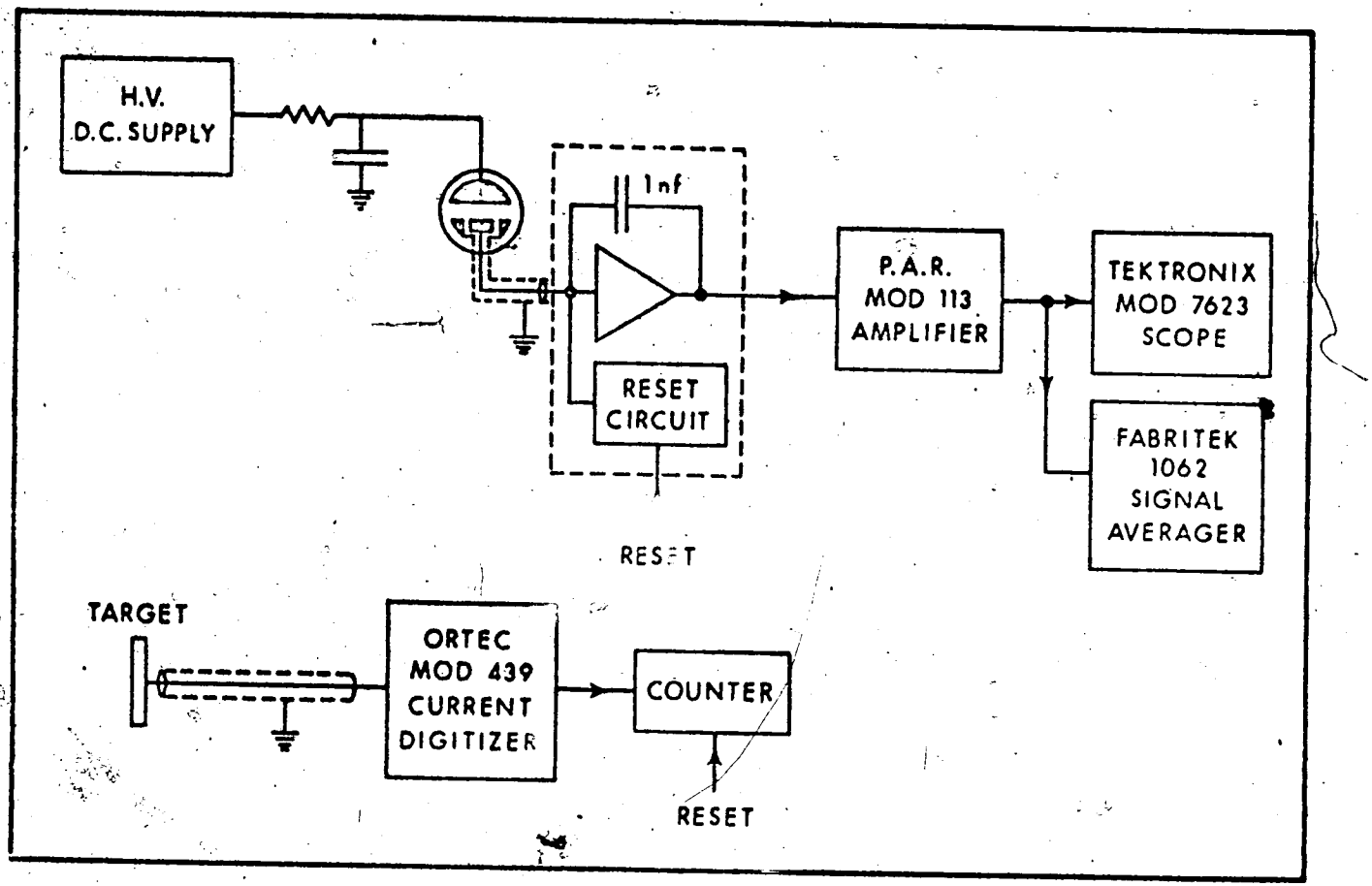

FIGURE VI-7 System for charge clearing experiment

VII RESULTS

A. Free Ion Yields

Figures VII-1 to VII-5 contain plots of free ion yield versus field strength. The solid lines through the points were obtained by methods that will be described in Chapter VIII.

Figure VII-1 shows the results for 2,3-dimethylbutane. Free ion yields are plotted for temperatures between 26.9°C and 227°C and field strengths in the range 3 to 62 kV/cm. The yields are increased by either an increase in the field strength or an increase in the temperature.

Figure VII-2 contains data for 3-methylpentane. Yields are given for temperatures between 26°C and 231.2°C and field strengths from 3 to 45 kV/cm. As with 2,3-dimethylbutane the free ion yield is seen to increase with both temperature and field strength.

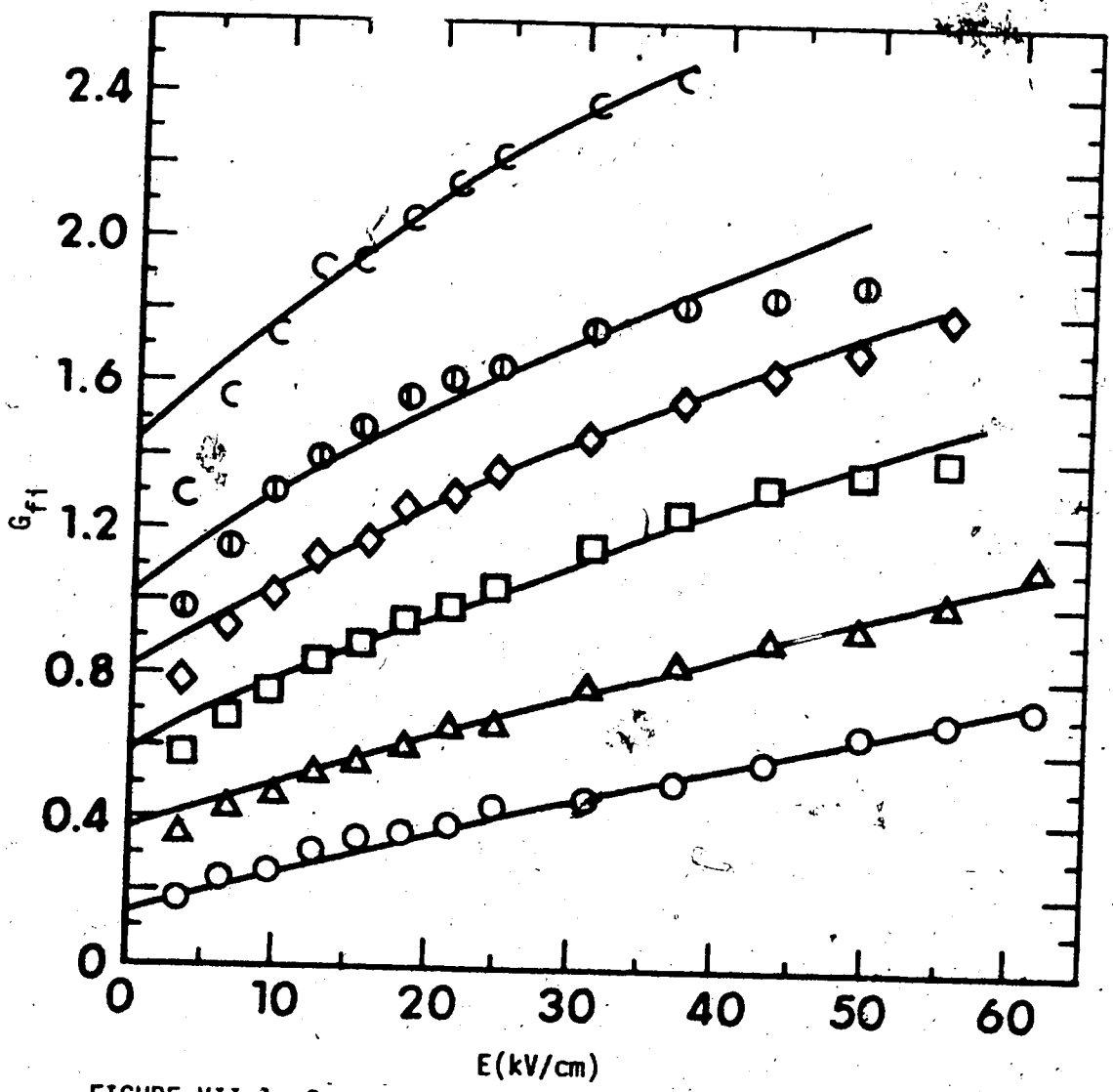

FIGURE VII-1 G_{fi} versus field strength 2,3-dimethylbutane

○, 26.9°C; △, 102°C, □, 156°C; ◇, 184°C; ⊕, 206°C;

C, 227.0°C (critical temp.)

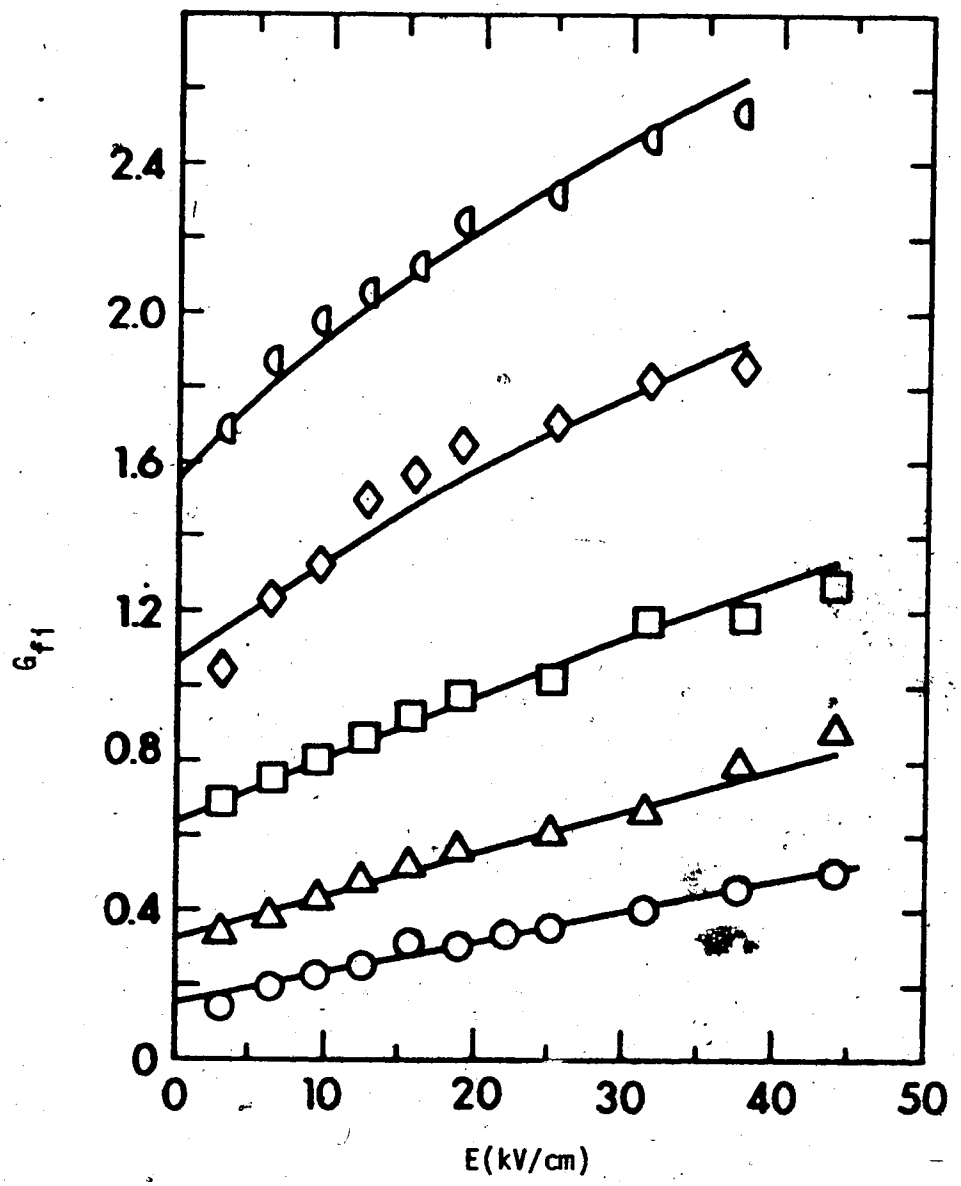

FIGURE VII-2 G_{fi} versus field strength 3-methylpentane

○, 26°C; △, 109°C; □, 171°C; ◇, 215°C;

◁, 231.2°C (critical temp.)

Results are shown in Figure VII-3 for 3,3-dimethylpentane. Data is given for field strengths between 3 and 57 kV/cm and temperatures from -40°C to 263°C.

Free ion yields from 2,2,4-trimethylpentane are shown in Figure VII-4. The field strengths are between 3 and 50 kV/cm and the temperature range is from -33°C to 271°C.

Yields from 2,2,4,4-tetramethylpentane are given in Figure VII-5 for temperatures between -1°C and 227°C and field strengths up to 45 kV/cm. Some yields for negative voltages are also shown and appear to be within experimental error of the yields for positive voltages.

Table VII-1 contains data on the five compounds used in this study. Room temperature and critical densities are shown for each of the paraffins.

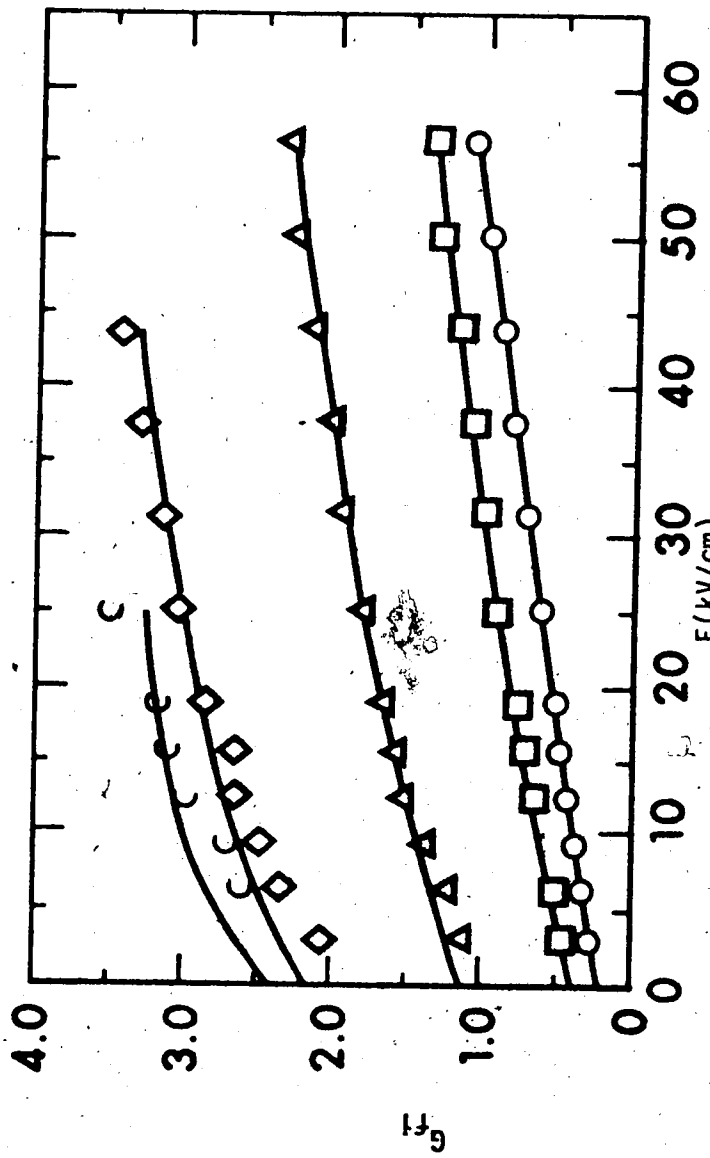

FIGURE VII-3 G_{fi} versus field strength 3,3-dimethylpentane

O, -40°C; □, 27°C; Δ, 169°C; ◇, 247°C; C, 263.0°C (critical temp.)

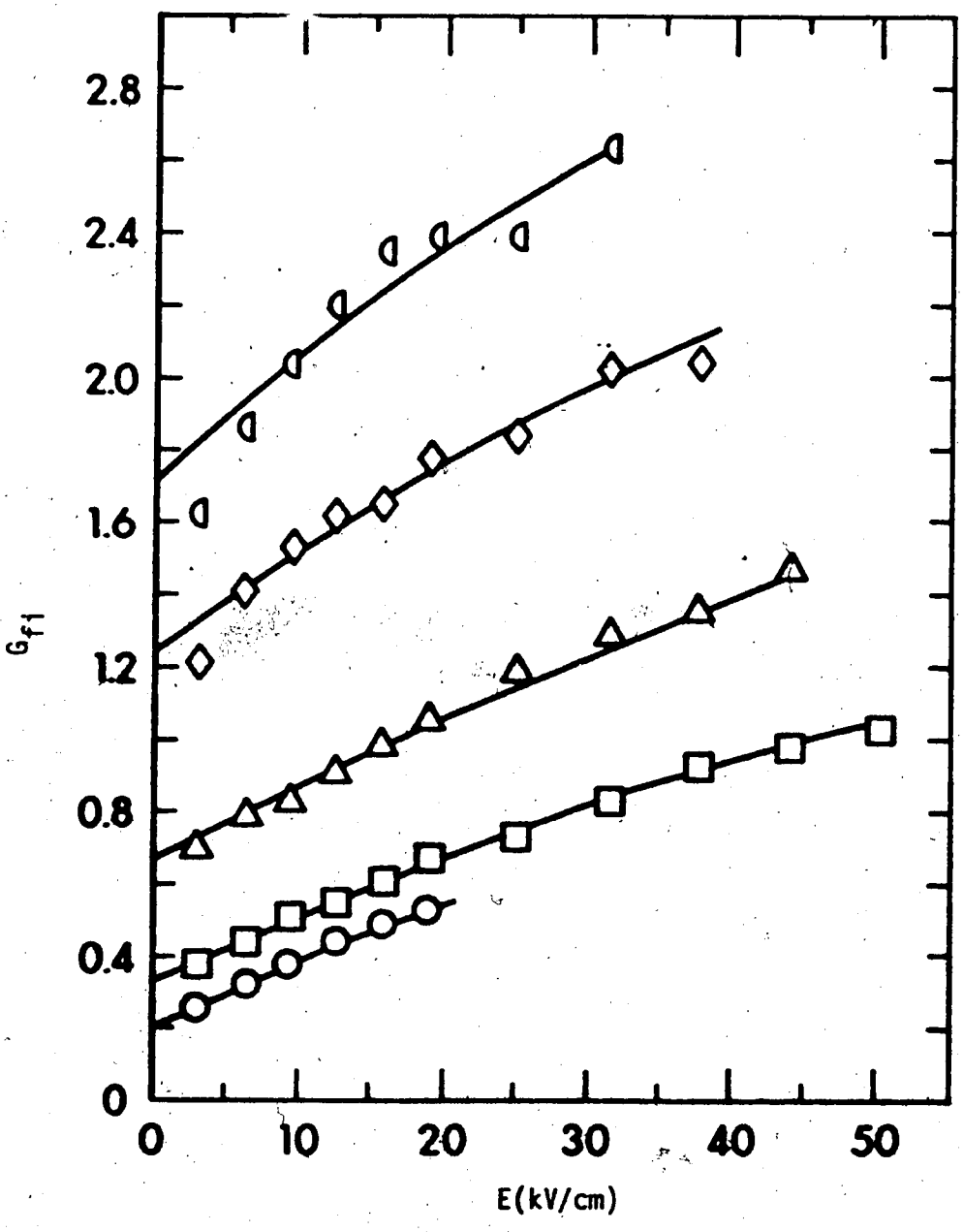

FIGURE VII-4 G_{fi} versus field strength, 2,2,4-trimethylpentane
○, -33°C; □, 26°C; △, 135°C; ◇, 225°C;
◁, 271°C (critical temp.)

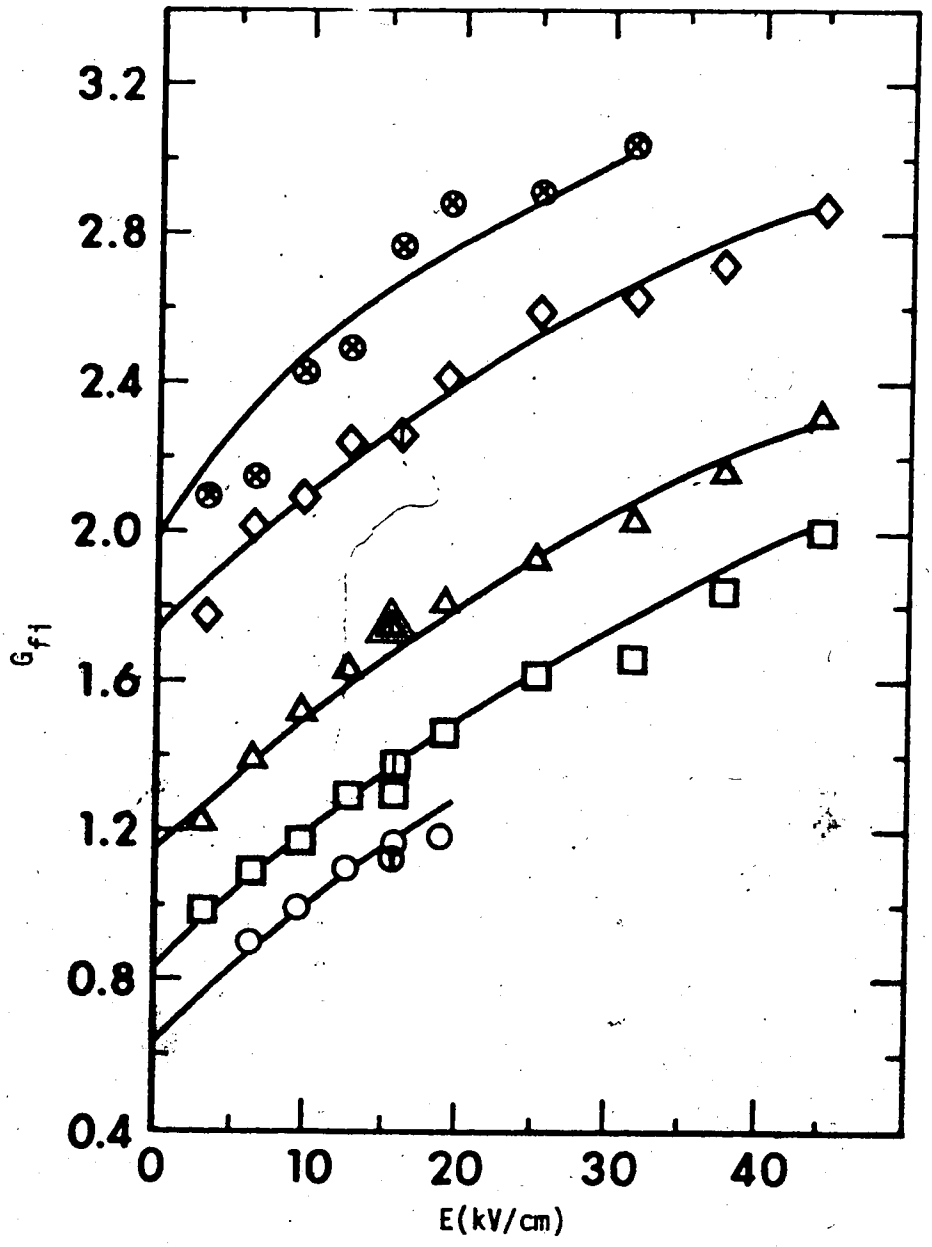

FIGURE VII-5 G_{fi} versus field strength, 2,2,4,4-tetramethylpentane
○, -1.0°C + V; ⊖, -1.0°C-V; □, 27°C + V;
⊟, 27°C - V; △, 115°C + V; ▲, 115°C - V;
◇, 198°C + V; ◈, 198°C - V; ○, 227°C + V.

TABLE VII-1

Physical Properties of Hydrocarbons

Compound	Temperature K	Densit g/ml
2,3-dimethylbutane	293	0.662
	298	0.657
	303	0.652
	500.2*	0.241
3-methylpentane	293	0.664
	298	0.660
	303	0.655
	504.3*	0.235
3,3-dimethylpentane	293	0.693
	298	0.689
	303	0.685
	536.1*	0.239
2,2,4-trimethylpentane	293	0.692
	298	0.688
	303	0.684
	544.3*	0.237
2,2,4,4-tetramethylpentane	293	0.719
	298	0.716
	303	0.712
	556.1*	0.237†

* critical temperature
† assumed value

B. Electron Mobilities

Electron mobilities as a function of field strength at various temperatures are shown in Figures VII-6 to VII-13. Results for 2,3-dimethylbutane are given in Figures VII-6 and VII-7. The mobilities are independent of field strength for temperatures from -46°C to 173°C.

Figures VII-8 and VII-9 show electron mobilities for 3-methylpentane. The curves demonstrate that the mobilities are field independent for temperatures from -20°C to 227°C.

Figures VII-10 and VII-11 contain electron mobilities in 3,3-dimethylpentane for temperatures between -120°C and 251°C. The mobilities are field independent for all temperatures studied.

Figure VII-12 shows electron mobilities in 2,2,4-trimethylpentane. sults are given for temperatures rom 26°C to 263°C and the mobilities exhibit field ndependence at all temperatures studied.

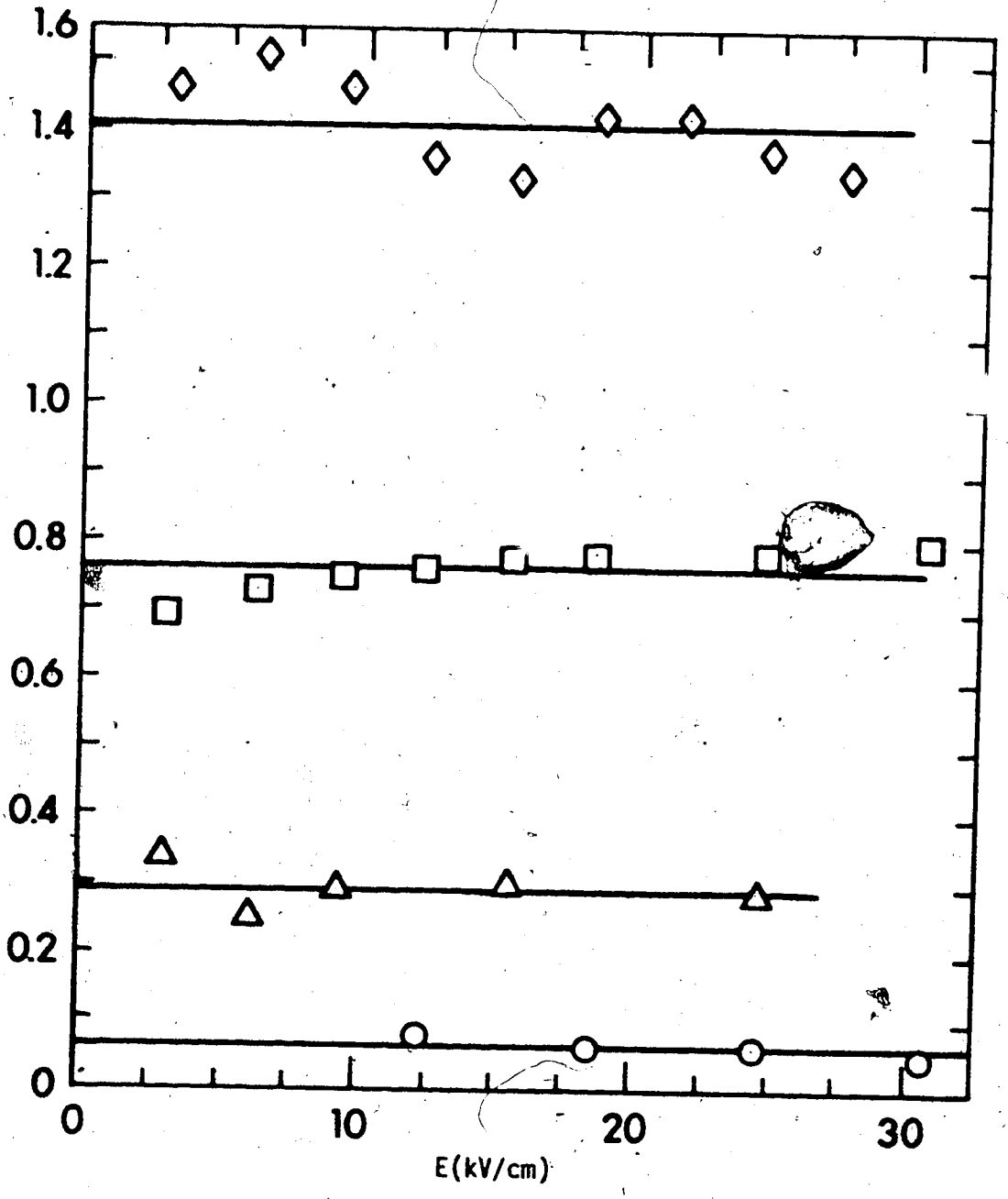

FIGURE VII-6. Electron mobility versus field strength 2,3-dimethyl butane. ○, -46°C; △, -6°C; □, 14°C; ◇, 27°C.

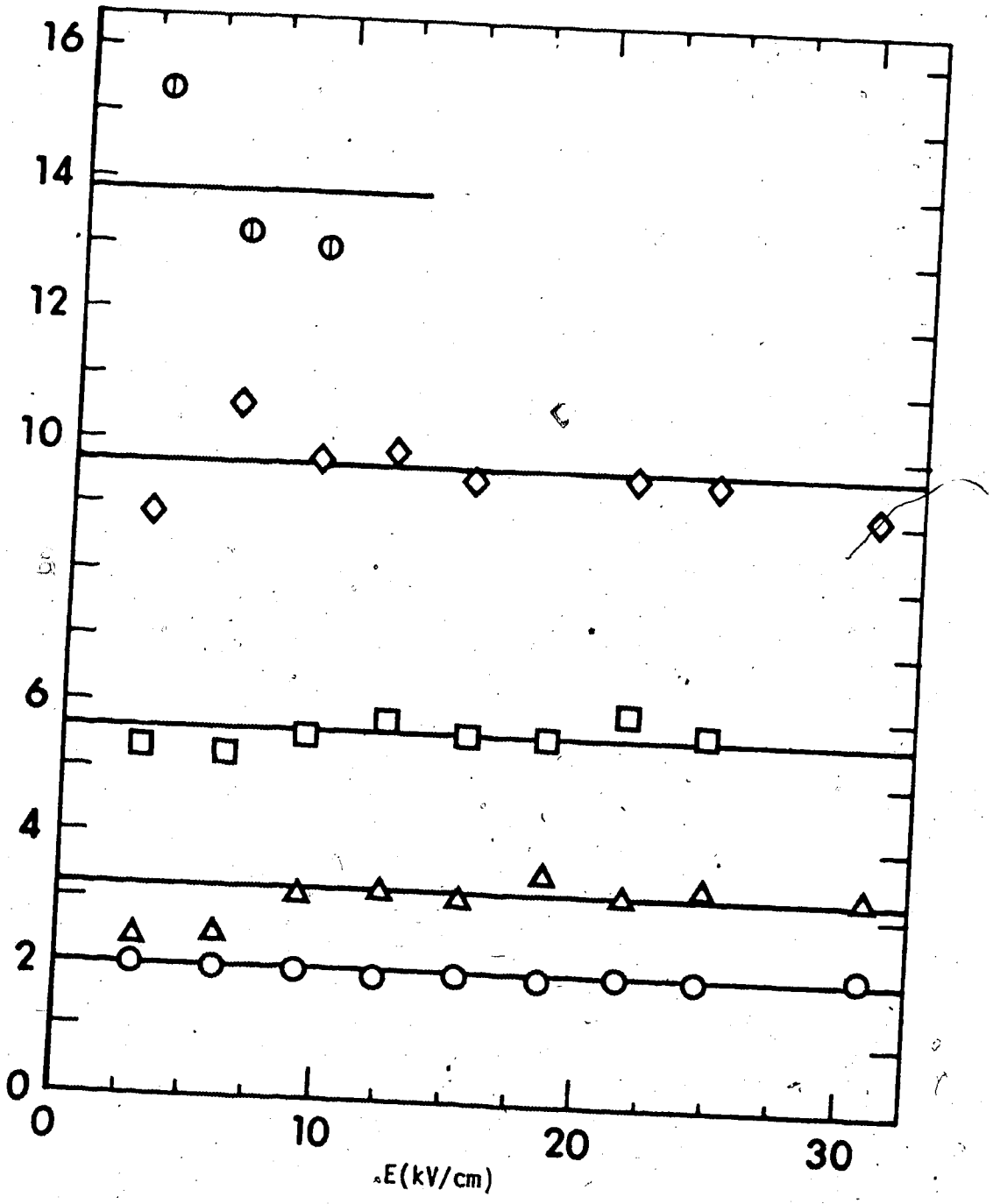

GURE VII-7. Electron mobility versus field strength 2,3-dimethyl-butane. ○, 47°C; △, 71°C; □, 123°C; ◇, 151°C; Φ, 173°C.

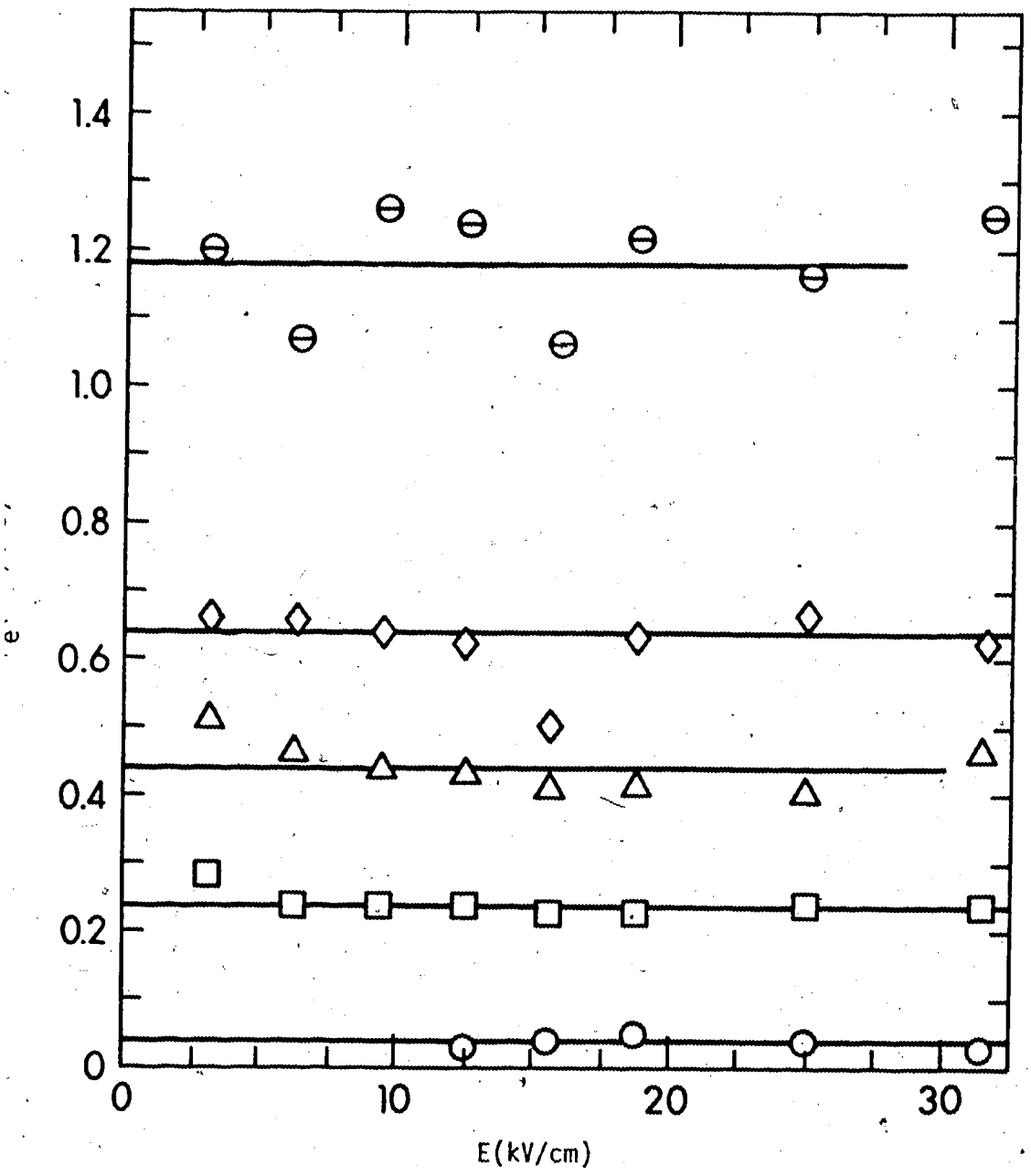

FIGURE VII-8. Electron mobility versus field strength 3-methylpentane ○, -20°C; □, 26°C; △, 47°C; ◇, 74°C; ⊖, 108°C.

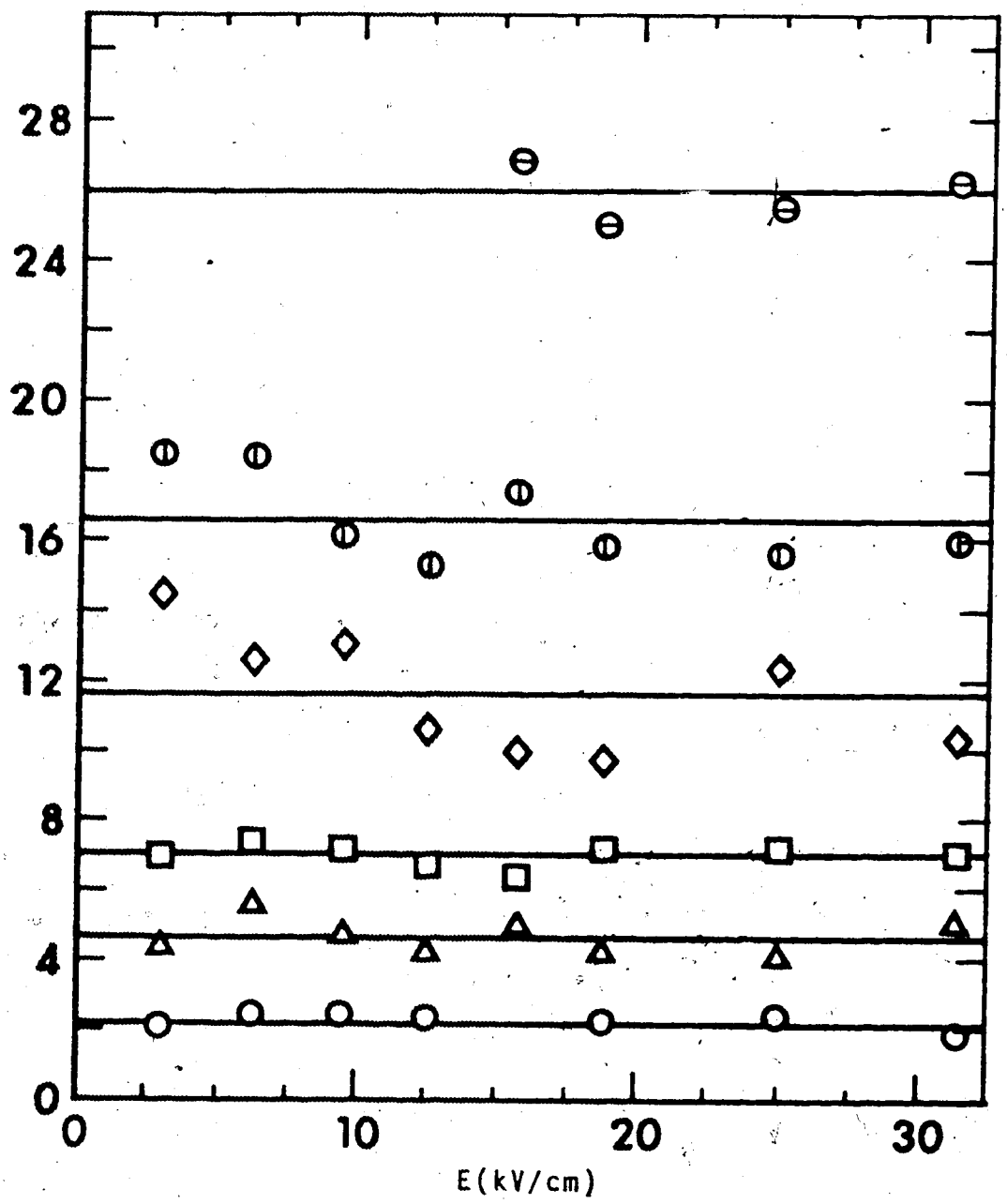

FIGURE VII-9. Electron mobility versus field strength 3-methylpentane. ○, 138°C; △, 153°C; □, 175°C; ◇, 194°C; ⊕, 207°C; ⊖, 227°C.

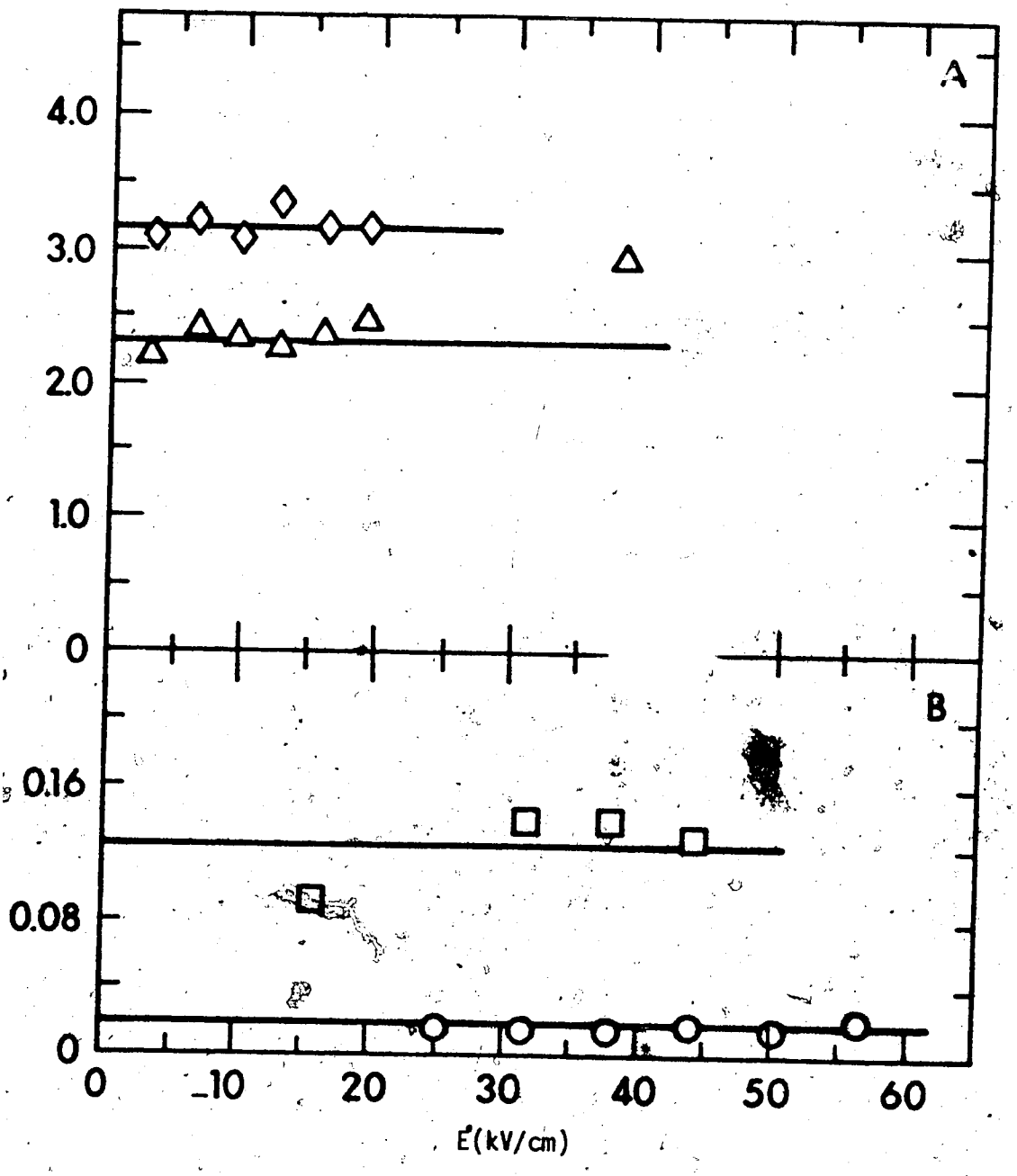

FIGURE VII-10. Electron mobility versus field strength, 3,3-dimethylpentane. A △, 26°C; ◇, 52°C.

B ○, -120°C; □, -91°C.

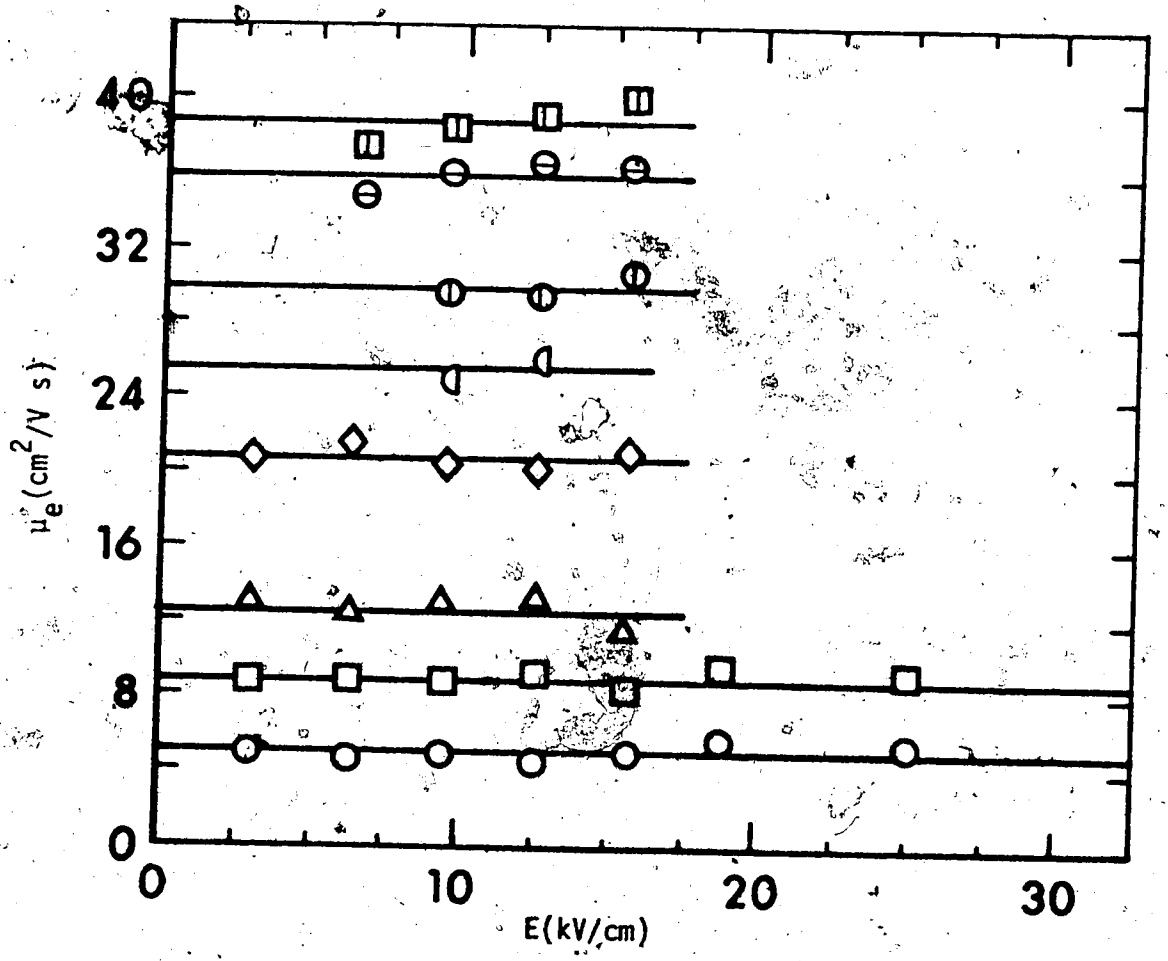

FIGURE VII-11. Electron mobility versus field strength, 3,3-dimethylpentane. ○, 95°C; □, 150°C; △, 177°C; ◇, 204°C; ⊕, 229°C; ⊖, 241°C; ⊞, 251°C; ◫, 263.0°C (critical temp.)

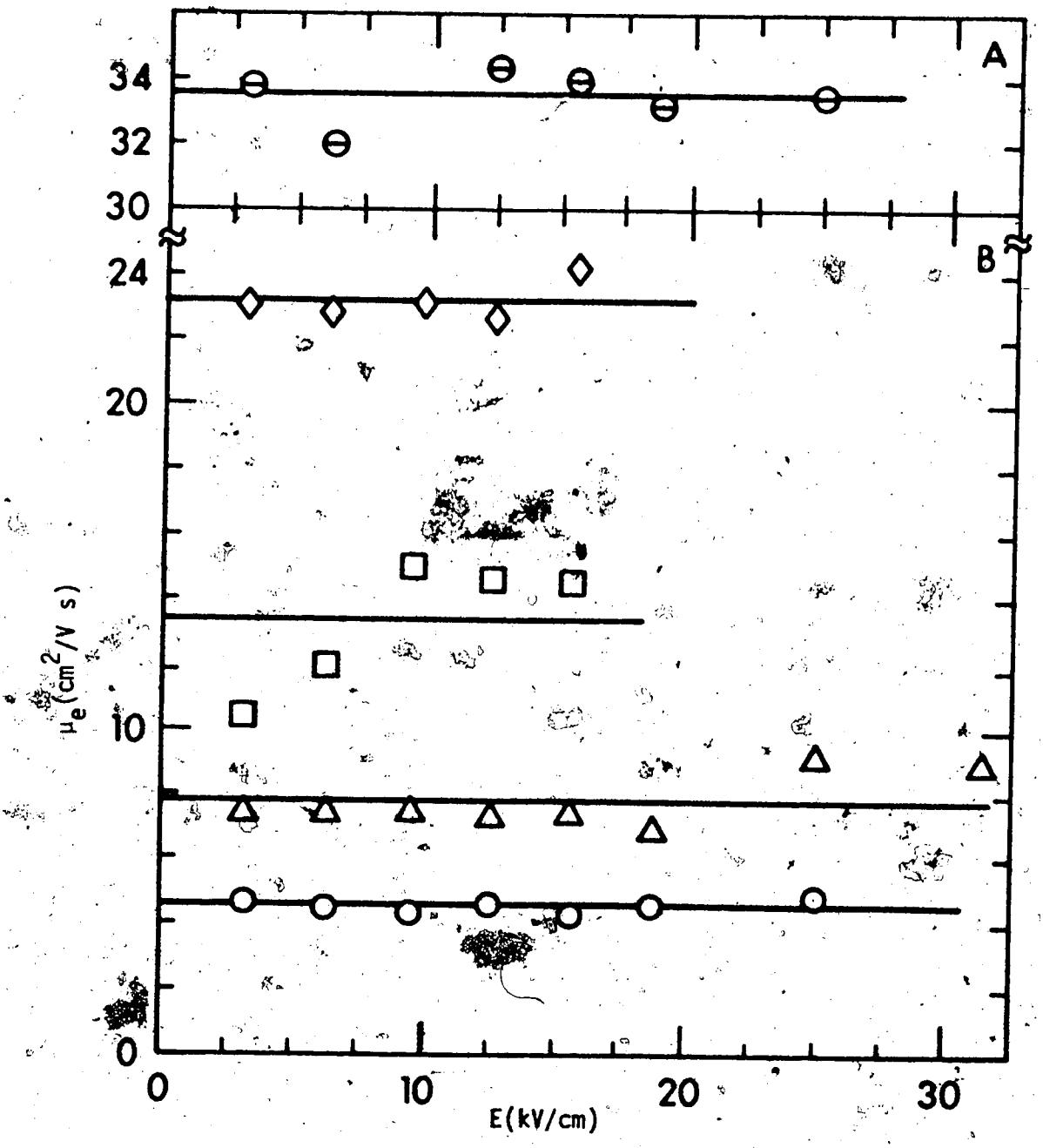

FIGURE VII-12. Electron mobility versus field strength, 2,2,4-trimethylpentane. A ⊖, 263°C.

B ○, 26°C; △, 115°C; □, 160°C; ◇, 193°C.

Electron mobilities in 2,2,4,4-tetramethylpentane are shown in Figure VII-13 for temperatures from -33°C to 235°C. Some negative voltages were examined and the results obtained appear to be within experimental error of those for positive voltages. For temperatures greater than 160°C the mobilities exhibit a field dependence. For these cases an average value of the mobility was obtained by drawing a horizontal line through the data for each temperature.

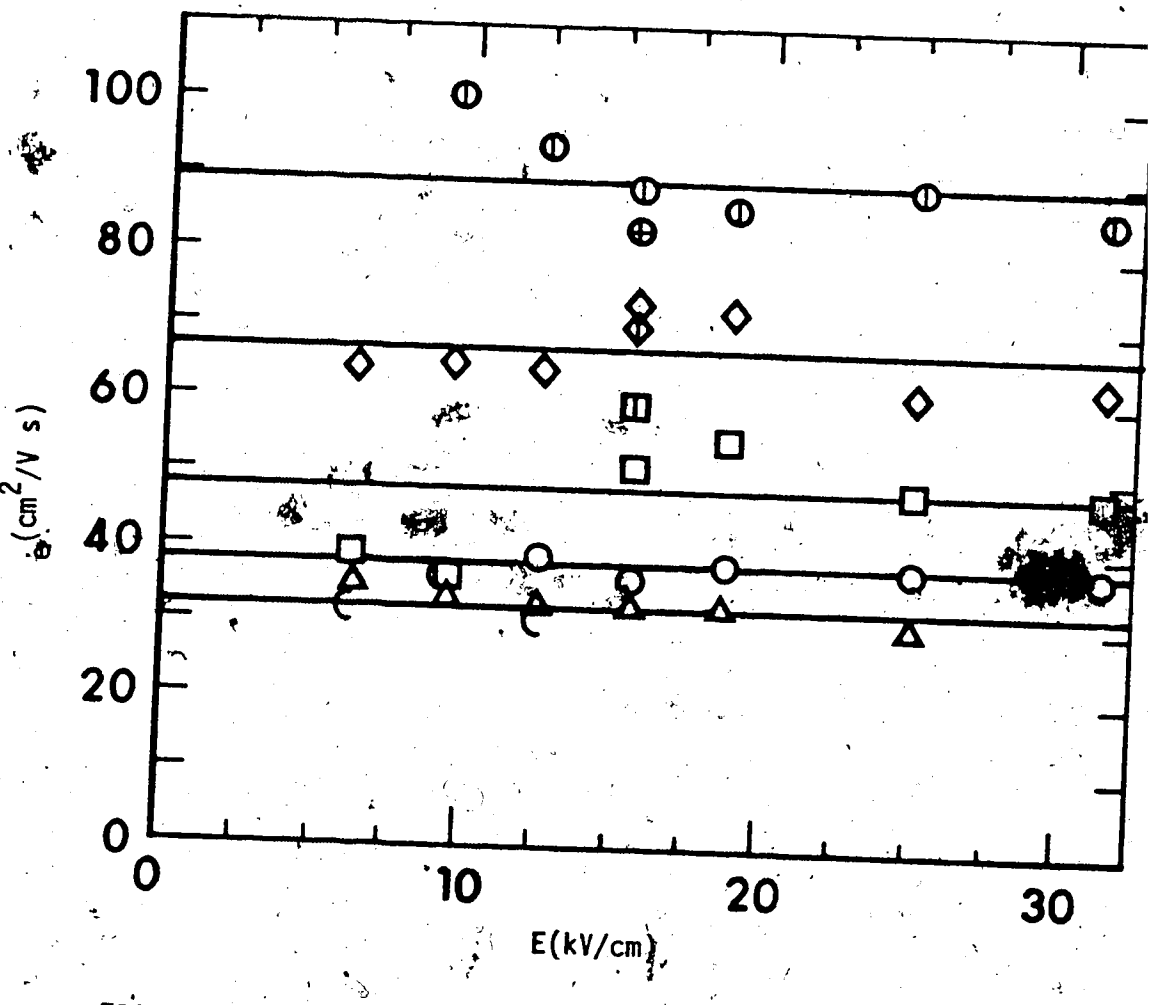

FIGURE VII-13. Electron mobility versus field strength, 2,2,4,4-tetramethylpentane. ○, -33°C; △, -1°C; □, 163°C + V; ▣, 163°C - V; ◇, 207°C + V; ◈, 207°C - V; ⊙, 235°C + V; ●, 235°C - V; ⊂, 283°C (critical temp.).

C. Arrhenius Plots of Electron Mobilities

Data used to make Arrhenius plots of electron mobilities, Figures VII-14 to VII-18, is given in Tables VII-2 to VII-6. Table VII-2 shows the results for 2,3-dimethylbutane and Figure VII-14 is a plot of the data for this compound. A similar treatment is given in Table VII-3 and Figure VII-15 for 3-methylpentane.

Table VII-4 and Figure VII-16 are for 3,3-dimethylpentane. The Arrhenius plot for this compound has some peculiar characteristics in that there is a maximum in the electron mobility just below the critical point and a sharp increase in mobility just above. Similar effects are seen in 2,2,4-trimethylpentane, Table VII-5 and Figure VII-17, and the data for 2,2,4,4-tetramethylpentane, Table VII-6 and Figure VII-18, also show a maximum in the liquid phase mobility. The unique feature in the Arrhenius plot for 2,2,4,4-tetramethylpentane is a minimum in the mobility around 300K.

TABLE VII-2

Electron Mobility as a Function of Temperature, 2,3-dimethylbutane

Electron Mobility $cm^2/V\ s$	Temperature K	1000/T(K)
0.062	277	4.40
0.085	249	4.02
0.29	267	3.75
0.50	281	3.56
0.76	287	3.48
1.1	298	3.35
1.2	296	3.38
1.4	300	3.33
1.9	320	3.13
3.3	344	2.91
3.8	365	2.74
5.6	396	2.53
9.7	424	2.36
11	433	2.31
14	446	2.24
16	455	2.20
16	463	2.16
20	473	2.11
23	487	2.05
26	494	2.02
26	500	2.00

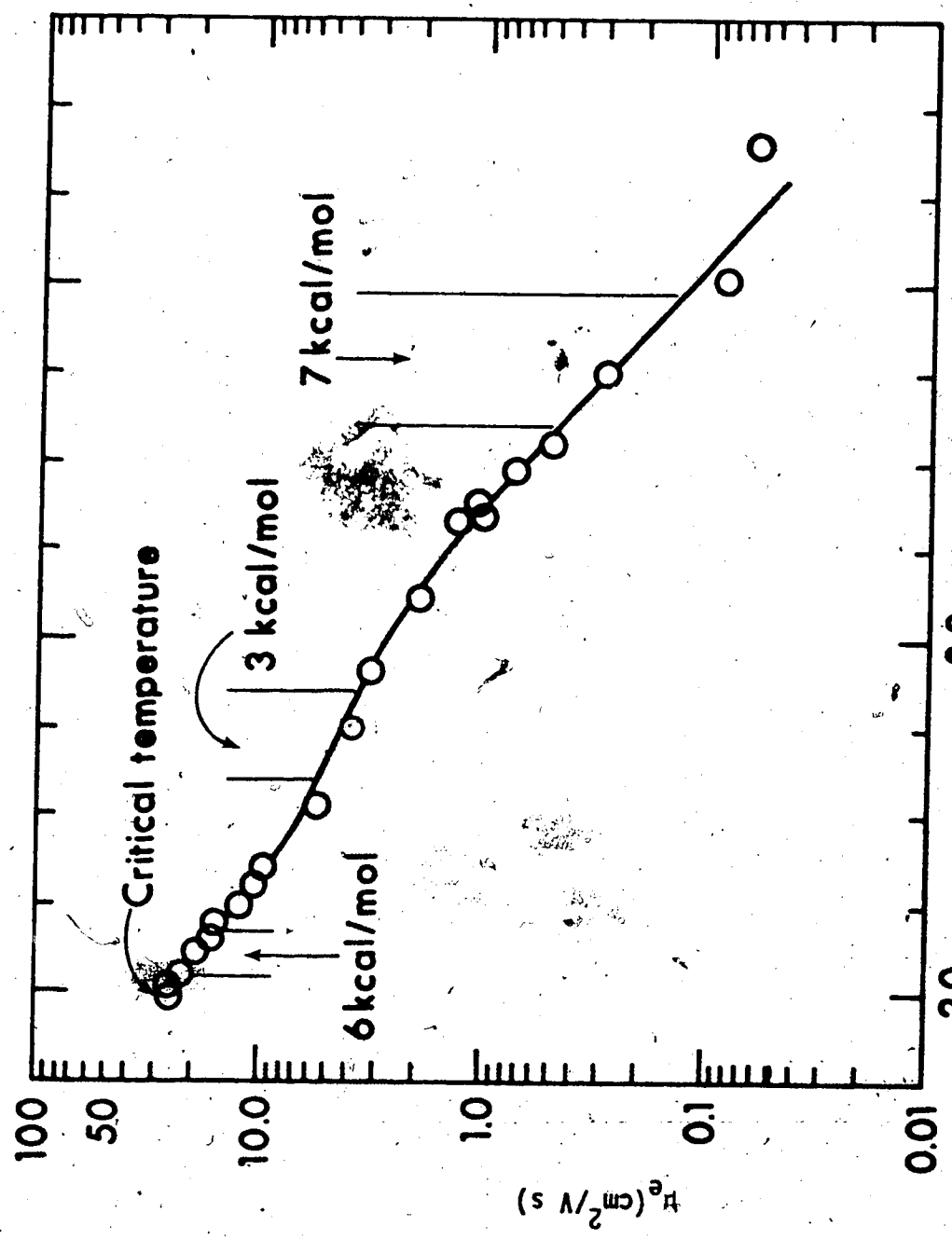

FIGURE VII-14. Electron mobility versus 1000/T 2,3 dimethylbutane.

TABLE VII-3

Electron Mobility as a Function of Temperature, 3-methylpentane

Electron mobility $cm^2/V\ s$	Temperature K	1000/T(K)
0.0074	215	4.65
0.24	299	3.34
0.44	320	3.13
0.64	347	2.88
1.2	381	2.63
2.2	411	2.43
4.6	426	2.35
5.3	438	2.28
7.0	448	2.23
12	467	2.14
17	480	2.08
18	500	2.00
19	504	99
21	509	1.97
24	517	1.93
26	525	1.91

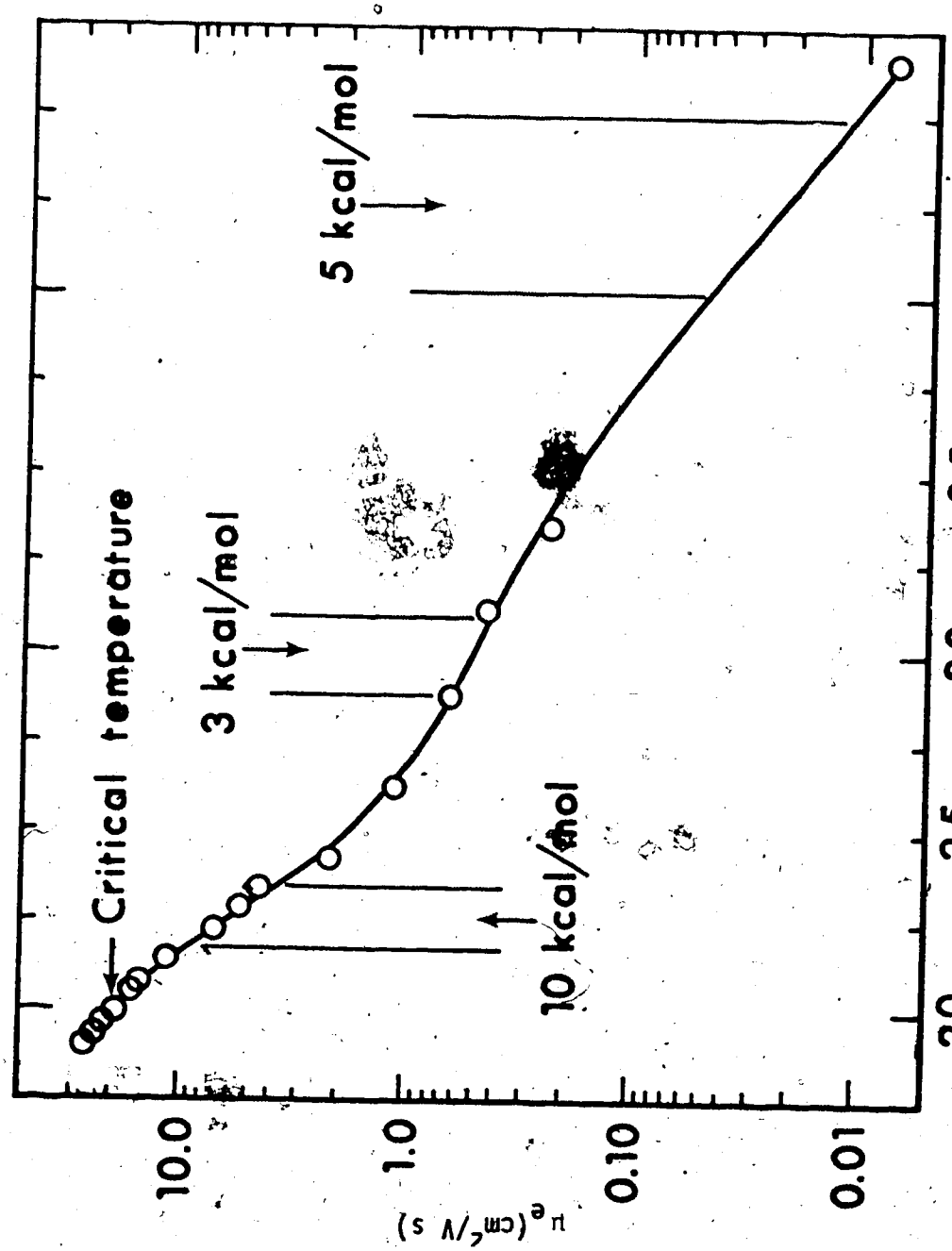

FIGURE VII-15. Electron mobility versus 1000/T, 3-methylpentane.

TABLE VII-4

Electron Mobility as a Function of Temperature, 3,3-dimethylpentane

Electron Mobility $cm^2/V\ s$	Temperature K	1000/T(K)
0.12	182	5.49
2.3	299	3.34
3.2	325	3.08
5.0	368	2.72
8.8	423	2.36
13	450	2.22
21	477	2.10
30	502	1.99
36	514	1.95
39	524	1.91
26	536	1.87
28	540	1.85
32	546	1.83
36	555	1.80

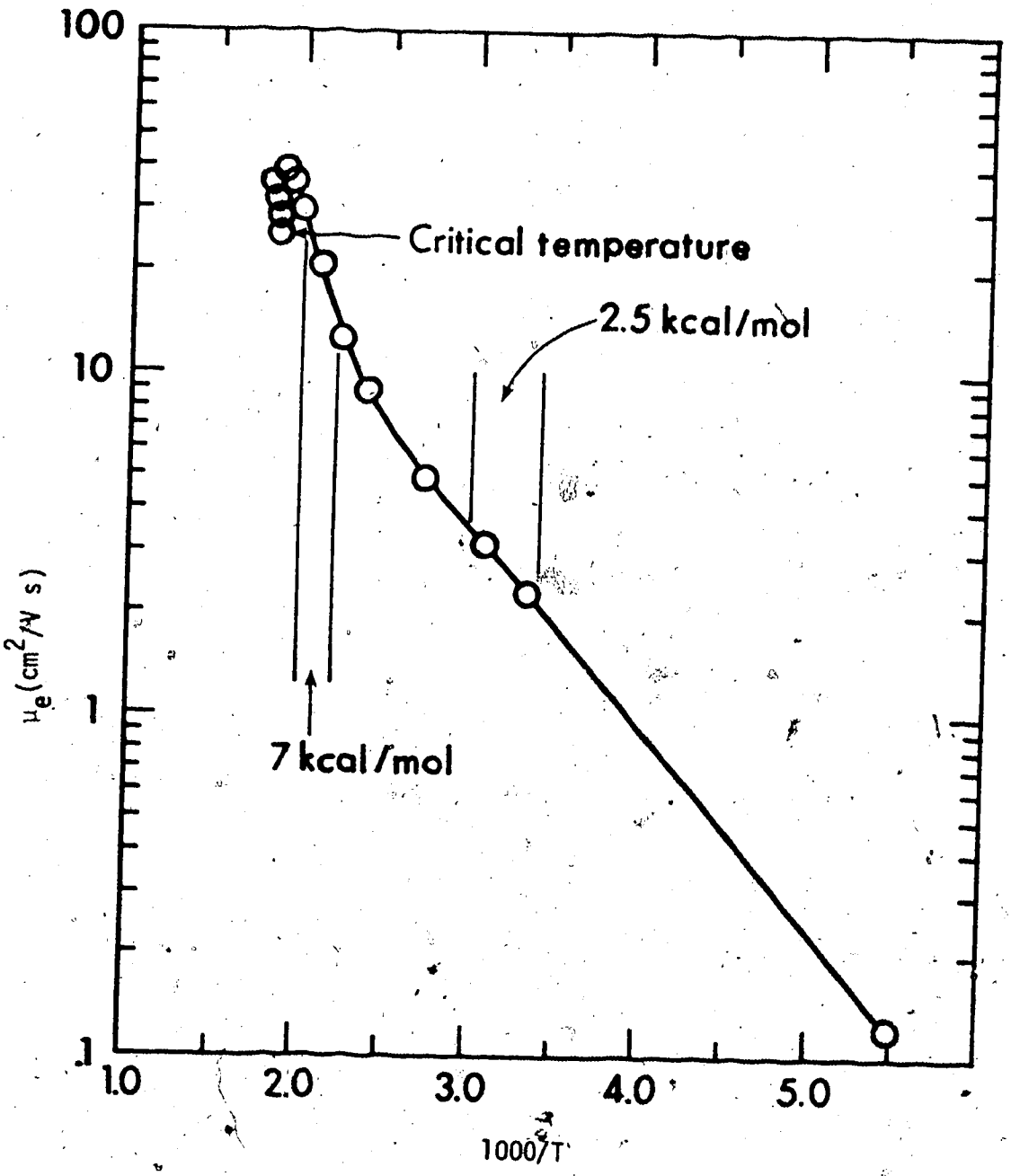

FIGURE VII-16. Electron mobility versus 1000/T, 3,3-dimethylpentane.

TABLE VII-5

Electron Mobility as a Function of Temperature, 2,2,4-trimethylpentane

Electron Mobility $cm^2/V\ s$	Temperature K	1000/T(K)
4.6	299	3.34
5.7	346	2.89
7.8	88	2.58
13	433	2.31
23	466	2.15
27	499	2.00
34	518	1.93
34	536	1.87
24	544	1.84
29	547	1.83
34	555	1.80
35	560	1.79

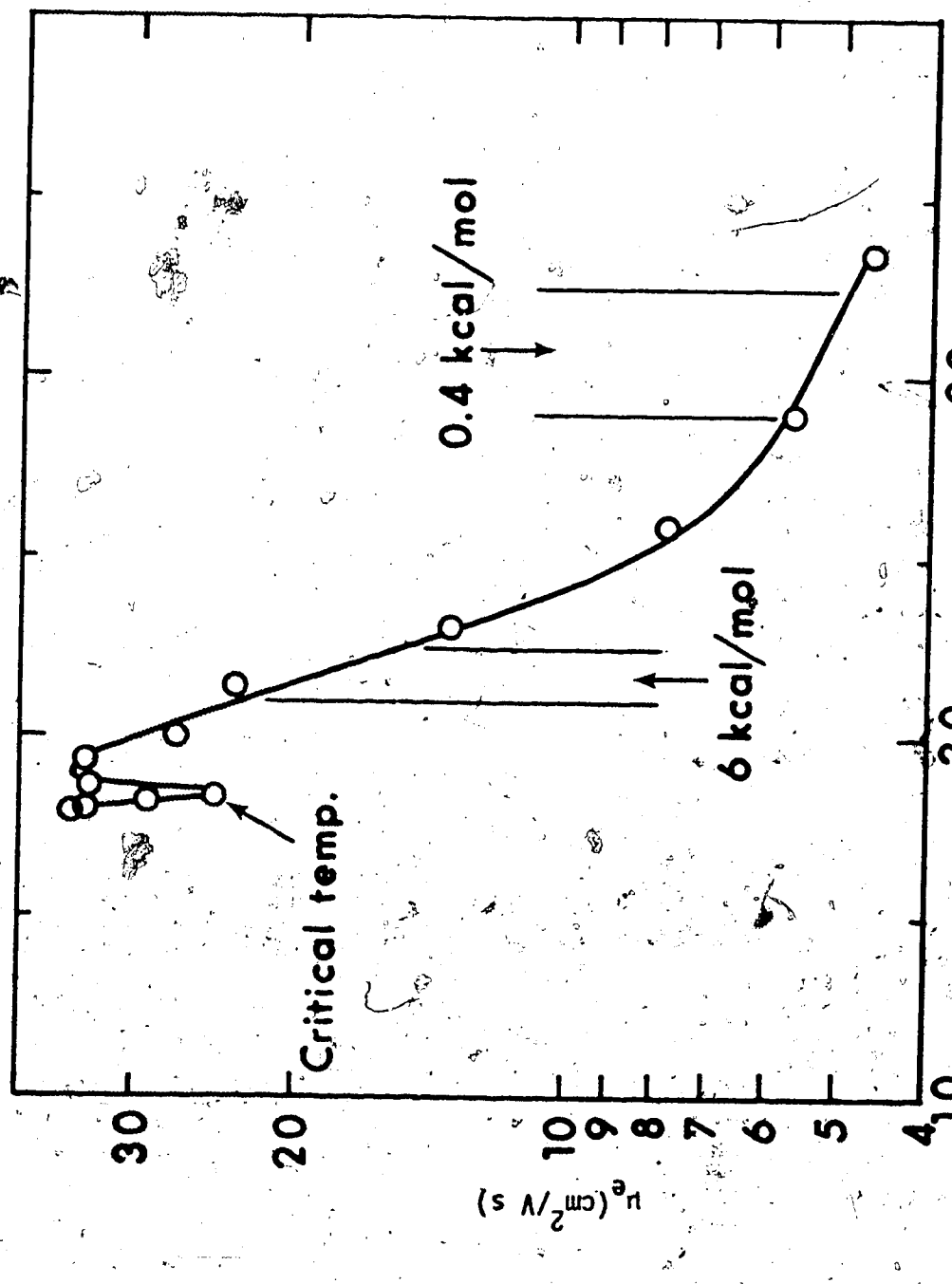

FIGURE VII-17. Electron mobility versus 1000/T, 2,2,4-trimethylpentane.

Electron Mobility as a Function of Temperature,

2,2,4,4-tetramethylpentane

Electron Mobility $cm^2/V\ s$	Temperature K	1000/T(K)
38	240	4.17
32	272	3.68
28	298	3.36
31	335	2.99
39	395	2.53
49	436	2.29
61	460	2.17
67	480	2.08
88	508	1.97
88	527	1.90
71	535	1.87
58	546	1.83
42	553	1.81
31	556	1.80

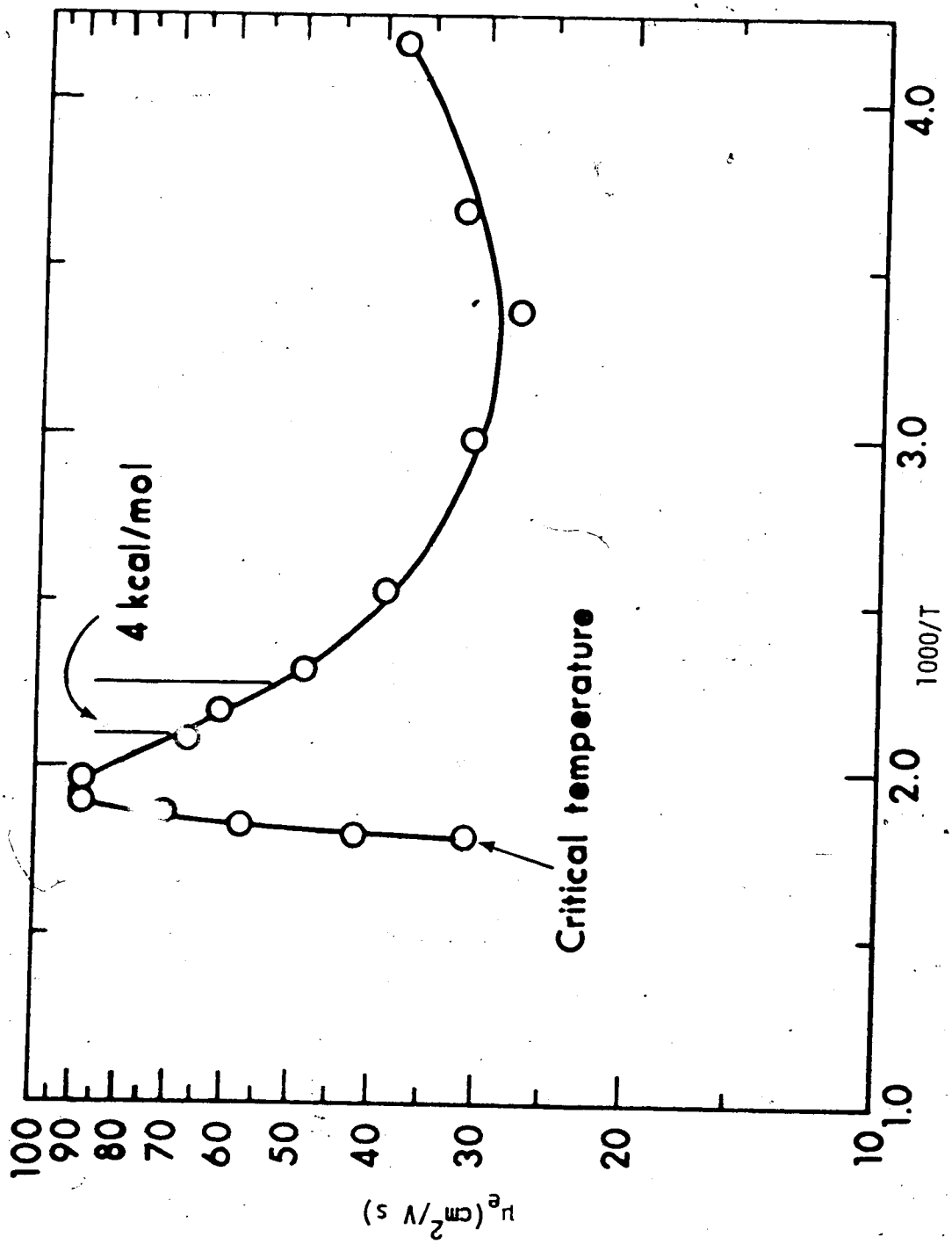

FIGURE VII-18. Electron mobility versus 1000/T 2,2,4,4-tetramethyl-pentane.

Figures VII-19 and VII-20 are plots of electron mobility and $b_{GP}d$ *versus* temperature. Figure VII-19 contains plots for 2,3-dimethylbutane and 2,2,4-trimethylpentane. In Figure VII-20, results are presented for 3-methylpentane and 3,3-dimethylpentane. The reasons for drawing the solid and dashed curves through the data will be given in Chapter VIII.

Figure VII-21 shows a plot of electron mobility and $b_{GP}d$ *versus* temperature for 2,2,4,4-tetramethylpentane.

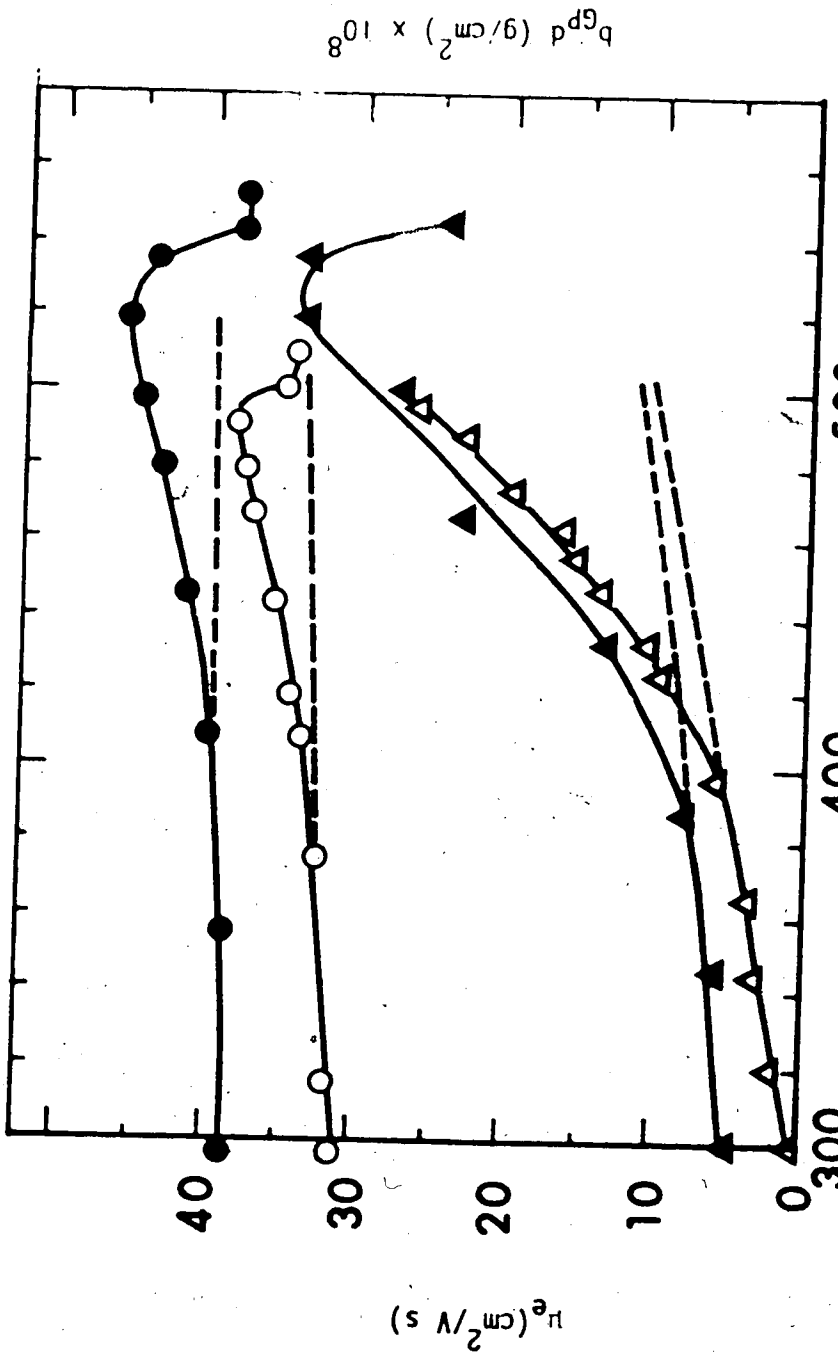

FIGURE VII-19. Electron mobility and $b_{GP}d$ versus temperature, 2,3-dimethylbutane O, $b_{GP}d$; Δ, μ_e. 2,2,4-trimethylpentane ●, $b_{GP}d$; ▲, μ_e.

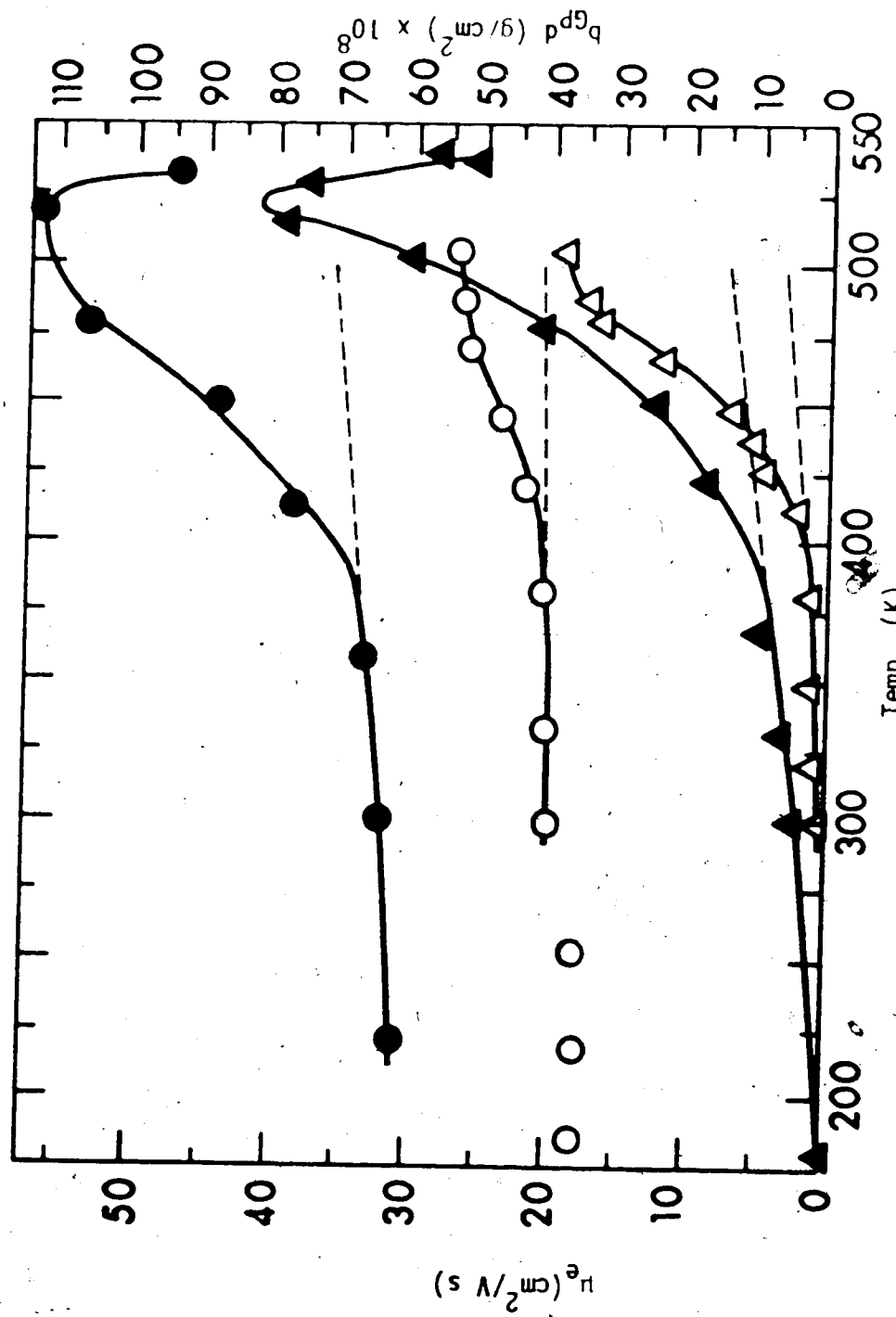

FIGURE VII-20. Electron mobility and $b_{GP}d$ versus temperature, 3-methylpentane, O, $b_{GP}d$; Δ, μ_e; 3,3-dimethylpentane ●, $b_{GP}d$; ▲, μ_e.

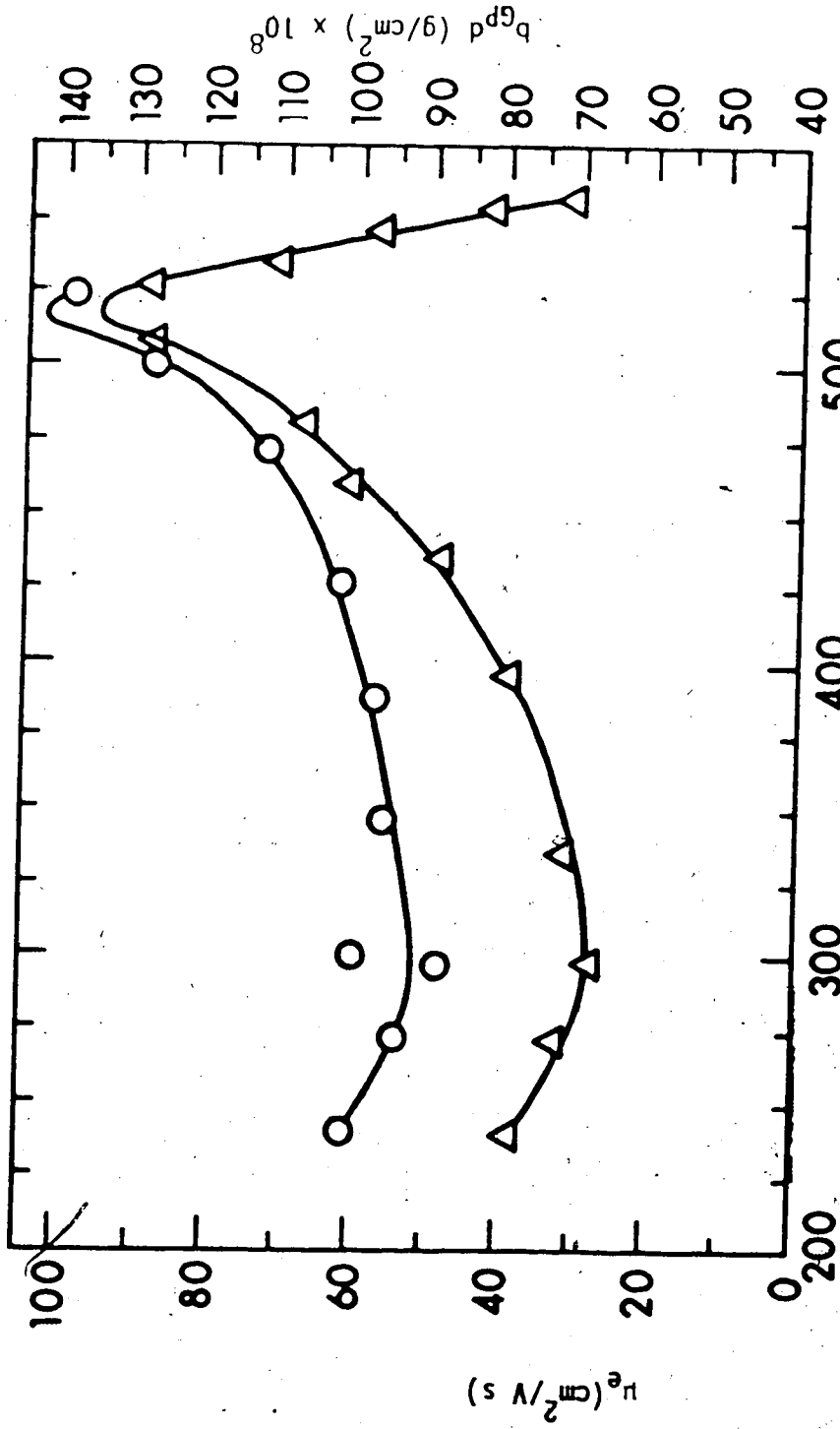

FIGURE VII-21. Electron mobility and $b_{GP}d$ in 2,2,4,4-tetramethylpentane; O, $b_{GP}d$; Δ, μ_e.

VIII D I S C U S S I O N

A. Theory

The free ion yield from the irradiation of a liquid can be measured by putting the liquid between the plates of a conductance cell and collecting the ions. The yield of ions per unit dose increases as the strength of the applied electric field is increased. The following set of equations qualitatively describe the system.

$$M \xrightarrow{\sim\sim} [M^+ + e^-] \qquad (7)$$

$$[M^+ + e^-] \xrightarrow{\text{columbic force}} [M], \text{ spur neutralization} \qquad (8)$$

$$[M^+ + e^-] \xrightarrow{\text{diffusion}} M^+ + e^-, \text{ free ions} \qquad (9)$$

$$M^+ + e^- \longrightarrow M, \text{ bulk medium neutralization} \qquad (10)$$

$$M^+ \xrightarrow{\text{electric field}} \text{collection at electrode} \qquad (11)$$

$$e^- \xrightarrow{\text{electric field}} \text{collection at electrode} \qquad (12)$$

At low applied electric field strengths 11 and 12 are in competition with 10 and the yield of ions collected at the electrodes increases as the field strength is increased. At higher field strengths the yield of reaction 9 is increased as a fraction of the ions are pulled out of the spur by the field. In this region process 10 becomes

negligible so that the free ion yield is identified as the zero field yield of reaction 9 plus the field induced increase in the yield of 9. To separate out the added yield due to field effects a plot of free ion yield versus field strength is made. An extrapolation to the vertical axis gives an intercept which is the zero field free ion yield.

A quantitative description of the system was developed by Onsager (6). He took into account the columbic force between a positive and negative species, the force created by the applied electric field, the orientation of the ion pair with respect to the direction of the applied field and the effect of diffusion. The expression derived is the following

$$\Phi(y,E,\theta) = e^{\frac{-\beta y}{2}(1+\cos\theta)} \int_{s=\frac{r}{y}}^{\infty} J_0\left\{2\left[\frac{-\beta y}{2}(1+\cos\theta)s\right]^{\frac{1}{2}}\right\} e^{-2}\,ds \quad \text{(ix)}$$

where $\Phi(y,E,\theta)$ is the probability that an ion pair, with initial separation distance y and at an angle θ with respect to the applied field E, will escape from the spur. The distance y is the separation distance between the two ions when both have reached thermal energy after being generated. The quantity r is the distance between the positive and negative species when the coulombic and thermal energy are equal, $r = \frac{\xi^2}{\varepsilon kT}$, where ξ is the charge on an electron, ε is the dielectric constant of the liquid, k is the Boltzmann

constant and T is the absolute temperature. The function J_o is the zero order Bessel function and β is defined by $\beta = (\xi E/300\ kT)$.

In order to apply equation (ix) to calculate free ion yields, it is necessary to average $\Phi(y,E,\theta)$ over all θ. This has been done by Terlecki and Fiutak (61), who obtained:

$$\Phi(y,E) = e^{-r/y}\left(1 + e^{-\beta y}\sum_{n=1}^{\infty}\frac{(\beta y)^n}{(n+1)!}\sum_{j=0}^{n-1}(n-j)\frac{(r/y)^{j+1}}{(j+1)!}\right) \qquad (x)$$

The fraction of electrons that escape from their parent ions and get collected depends on $\Phi(y,E)$ and on the distribution of thermalization ranges. To obtain the theoretical values of G_{fi}^{E} one must find a suitable distribution function. For all the calculations in this work F(y) is defined as follows (49)

$$F(y) = 0.96(4y^2/\pi^{3/2}\, b_{GP}^{3})\exp(-y^2/b_{GP}^{2}) \qquad y < 2.4\ b_{GP} \qquad (xia)$$

$$F(y) = 0.96[(4y^2/\pi^{3/2} b_{GP}^{3})\exp(-y^2/b_{GP}^{2}) + 0.5\ b_{GP}^{2}/y^3] \qquad (xib)$$

Expression (xia) is a three dimensional Gaussian distribution and (xib) is a Gaussian modified by the addition of a small power function tail at large y values. The constant 0.96 is a nomalization factor and b_{GP} is the adjustable dispersion parameter which is also the most probable value

of y. The distribution function F(y) is used to calculate G_{fi}^{E} with the following equation,

$$G_{fi}^{E} = G_{tot}\int_{0}^{\infty} F(y)\Phi(y,E)dy \qquad \text{(xii)}$$

where G_{tot} is G(total ionization) which was assumed equal to 4.4 for all calculations presented here.

The curves drawn through the data in Figures VII-1 to VII-5 were calculated by equation (xii). The procedure followed involved taking a preliminary value of b_{GP} and calculating G_{fi}^{E} for each experimental value of E. Calculated and experimental yields were then compared using the formula (xiii).

$$\text{Average \% error} = \frac{100\sum G_{fi}calc^{E} = G_{fi}exp^{E}}{\sum G_{fi}exp^{E}} \qquad \text{(xiii)}$$

The b_{GP} value was determined by repeating the calculation several times and taking the b_{GP} which gave the minimum average % error.

To make the calculations to determine b_{GP} it is necessary to assign values to the dielectric constant. For this work the room temperature dielectric constants were obtained from the literature (62) and values for all other temperatures studied were calculated using the Lorenz Lorentz equation (63).

Liquid densities were also required and experimental

alues have not been determined for the entire liquid range of these hydrocarbons. Those that have been measured are listed in Table VII-1 (64) while all other required values were determined by analogy. The procedure followed was to first obtain the density temperature curves for n-hexane, n-heptane, and n-octane, for their entire liquid range, from the literature (65). Density temperature curves were then drawn, for the five liquids, in such a way that their shapes were analogous to the experimental curve shapes for the straight chain hydrocarbons.

B. Density Normalized Ranges

A useful quantity is obtained by multiplying the b_{GP} value by the absolute density of the fluid. Because b_{GP} represents the most probable value of y it is reasonable to assume that it will be proportional to the mean free path for the electron in the liquid. Making this assumption we write

$$b_{GP} = C\text{mfp} \qquad \text{(xiv)}$$

where C is a constant and mfp is the mean free path for the electron. The mean free path can be related to the number density n by:

$$\text{mfp} = 1/n\sigma \qquad \text{(xv)}$$

where σ is the collision cross section per molecule. Relating

n to the absolute density, d, by the equation:

$$n = \frac{dN}{M} \qquad \text{(xiv)}$$

gives

$$b_{GP} = \frac{CM}{dN\sigma} \qquad \text{(xvii)}$$

and

$$b_{GP}d = \frac{CM}{N\sigma} \qquad \text{(xviii)}$$

where M and N are the molecular weight of the substance and Avogadro's number, respectively. If σ is considered to be a microscopic property and temperature independent then it follows that $b_{GP}d$ should be temperature independent. Table VIII-1 contains $b_{GP}d$ values for all five compounds at various temperatures. The values are more or less temperature independent below 400°K. The increase in $b_{GP}d$ above 400°K can be related to the electron mobility and will be discussed later.

C., Electron Mobility

Plots of electron mobility versus field strength for the five hydrocarbons studied are shown in Figures VII-6 to VII-13. Although there is considerable scatter in some of the plots, it appears that most of the electron mobilities determined are field independent. Exceptions are the results for 2,2,4,4-tetramethylpentane at 235°C shown in Figure VII-13. In this case there is a trend towards lower mobilities at higher field strengths. Because of the dif-

TABLE VII I

$b_{GP}d^{*}$ a Function of Temperature

2,3-dimethylbutane		3-methylpentane		3,3-dimethylpentane	
$b_{GP}d$	(Temp. K)	$b_{GP}d$	(Temp. K)	$b_{BP}d$	(Temp. K)
42.6	(300)	36.0	(184)	66.2	(183)
43.5	(325)	35.7	(217)	62.0	(233)
45.2	(375)	35.6	(252)	64.0	(299)
47.2	(407)	40.1	(299)	66.7	(359)
49.2	(429)	40.3	(326)	76.7	(412)
51.3	(443)	41.6	(382)	78.1	(442)
54.4	(467)	43.4	(416)	87.6	(450)
55.6	(479)	47.3	(444)	106.0	(480)
56.6	(491)	51.9	(470)	113.0	(520)
50.2	(500)†	53.1	(488)	94.8	(536)†
48.9	(510)	53.9	(504)†	94.5	(544)

2,2,4-trimethylpentane		2,2,4,4-tetramethylpentane	
$b_{GP}D$	(Temp. K)	$b_{GP}d$	(Temp. K)
61.1	(240)	101.4	(240)
58.3	(299)	93.9	(272)
57.2	(356)	88.2	(297)
59.5	(408)	100.0	(300)
63.3	(446)	96.1	(346)
66.0	(481)	97.3	(388)
69.3	(498)	102.3	(427)
70.8	(519)	112.6	(471)
67.5	(535)	128.0	(500)
55.7	(544)†	138.0	(523)
55.4	(552)		

† Critical temperature * $b_{GP}d$ is in units of 10^{-8} g/cm^2

ficulty in drawing a sloped line through the points the 235°C results have been treated in the same way as all other results by drawing the best horizontal line.

A comparison of electron mobilities, obtained in the present work, with the literature values is shown in Table VIII-2. In some cases, 3-methylpentane and 2,2,4-trimethylpentane, the discrepancy is as large as 25%. The fact that the room temperature mobilities range over a factor of 100 in the five compounds indicates that the discrepancy places no severe limitation on interpretation.

Table VIII-2 illustrates that more branched paraffins shows higher room temperature electron mobilities. This tendency is observed for a wide range of compounds (58) and is associated with the degree of sphericity of the molecule.

The Arrhenius plots in Figures VII-14 to VII-18 show that electron mobilities at the critical temperatures are between 19 and 31 $cm^2/V\ s$ for all five paraffins. Mobilities which range over a factor of 100 at room temperatur converge to a 1.6 fold range at the critical tempera ure This behavior parallels that observed in the series of compounds: 2,2-dimethylbutane, 2,2,-dimethylpropane, n-pentane and cyclopentane (66). In that study electron mobilities showing a 500-fold variation at 295K converged to be within a factor of 2 of each other at the critical temperature (66).

TABLE VIII-2

Electron Mobility

Compound	Temperature °K	μ_e $cm^2/V\ s$	Reference
2,3-dimethylbutane	299	1.2	this work
	293	1.1	(58)
3-methylpentane	298	0.24	this work
	293	0.18	(58)
3,3-dimethylpentane	299	2.3	this work
	293	2.3	(58)
2,2,4-trimethylpentane	299	5 ± 2	this work
	296	7 ± 2	(59)
2,2,4,4-tetramethylpentane	298	28	this work
	295	24	(37)
	335	31	this work
	324	32	(37)
	395	39	this work
	385	44	(37)

The Arrhenius plots for electron mobilities have a rather complex shape, Figures VII-14 to VII-18. For all compounds, except 2,2,4,4-tetramethylpentane, there is a portion of the curves where a gradual curvature is observed. At low temperatures 2,2,4,4-tetramethylpentane shows a negative temperature coefficient, a phenomenon that has been observed before in 2,2-dimethylbutane (66), methane (67), and neopentane (49). Activation energies calculated from the most gentle slopes in Figures VII-14 to III-17 are between 0.4 and 3 kcal/mol. It is not meaningful to make the calculation for 2,2,4,4-tetramethylpentane because of the negative temperature coefficient at low temperature. A rough trend is observed in the size of the activation energies for these compounds, with the least branched, 3-methylpentane, yielding 3 kcal/mol and the most branched, 2,2,4-trimethylpentane, giving 0.4 kcal/mol. Values calculated from the steepest portion of the curve also show the trend, 10 kcal/mol for 3-methylpentane and 4 kcal/mol for 2,2,4,4-tetramethylpentane. The other three compounds are characterized by intermediate values of 6 or 7 kcal/mol. The temperature coefficients from the steepest portion of the curves are determined by a combination of thermal activation effects and collisional cross section changes. A qualitative understanding of the cross section changes can be achieved by considering the effect of density changes. When an electron passes through a high density liquid it

is forced to pass so near to the molecules that it experiences mainly repulsion from the hard core (Hartree field) of the molecules (68). For lower density liquids the molecules are further apart and the electron is subjected to more of the attractive polarization interactions which tend to counterbalance the hard core repulsions. Thus a decrease in density (increase in temperature) leads to a smaller interaction cross section and increase in electron mobility.

In Figures VII-16, VII-17 and VII-18 these are maxima in the electron mobilities below the critical temperature. These maxima can be explained by considering that as the density is decreased there will be a point where a balance exists between the hard core repulsions and attractive polarization interactions. At this point the scattering cross section reaches a minimum and the electron mobility is a maximum. The above argument has been used to explain the electron mobility maximum in liquid argon (69).

The curves in VII-14 and VII-15 show a downward curvature at lower temperatures. As shown in the Figures the activation energies calculated from these plots are 7 kcal/mol and 5 kcal/mol for 2,3-dimethylbutane and 3-methylpentane, respectively. Electron mobilities in cis-butene-2 and isobutene (70) have been observed to behave in a similar way. For these two olefins the middle portion of

the Arrhenius plot had a gentle slope (~3 kcal/mol) while at lower temperatures a value of 5 kcal/mol was obtained. It therefore appears possible that the larger activation energies at lower temperatures in 3-methylpentane and 2,3-dimethylbutane are caused by the presence of small amounts of olefinic impurities.

Plots of electron mobility and $b_{GP}d$ as a function of temperature are shown in Figures VII-19 to VII-21. For the four compounds in Figures VII-19 and VII-20 there appears to be a distinct change in the behavior of both $b_{GP}d$ and μ_e at about 400°K. As mentioned above, $b_{GP}d$ represents the most probable value of a Gaussian distribution of thermalization ranges multiplied by the liquid density. In other words it is determined by the behavior of epithermal electrons (electrons that have not yet been thermalized). Since μ_e is a property of thermalized electrons, the parallel behavior between $b_{GP}d$ and μ_e, in Figures III-19 to III-21, indicates that epithermal and thermalized electrons show parallel behavior.

To make a comparison between the behavior of thermal and epithermal electrons it is necessary to realize that the former are sensitive to thermal activation effects and the latter are not. This explains why the $b_{GP}d$ values are more or less temperature independent below 400°K while the electron mobilities are quite sensitive to temperature in this region, Figures VII-19 and VII-20. The gradual changes

that do occur in the $b_{GP}d$ values below 400°K are due to changes in the epithermal electron cross sections, equation (xviii). The changes in the electron mobilities in this region are due to thermal activation effects with probably some contribution from changes in the thermal electron cross sections. The dashed curves in Figure VII-19 and VII-20 are an attempt to extrapolate the behavior of $b_{GP}d$ and μ_e, below 400°C, to higher temperatures. The electron mobilities from these dashed curves can be thought of as the values that would be obtained if only thermal activation effects and small thermal electron cross sectional changes had remained operative up to a temperature of 500°K. The $b_{GP}d$ values from the dashed curves are the predicted values for the situation where the epithermal electron cross sections continue to change gradually up to a temperature of 500°K. If one assumes that the changes in the epithermal and thermal electron cross sections are proportional to each other above 400°C,

$$\frac{\Delta\sigma_T}{\sigma_T} = \frac{\Delta\sigma_{E.T.}}{\sigma_{E.T.}} \qquad \text{(xix)}$$

where σ_T and $\sigma_{E.T.}$ are the thermal and epithermal cross sections respectively, then equation (xx) can be written

$$\frac{((\mu_e)_T - \mu_T)d}{((b_{GP}d)_e)_T - (b_{GP}d)} = C \qquad (xx)$$

Here $(\mu_e)_T$ is the experimental mobility and μ_T is the mobility from the dashed curve. The quantity C is a constant, $((b_{GP}d)_e)_T$ is the experimental density normalized range and $(b_{GP}d)$ is the value from the dashed curve. Figure VIII-1 contains a plot of the left side of equation (xx) against temperature for four of the compounds. As predicted by (xx) the temperature independence is observed and each compound has a different C value.

The plot for 2,2,4,4-tetramethylpentane in Figure VII-21 shows that this compound can not be treated in the same way as the other four. There is no part of the curve where $b_{GP}d$ is more or less temperature independent, indicating that the cross section for epithermal electrons is quite sensitive to small density changes. The same is true for the electron mobilities. Parallel behavior between $b_{GP}d$ and μ_e indicates that the thermal and epithermal electron cross sections behave in a similar way in this liquid.

In conclusion several points should be emphasized.

1. Electron mobilities in liquid paraffins can vary over several orders of magnitude, for a series of compounds showing a large structure effect. At the

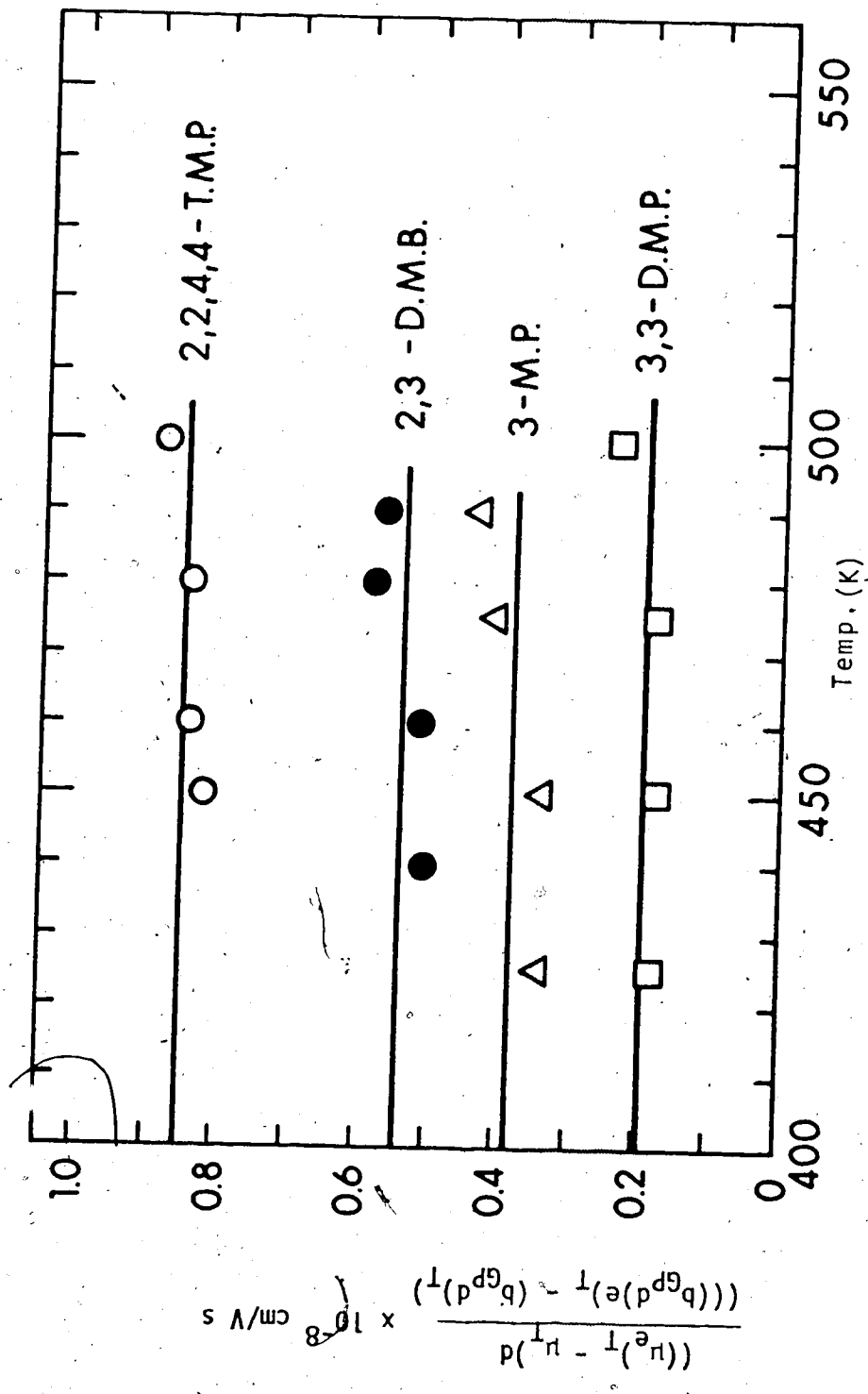

FIGURE VIII-1 $\frac{((\mu_e)_T - \mu_T)_d}{(((b_{GP}{}^d)e)_T - (b_{GP}{}^d)_T)}$ versus temperature.

critical temperature the structure effect is much reduced and mobilities tend to be within a factor of two from one paraffin to another.

2. The liquid phase temperature coefficients of electron mobility tend to be larger in straight paraffins than in more branched ones.

3. The changes in liquid phase mobilities with temperature are due to a combination of thermal activation effects and thermal electron collisional cross sectional changes.

4. For the five paraffins in this study it appears that the thermal and epithermal electron cross sections vary with density in a similar way.

REFERENCES

1. P. Curie, —— C. R., 134, 420 (1902).
2. A. N. Gerritsen and J. Kolhaas, Physica 10, 49 (1943).
3. G. R. Freeman, J. Chem. Phys. 38, 1022 (1963).
4. G. R. Freeman, J. Chem. Phys. 39, 988 (1963).
5. G. R. Freeman, J. Chem. Phys. 39, 1580 (1963).
6. L. Onsager, Phys. Rev. 54, 554 (1938).
7. H. Ullmaier, Z. Physik 178, 44 (1964).
8. A. Hummel and A. O. Allen, Disc. Faraday Soc. 36, 95 (1963).
9. A. Hummel and A. O. Allen, J. Chem. Phys. 44, 3431 (1966).
10. G. R. Freeman and J. M. Fayadh, J. Chem. Phys. 43 86 (1965).
11. A. Hummel, A. O. Allen, and F. H. Watson Jr., J. Chem. Phys. 44, 3431 (1966).
12. O. Leblanc Jr., J. Chem. Phys. 30, 1443 (1959).
13. O. Czowski, Z. Physik. Chem. 221, 288 (1962).
14. P. Chong and Y. Inuishi, Tech. Rept. Osaka University, 10, 545 (1960).
15. M. S. Malkin and H. L. Schultz, Phys. Rev. 83, 1051 (1951).
16. R. L. Williams, Can. J. Phys. 35, 134 (1957).
17. D. W. Swan, Proc. Phys. Soc. 83, 662 (1964).
18. H. Schnyders, S. A. Rice, and L. Meyer, Phys. Rev. 150, 127 (1966).

19. L. S. Miller, S. Howe, and W. E. Spear, Phys. Rev. 166, 871 (1968).

20. A. H. Samuel, F. O. Halliday, A. K. Keast and S. I. Tiamuty, Science 144, 839 (1964).

21. P. H. Tewari and G. R. Freeman, J. Chem. Phys. 49, 4394 (1968).

22. P. H. Tewari and G. R. Freeman, J. Chem. Phys. 51, 1276 (1969).

23. R. M. Minday, L. D. Schmidt, and H. T. Davis, J. Chem. Phys. 50, 1473 (1969).

24. W. F. Schmidt and A. O. Allen, J. Chem. Phys. 50, 5037 (1969).

25. E. E. Conrad and J. Silverman, J. Chem. Phys. 51, 450 (1969).

26. W. F. Schmidt, Z. Naturforsch., 236, 126 (1968).

27. W. F. Schmidt and A. O. Allen, Science, 160, 301 (1968).

28. W. F. Schmidt and A. O. Allen, J. Phys. Chem. 72, 3730 (1968).

29. H. A. Ullmaier, Phys. Med. Biol. 11, 95 (1966).

30. N. V. Klassen and W. F. Schmidt, Can. J. Chem. 47, 4286 (1969).

31. J. A. Leone and W. H. Hamill, J. Chem. Phys. 49, 5304 (1968).

32. J. Mathieu, D. Blanc, P. Caminade, and J. P. Patau, J. Chim. Phys. 64, 1679 (196

33. W. F. Schmidt and A. O. Allen, J. Chem. Phys. 52, 2345 (1970).

34. W. F. Schmidt, Radiat. Res. 42, 73 (1970).

35. J.-P. Dodelet and G. R. Freeman, Can. J. Chem. 49, 2643 (1971).

36. M. G. Robinson, P. G. Fuochi, and G. R. Freeman, Can. J. Chem. 49, 984 (1971).

37. J.-P. Dodelet and G. R. Freeman, Can. J. Chem. 50, 2667 (1972).

38. J.-P. Dodelet, P. G. Fuochi, and G. R. Freeman, Can. J. Chem. 50, 1617 (1972).

39. P. G. Fuochi and G. R. Freeman, J. Chem. Phys. 56, 2333 (1972).

40. A. Jahns and W. Jacobi, Z. Naturforsch. 21a, 1400 (1966).

41. M. G. Robinson and G. R. Freeman, J. Chem. Phys. 59, 1293 (1973).

42. J.-P. Dodelet, K. Shinsaka, and G. R. Freeman, J. Chem. Phys. 59, 1293 (1973).

43. J.-P. Dodelet, K. Shinsaka, U. Kortsch, and G. R. Freeman, J. Chem. Phys. 59, 2376 (1973).

44. G. Bakale, E. C. Gregg, and R. D. McCreary, J. Chem. Phys. 57, 4246 (1972).

45. G. Bakale and W. F. Schmidt, Naturforsch . A, 28, 511 (1973).

46. G. Bakale and W. F. Schmidt, Chem. Phys. Letts. 22,

164 (1973).

47. G. C. Abell and K. Funabashi, J. Chem. Phys. 58, 1079 (1973).

48. A. O. Allen and R. A. Holroyd, J. Phys. Chem. 78, 796 (1974).

49. K. Shinsaka and G. R. Freeman, Can. J. Chem. 52, 3556 (1974).

50. T. Kimura and G. R. Freeman, J. Chem. Phys. 60, 4081 (1974).

51. M. Miyajima, T. Takahashi, S. Konno, T. Hamada, S. Kubota, H. Shibamura, and T. Doke, Phys. Rev. A9, 1438 (1974).

52. M. Miyajima, T. Takahashi, S. Konno, T. Hamada, S. Kubota, H. Shibamura, and T. Doke. Phys. Rev. A10, 1452 (1974).

53. T. Takahashi, S. Konno, J. Hamada, M. Miyajima, S. Kubota, A. Nakamoto, A. Hitachi, E. Shibamura, and T. Doke, Phys. Rev. A12, 1771 (1975).

54. J. Casanovas, R. Grob, D. Blanc, G. Brunet, and J. Mathieu, J. Chem. Phys. 63, 3673 (1975).

55. K. Shinsaka, J.-P. Dodelet, and G. R. Freeman, Can. J. Chem. 53, 2714 (1975).

56. J.-P. Dodelet, F. Y. Jou, and G. R. Freeman, J. Phys. Chem. 79, 3876 (1975).

57. J.-P. Dodelet and G. R. Freeman, Can. J. Chem. 53, 1263 (1975).

58. J.-P. Dodelet, K. Shinsaka, and G. R. Freeman, Can. J. Chem. 54, 744 (1976).

59. W. F. Schmidt and A. O. Allen, J. Chem. Phys. 52, 4788 (1970).

60. I. Kalinowski, J. G. Rabe, and W. F. Schmidt, Z. Naturforsch. 30, 568 (1975).

61. J. Terlecki and J. Fiutak, Int. J. Radiat. Phys. Chem. 4, 469 (1972).

62. R. C. Weast, (Editor) Handbook of Chemistry and Physics, 49th Edn., Chemical Rubber Co., Cleveland, Ohio, 1968.

63. N. E. Hill, W. E. Vaughan, A. H. Price, and M. Davies, "Dielectric Properties and Molecular Behavior", Van Nostrand Reinhold Co., Toronto, 1969, p.191.

64. R. R. Driesback (Editor), "Physical Properties of Chemical Compounds", American Chemical Society, Washington, D. C., Vol. 2, 1959.

65. R. W. Gallant, Physical Properties of Hydrocarbons, Vol. 1 and Vol. 2, Gulf Publishing Company, Houston, Texas (1968).

66. J.-P. Dodelet and G. R. Freeman (in press).

67. M. G. Robinson and G. R. Freeman, Can. J. Chem. 52, 440 (1974).

68. J. Lekner, Phys. Rev. 158, 130 (1967).

69. J. Lekner, Phys. Letts. 27A, 341 (1968).

70. J.-P. Dodelet and G. R. Freeman (in press).

APPENDIX

A. Derivation of Equation (iii)

$$H_2O \longrightarrow H,OH \qquad (30)$$

$$H,OH + HCH_2OH \longrightarrow H_2,H_2O + \cdot CH_2OH \qquad (31)$$

$$N_2O + \cdot CH_2OH \longrightarrow N_2 + \cdot OCH_2OH \qquad (32)$$

$$\cdot OCH_2OH + H_2O \longrightarrow HOCH_2OH + OH \qquad (33)$$

$$\cdot OCH_2OH + HCH_2OH \longrightarrow HOCH_2OH + \cdot CH_2OH \qquad (34)$$

$$HOCH_2OH \rightleftharpoons CH_2O + H_2O \qquad (35)$$

$$2 \cdot CH_2OH \longrightarrow P_1 \qquad (36)$$

$$\cdot OCH_2OH + CH_2OH \longrightarrow P_2 \qquad (37)$$

$$2 \cdot OCH_2OH \longrightarrow P_3 \qquad (38)$$

If one considers reactions (31), 32), and (33) as the important propagation reactions then the steady state analysis is as follows:

$$\frac{d[OH]}{dT} = k_{33}[\cdot OCH_2OH] - k_{31}[OH][HCH_2OH] = 0 \qquad (1)$$

$$k_{33}[\cdot OCH_2OH] = k_{31}[OH][HCH_2OH] \qquad (2)$$

Here the rate of production of OH in reaction (30) is neglected because the chain length is greater than 10 for most of the conditions studied and this means that reaction

(33) is at least 10 times faster than reaction (30).

$$\frac{d[\cdot CH_2OH]}{dT} = 2I + k_{31}[OH][HCH_2OH] - k_{32}[N_2O][\cdot CH_2OH] - 2k_{36}[\cdot CH_2OH]^2 - k_{37}[\cdot OCH_2OH][\cdot CH_2OH] = 0 \quad (3)$$

Equation (3) involves the assumption that reaction (36) and (37) are the only important termination reactions. Substituting the equality in equation (2) into equation (3) gives

$$\frac{d[\cdot CH_2OH]}{dT} = 2I + k_{33}[\cdot OCH_2OH] - k_{32}[N_2O][\cdot CH_2OH] - 2k_{36}[\cdot CH_2OH]^2 - k_{37}[\cdot OCH_2OH][\cdot CH_2OH] = 0 \quad (4)$$

Since the rate of initiation is equal to rate of termination we have

$$I = k_{36}[\cdot CH_2OH]^2 + k_{37}[\cdot OCH_2OH][\cdot CH_2OH] \quad (5)$$

where I is the rate of initiation. By rearranging equation (5) we obtain

$$[\cdot OCH_2OH] = \frac{I - k_{36}[\cdot CH_2OH]^2}{k_{37}[\cdot CH_2OH]} = \frac{I}{k_{37}[\cdot CH_2OH]} - \frac{k_{36}}{k_{37}}[\cdot CH_2OH] \quad (6)$$

Substituting equation (6) into equation (4) gives

$$2I + k_{33}\left(\frac{I}{k_{37}[\cdot CH_2OH]} - \frac{k_{36}}{k_{37}}[\cdot CH_2OH]\right) - k_{32}[N_2O][\cdot CH_2OH]$$
$$- 2k_{36}[\cdot CH_2OH]^2 - k_{37}[\cdot CH_2OH]\left(\frac{I}{k_{37}[\cdot CH_2OH]} - \frac{k_{36}}{k_{37}}[\cdot CH_2OH]\right) = 0 \quad (7)$$

Multiplying and removing brackets gives

$$2I + \frac{k_{33}I}{k_{37}[\cdot CH_2OH]} - \frac{k_{33}k_{36}}{k_{37}}[\cdot CH_2OH] - k_{32}[N_2O][\cdot CH_2OH]$$
$$- 2k_{36}[\cdot CH_2OH]^2 - I + k_{36}[\cdot CH_2OH]^2 = 0 \quad (8)$$

If we multiply equation (8) by $k_{37}[\cdot CH_2OH]$ the result is equation (9)

$$k_{37}I[\cdot CH_2OH] + k_{33}I - k_{33}k_{36}[CH_2OH]^2$$
$$- k_{32}k_{37}[N_2O][\cdot CH_2OH]^2 - k_{36}k_{37}[\cdot CH_2OH]^3 = 0 \quad (9)$$

Multiplying through by -1 and rearranging gives the desired result.

$$k_{36}k_{37}[\cdot CH_2OH]^3 + (k_{32}k_{37}[N_2O] + k_{33}k_{36})[\cdot CH_2OH]^2$$
$$-k_{37}I[\cdot CH_2OH] - k_{33}I = 0 \quad (10)$$

Derivation of Equation (v)

If we assume that termination is by equation (37) only then

$$\frac{d[\cdot OCH_2OH]}{dT} = k_{32}[N_2O][\cdot CH_2OH] - k_{33}[\cdot OCH_2OH]$$

$$- k_{37}[\cdot OCH_2OH][\cdot CH_2OH] = 0 \qquad (11)$$

rate of initiation equals rate of termination so that

$$[\cdot OCH_2OH] = \frac{I}{k_{37}[\cdot CH_2OH]} \qquad (12)$$

Substituting equation (12) into equation (11) leads to (13)

$$k_{32}[N_2O][\cdot CH_2OH] - \frac{k_{33}I}{k_{37}[\cdot CH_2OH]} - I = 0 \qquad (13)$$

Multiplying through by $k_{37}[\cdot CH_2OH]$ yields

$$k_{32}k_{37}[N_2O][\cdot CH_2OH]^2 - k_{37}I[\cdot CH_2OH] - k_{33}I = 0 \qquad (14)$$

solving the quadratic equation for $[\cdot CH_2OH]$ gives

$$[\cdot CH_2OH] = \frac{+k_{37}I}{2k_{32}k_{37}[N_2O]} + \frac{\sqrt{k_{37}^2I^2 + 4k_{32}k_{37}k_{33}I[N_2O]}}{\sqrt{4k_{32}^2k_{37}^2[N_2O]^2}}$$

$$= \frac{I}{2k_{32}[N_2O]} + \sqrt{\frac{I^2}{4k_{32}^2[N_2O]^2} + \frac{k_{33}I}{k_{32}k_{37}[N_2O]}} \qquad (15)$$

$$\frac{d(N_2)}{dT} = k_{32}[N_2O][\cdot CH_2OH] + I \qquad (16)$$

$$= \frac{3I}{2} + \sqrt{\frac{I^2}{4} + \frac{k_{33}k_{32}I[N_2O]}{k_{37}}}$$

The $I^2/4$ term and $3I/2$ term can be considered negligible for chain lengths greater than 10 so that

$$\frac{d(N_2)}{dT} = \left(\frac{k_{33}k_{32}}{k_{37}}\right)^{\frac{1}{2}} (I)^{\frac{1}{2}} [N_2O]^{\frac{1}{2}} \qquad (17)$$

$I = 10^{-2}D\ G(\text{int})$ and $G(N_2) = \frac{d(N_2)}{dT}/10^{-2}D$

therefore

$$G(N_2) = G(CH_2O) = \left(\frac{k_{33}k_{32}}{k_{37}}\right)^{\frac{1}{2}} \frac{(G\text{int})^{\frac{1}{2}}}{(10^{-2}D)^{\frac{1}{2}}} [N_2O]^{\frac{1}{2}} \qquad (18)$$

which is the desired result.

Equation (vi) can easily be derived by setting $I = k_{36}[\cdot CH_2OH]^2$ and $g(N_2) = \frac{d(N_2)}{dT}/10^{-2}D$. Using the relation that $\frac{d(N_2)}{dT} = k_{32}[\cdot CH_2OH][N_2O]$ gives the desired result, equation (vi).

B. Derivation of Equation (vii)

The reaction mechanism for the 2-propanol system can be written as follows:

$$H_2O \longrightarrow H,OH \qquad (30)$$

$$H,OH + HC(CH_3)_2OH \longrightarrow H_2,H_2O + \cdot C(CH_3)_2OH \qquad (31)$$

$$N_2O + \cdot C(CH_3)_2OH \longrightarrow N_2 + \cdot OC(CH_3)_2OH \qquad (32)$$

$$\cdot OC(CH_3)_2OH + H_2O \longrightarrow HOC(CH_3)_2OH + OH \quad (33)$$

$$\cdot OC(CH_3)_2OH + HC(CH_3)_2OH \longrightarrow HOC(CH_3)_2OH + \cdot C(CH_3)_2OH \quad (34)$$

$$HOC(CH_3)_2OH \rightleftharpoons C(CH_3)_2O + H_2O \quad (35)$$

$$2\cdot C(CH_3)_2OH \longrightarrow P_1 \quad (36)$$

$$\cdot OC(CH_3)_2OH + \cdot C(CH_3)_2OH \longrightarrow P_2 \quad (37)$$

$$2\cdot OC(CH_3)_2OH \longrightarrow P_3 \quad (38)$$

Considering reaction (31), (32) and (34) as the important propagation reactions leads to the following equations.

$$\frac{d[OH]}{dT} = k_{34}[\cdot OC(CH_3)_2OH][HC(CH_3)_2OH] - k_{31}[\cdot OH][HC(CH_3)_2OH] = 0 \quad (19)$$

Here the rate of production of OH in reaction (30) is neglected for the same reason as given in Appendix A.

$$\frac{d[\cdot C(CH_3)_2OH]}{dT} = 2I + k_{31}[OH][HC(CH_3)_2OH] - k_{32}[N_2O][\cdot C(CH_3)_2OH] - 2k_{36}[\cdot C(CH_3)_2OH]^2 - k_{37}[\cdot OC(CH_3)_2OH][\cdot C(CH_3)_2OH] = 0 \quad (20)$$

Here it is assumed that termination is by reaction (36) and (37). Substituting equation (19) into equation (20) leads to (21)

$$\frac{d[\cdot C(CH_3)_2OH]}{dT} = 2I + k_{34}[\cdot OC(CH_3)_2OH][HC(CH_3)_2OH] - k_{32}[N_2O][\cdot C(CH_3)_2OH] - 2k_{36}[\cdot C(CH_3)_2OH]^2 - k_{37}[\cdot OC(CH_3)_2OH][\cdot C(CH_3)_2OH] = 0 \quad (21)$$

The steps followed from this point are the same as equations (5), (6), (7), (8) and (9) shown in the derivation in Appendix A leading to the desired result

$$k_{36}k_{37}[\cdot C(CH_3)_2OH]^3 + (k_{32}k_{37}[N_2O] + k_{34}k_{36}[HC(CH_3)_2OH])[\cdot C(CH_3)_2OH]^2 - k_{37}I[\cdot C(CH_3)_2OH] - k_{34}I[HC(CH_3)_2OH] = 0 \quad (22)$$

Derivation of Equation (viii)

Assuming that termination is by reaction (37) only, leads to the expression

$$\frac{d[\cdot OC(CH_3)_2OH]}{dT} = k_{32}[N_2O][\cdot C(CH_3)_2OH] - k_{34}[HC(CH_3)_2OH][OC(CH_3)_2OH] - k_{37}[\cdot OC(CH_3)_2OH][\cdot C(CH_3)_2OH] = 0 \quad (23)$$

The derivation from this point follows the same steps as shown in equations (12-17) in Appendix A, giving the desired result.

$$G((CH_3)_2CO) = G(N_2) = G(int)\left(\frac{k_{34}k_{32}}{k_{37}}\right)^{\frac{1}{2}} \frac{[N_2O]\,[HC(CH_3)_2OH]^{\frac{1}{2}}}{(10^{-2}\ D)^{\frac{1}{2}}} \qquad (24)$$

C. Derivation of Equation (x)

Assuming termination is by reactions (37) and (38) and propagation by (32) and (34) gives

$$\begin{aligned}\frac{d[\cdot OC(CH_3)_2OH]}{dT} &= k_{32}[N_2O][\cdot C(CH_3)_2OH] \\ &\quad - k_{34}[\cdot OC(CH_3)_2OH][HC(CH_3)_2OH] \\ &\quad - k_{37}[\cdot OC(CH_3)_2OH][\cdot C(CH_3)_2OH] \\ &\quad - 2k_{38}[\cdot OC(CH_3)_2OH]^2 = 0\end{aligned} \qquad (25)$$

From rate of initiation equals rate of termination we get

$$\begin{aligned}I &= k_{37}[\cdot OC(CH_3)_2OH][\cdot C(CH_3)_2OH] \\ &\quad + k_{38}[OC(CH_3)_2OH]^2\end{aligned} \qquad (26)$$

so that

$$[\cdot C(CH_3)_2OH] = \frac{I}{k_{37}[\cdot OC(CH_3)_2OH]} - \frac{k_{38}}{k_{37}}[\cdot OC(CH_3)_2OH] \qquad (27)$$

Substitution of equation (27) into equation (25) yields

$$k_{32}[N_2O]\left(\frac{I}{k_{37}[\cdot OC(CH_3)_2OH]} - \frac{k_{38}}{k_{37}}[\cdot OC(CH_3)_2OH]\right)$$

$$- k_{34}[\cdot OC(CH_3)_2OH][HC(CH_3)_2OH]$$

$$- k_{37}[\cdot OC(CH_3)_2OH]\left(\frac{I}{k_{37}[\cdot OC(CH_3)_2OH]} - \frac{k_{38}}{k_{37}}[\cdot OC(CH_3)_2OH]\right)$$

$$- 2k_{38}[\cdot OC(CH_3)_2OH]^2 = 0 \qquad (28)$$

and multiplying and removing brackets gives

$$\frac{k_{32}[N_2O]I}{k_{37}[\cdot OC(CH_3)_2OH]} - \frac{k_{32}k_{38}}{k_{37}}[N_2O][\cdot OC(CH_3)_2OH]$$

$$- k_{34}[\cdot OC(CH_3)_2OH][HC(CH_3)_2OH]$$

$$- I + k_{38}[\cdot OC(CH_3)_2OH]^2$$

$$- 2k_{38}[\cdot OC(CH_3)_2OH]^2 = 0 \qquad (29)$$

multiplying equation (29) by $k_{37}[\cdot OC(CH_3)_2OH$ followed by multiplication by -1 gives the desired result.

$$k_{37}k_{38}[\cdot OC(CH_3)_2OH]^3$$

$$+ (k_{32}k_{38}[N_2O] + k_{34}k_{37}[HC(CH_3)_2OH])[\cdot OC(CH_3)_2OH]^2$$

$$+ k_{37}I[\cdot OC(CH_3)_2OH] - k_{32}I[N_2O] = 0 \qquad (30)$$